United States Department of Agriculture – Forest Service
Research Agreement No. 12318720C0009

CRASH-TESTED BRIDGE RAILINGS AND TRANSITIONS FOR WOOD BRIDGES – PHASE IIA

Submitted by

Jared T. Duren, M.S.C.E.
Former Graduate Research Assistant

Ronald K. Faller, Ph.D., P.E.
MwRSF Director and Research Professor

Tewodros Y. Yosef, Ph.D.
Post-Doctoral Research Associate

Robert W. Bielenberg, M.S.M.E.
Research Engineer

Scott K. Rosenbaugh, M.S.C.E.
Research Engineer

Joshua S. Steelman, Ph.D., P.E.
Associate Professor

James P. Wacker, P.E.
Research Engineer, U.S. Department of Agriculture, Forest Service, Forest Products Laboratory

MIDWEST ROADSIDE SAFETY FACILITY
Nebraska Transportation Center
University of Nebraska-Lincoln

Main Office
Prem S. Paul Research Center at Whittier School
Room 130, 2200 Vine Street
Lincoln, Nebraska 68583-0853
(402) 472-0965

Outdoor Test Site
4630 N.W. 36th Street
Lincoln, Nebraska 68524

Submitted to

U.S. Department of Agriculture
Forest Service
Forest Products Laboratory
One Gifford Pinchot Dr.
Madison, Wisconsin 53726

MwRSF Research Report No. TRP-03-465-23

March 20, 2023

TECHNICAL REPORT DOCUMENTATION PAGE

1. Report No. TRP-03-465-23	**2. Government Accession No.**	**3. Recipient's Catalog No.**
4. Title and Subtitle Crash-Tested Bridge Railings and Transitions for Wood Bridges – Phase IIa		**5. Report Date** March 20, 2023 **6. Performing Organization Code**
7. Author(s) Duren, J.T., Faller, R.K., Yosef, T.Y., Bielenberg, R.W., Rosenbaugh, S.K., Steelman, J.S., and Wacker, J.P.		**8. Performing Organization Report No.** TRP-03-465-23
9. Performing Organization Name and Address Midwest Roadside Safety Facility (MwRSF) Nebraska Transportation Center University of Nebraska-Lincoln Main Office: Prem S. Paul Research Center at Whittier School Room 130, 2200 Vine Street Lincoln, Nebraska 68583-0853 Outdoor Test Site: 4630 N.W. 36th Street Lincoln, Nebraska 68524		**10. Work Unit No.** **11. Contract**
12. Sponsoring Agency Name and Address U.S. Department of Agriculture Forest Service Forest Products Laboratory One Gifford Pinchot Drive Madison, Wisconsin 53726		**13. Type of Report and Period Covered** Final Report: 2018-2022 **14. Sponsoring Agency Code** Research Agreement No. 18-JV-11111107-037
15. Supplementary Notes Prepared in cooperation with U.S. Department of Transportation, Federal Highway Administration.		

16. Abstract

In this study, an updated design configuration for a Manual for Assessing Safety Hardware (MASH 2016) Test Level 4 (TL-4) crashworthy glulam timber rail with a curb bridge railing system was developed. Many similar systems were developed in the past to meet previous impact safety criteria, but an updated design was necessary to meet current MASH impact safety criteria. A thorough review of similar systems developed under previous crash testing standards was performed during the development of the bridge railing system. The most recent iteration of this type of system, developed by MwRSF in the 1990s under NCHRP Report No. 350, served as an initial basis for the updated system.

In order to create a new system deemed acceptable under MASH criteria, simulation using BARRIER VII software was performed with models originally developed for the NCHRP Report No. 350 system. The original models were examined piece by piece and general updates were made to utilize the increased capacities of BARRIER VII. After a series of modifications to the bridge railing system model, including increasing the size and height of multiple components, the simulation effort demonstrated that the modified TL-4 bridge railing was acceptable under MASH criteria. Additional research on connection details and timber deck strengths, the development of an approach guardrail transition system, and component and full-scale testing programs are yet to be performed to complete Phase IIa of this project.

17. Key Words Highway Safety, Crash Test, Roadside Safety Appurtenances, Compliance Test, Bridge Railings, Timber Bridges, Timber Railings, and Wood Railings		**18. Distribution Statement** No restrictions. Document available from: National Technical Information Services, Springfield, Virginia 22161	
19. Security Classification (of this report) Unclassified	**20. Security Classification (of this page)** Unclassified	**21. No. of Pages** 130	**22. Price**

DISCLAIMER STATEMENT

This report was completed with funding from the U.S. Department of Agriculture – Forest Service – Forest Products Laboratory. The contents of this report reflect the views and opinions of the authors who are responsible for the facts and the accuracy of the data presented herein. The contents do not necessarily reflect the official views or policies of the U.S. Department of Agriculture. This report does not constitute a standard, specification, regulation, product endorsement, or an endorsement of manufacturers.

ACKNOWLEDGEMENTS

The authors wish to acknowledge the U.S. Department of Agriculture - Forest Service - Forest Products Laboratory for sponsoring this project. Acknowledgement is also given to the following individuals who contributed to the completion of this research project.

Midwest Roadside Safety Facility
J.C. Holloway, M.S.C.E., Research Engineer & Assistant Director –Physical Testing Division
K.A. Lechtenberg, M.S.M.E., Research Engineer
C.S. Stolle, Ph.D., Research Assistant Professor
M. Asadollahi Pajouh, Ph.D., P.E., Research Assistant Professor
B.J. Perry, M.E.M.E., Research Associate Engineer
A.T. Russell, B.S.B.A., Testing and Maintenance Technician II
E.W. Krier, B.S., Engineering Testing Technician II
D.S. Charroin, Engineering Testing Technician II
R.M. Novak, Engineering Testing Technician II
S.M. Tighe, Engineering Testing Technician I
T.C. Donahoo, Engineering Testing Technician I
J.T. Jones, Engineering Testing Technician I
C. Charroin, Engineering Construction Testing Technician I
T. Shapland, Engineering Construction Testing Technician I
E.L. Urbank, B.A., Research Communication Specialist
Z.Z. Jabr, Engineering Technician
Undergraduate and Graduate Research Assistants

U.S. Department of Agriculture Forest Service – Forest Products Laboratory
Michael Ritter, P.E., Assistant Director (retired)

SI* (MODERN METRIC) CONVERSION FACTORS

APPROXIMATE CONVERSIONS TO SI UNITS

Symbol	When You Know	Multiply By	To Find	Symbol
		LENGTH		
in.	inches	25.4	millimeters	mm
ft	feet	0.305	meters	m
yd	yards	0.914	meters	m
mi	miles	1.61	kilometers	km
		AREA		
in^2	square inches	645.2	square millimeters	mm^2
ft^2	square feet	0.093	square meters	m^2
yd^2	square yard	0.836	square meters	m^2
ac	acres	0.405	hectares	ha
mi^2	square miles	2.59	square kilometers	km^2
		VOLUME		
fl oz	fluid ounces	29.57	milliliters	mL
gal	gallons	3.785	liters	L
ft^3	cubic feet	0.028	cubic meters	m^3
yd^3	cubic yards	0.765	cubic meters	m^3
		NOTE: volumes greater than 1,000 L shall be shown in m^3		
		MASS		
oz	ounces	28.35	grams	g
lb	pounds	0.454	kilograms	kg
T	short ton (2,000 lb)	0.907	megagrams (or “metric ton”)	Mg (or "t")
		TEMPERATURE (exact degrees)		
°F	Fahrenheit	5(F-32)/9 or (F-32)/1.8	Celsius	°C
		ILLUMINATION		
fc	foot-candles	10.76	lux	lx
fl	foot-Lamberts	3.426	candela per square meter	cd/m^2
		FORCE & PRESSURE or STRESS		
lbf	poundforce	4.45	newtons	N
lbf/in^2	poundforce per square inch	6.89	kilopascals	kPa

APPROXIMATE CONVERSIONS FROM SI UNITS

Symbol	When You Know	Multiply By	To Find	Symbol
		LENGTH		
mm	millimeters	0.039	inches	in.
m	meters	3.28	feet	ft
m	meters	1.09	yards	yd
km	kilometers	0.621	miles	mi
		AREA		
mm^2	square millimeters	0.0016	square inches	in^2
m^2	square meters	10.764	square feet	ft^2
m^2	square meters	1.195	square yard	yd^2
ha	hectares	2.47	acres	ac
km^2	square kilometers	0.386	square miles	mi^2
		VOLUME		
mL	milliliter	0.034	fluid ounces	fl oz
L	liters	0.264	gallons	gal
m^3	cubic meters	35.314	cubic feet	ft^3
m^3	cubic meters	1.307	cubic yards	yd^3
		MASS		
g	grams	0.035	ounces	oz
kg	kilograms	2.202	pounds	lb
Mg (or "t")	megagrams (or “metric ton”)	1.103	short ton (2,000 lb)	T
		TEMPERATURE (exact degrees)		
°C	Celsius	1.8C+32	Fahrenheit	°F
		ILLUMINATION		
lx	lux	0.0929	foot-candles	fc
cd/m^2	candela per square meter	0.2919	foot-Lamberts	fl
		FORCE & PRESSURE or STRESS		
N	newtons	0.225	poundforce	lbf
kPa	kilopascals	0.145	poundforce per square inch	lbf/in^2

*SI is the symbol for the International System of Units. Appropriate rounding should be made to comply with Section 4 of ASTM E380.

TABLE OF CONTENTS

LIST OF FIGURES

LIST OF TABLES

1 INTRODUCTION

1.1 Background

Between 1988 and 2013, numerous bridge railing systems were developed for use on timber deck bridges per the impact safety criteria found in the National Cooperative Highway Research Program (NCHRP) Report No. 350, *Recommended Procedures for the Safety Performance Evaluation of Highway Features* [1]; the American Association of State Highway and Transportation Officials (AASHTO) *Guide Specifications for Bridge Railings* [2]; and the AASHTO *Manual for Assessing Safety Hardware (MASH) 2009* [3]. In 2016, AASHTO's MASH was updated. Both MASH 2009 [3] and MASH 2016 [4] included updated impact conditions and safety evaluation criteria, which reflected current vehicles and characteristics, new hardware categories, improved crash test documentation, objective vehicle damage criteria, and refined occupant risk limits.

To date, two bridge railing systems have been developed for use on wood bridges using the updated MASH 2016 impact conditions and evaluation criteria, only one of which has been crash tested. The only crash tested system to meet MASH impact safety criteria was a Test Level 1 (TL-1) low-height, curb-type, glued-laminated (glulam) timber bridge railing system [5-6]. The other wood bridge railing system to be developed under MASH criteria was a Test Level 3 (TL-3) W-beam system [7]. Thus, a need exists to develop new and/or modify existing bridge railing and approach guardrail transition systems for use on wood bridges under the MASH 2016 impact safety standards. For this effort, these systems need to be subjected to full-scale crash testing and evaluation. In some scenarios, it may be possible to utilize static and/or dynamic component testing to demonstrate equivalency when crashworthy bridge railing systems are installed on alternative bridge deck types.

In collaboration with the United States Department of Agriculture – Forest Service – Forest Products Laboratory (USDA – FS – FPL), the Midwest Roadside Safety Facility (MwRSF) of the University of Nebraska-Lincoln (UNL) initiated a multiphase project to: (1) identify bridge railing systems that were previously developed under prior safety criteria, (2) document bridge railings currently in use in the field, (3) create a research plan to update selected bridge railing and approach guardrail transition systems, and (4) redesign these systems to meet current AASHTO MASH 2016 impact safety standards. The aforementioned research activities were performed in Phase I of this project and can be found in reference [8].

Phase IIa of the research program was initiated with additional funding provided by the USDA – FS – FPL and targeted the development of the top priority system identified in Phase I, a glulam timber rail with curb bridge railing system designed to meet MASH TL-4 impact safety criteria. This research report contains information on Phase IIa research project. However, it should be noted that only partial funding had been provided to date to support on Phase IIa bridge railing design effort.

Due to its prominence in timber bridge railing systems, background information on glulam timber is necessary to understand the research compiled in this study. Glulam timber is a construction material consisting of multiple pieces of wood, or wood laminations, that are bonded together using extremely durable adhesives. A schematic of glulam timber is provided in Figure 1. Glulam members can be fabricated to virtually any reasonable size and length. Because glulam

members are built-up sections of smaller pieces of wood, it is much easier to obtain a high-quality wood member than simply using sawn timber. Different combinations of timber species and grades can also be created to optimize the member for different types of loading, including for impact loading scenarios. For these reasons, glulam timber has continued to be used in the roadside safety industry.

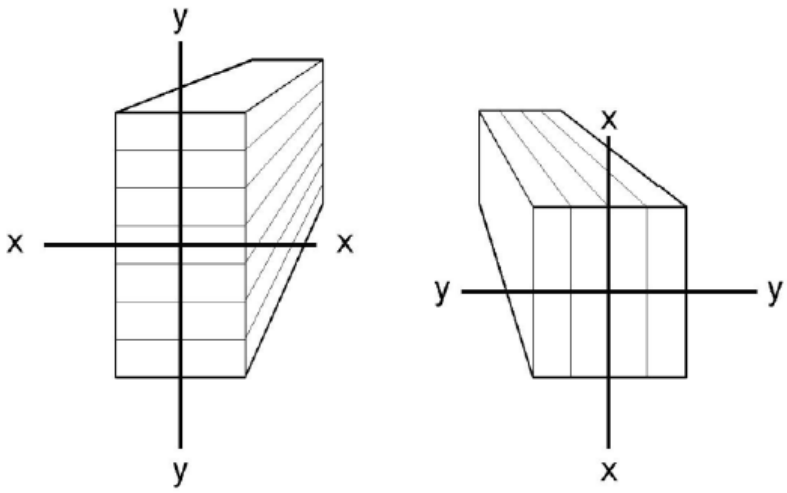

Figure 1. Schematic of Glulam Timber [9]

1.2 Project Objectives

The primary objective of the Phase IIa research study was to develop a glulam timber rail with a curb bridge railing system in compliance with MASH 2016 Test Level 4 (TL-4) safety performance criteria for use on both transverse and longitudinal glulam timber bridge decks as well as reinforced-concrete bridge decks. This study (i.e., Phase IIa) contains only the initial efforts to develop this updated bridge railing system. In future tasks under Phase IIb, the final system details as well as an approach guardrail transition will also be configured to connect W-beam guardrail systems to the glulam timber rail with the curb bridge railing system. The approach guardrail transition shall be configured to meet MASH 2016 TL-3 safety performance criteria.

The bridge railing system was configured to use glulam timber for all wood components, such as the upper rail, lower curb rail, scuppers, spacer blocks, and support posts. The bridge railing system will later be constructed and the critical timber deck configuration will be crash tested to allow its use on alternative timber and reinforced-concrete slab decks. A critical deck thickness and deck cantilever, or overhang, will later be determined. The research and development effort utilized survey data, a literature review, and partner expertise to determine the practical ranges for glulam deck panel dimensions (i.e., widths, lengths, and thicknesses) as well as ranges for deck cantilevers for transverse glulam timber decks. The initial development effort considered common timber species, such as Southern Yellow Pine (SYP) and Douglas Fir (DF), for the bridge railing system's structural components.

In testing, the glulam timber decks will be configured with a 2-in. thick asphalt wearing surface to represent the opening of the new bridge structure with railings. As such, the development of the bridge railing and transition systems will need to consider this initial condition. Further,

roadways associated with real-world bridge structures often require a future asphalt overlay, which can add 2 in. to the overall surfacing on the timber deck. The development effort considered an overall surface thickness of 4 in. when determining the geometric and structural requirements of the bridge railing system to meet the MASH 2016 TL-4 impact safety criteria.

Over time, timber bridge deck systems can be susceptible to the long-term effects of excess moisture on the members, which can result in degraded structural capacity and cause timber elements to swell, shift, and/or rotate. For this study, it was desirable for the project team to brainstorm, consider, and possibly implement cost-effective measures that are targeted to reduce exposure of timber deck elements under the asphalt wearing surface to hydraulic water runoff and prolonged water accumulation near the bridge railing system. Considerations for such environmental factors will be contained in the research efforts to be performed beyond the work reported herein.

2 USDA – FS – FPL MASH TL-4 BRIDGE RAILING

2.1 Introduction

In the 2020 report, Crash-Tested Bridge Railings and Transitions for Wood Bridges – Phase I, researchers compiled significant information pertaining to bridge railing systems that either utilized timber components or were developed for use on timber deck bridges [8]. Further, the project team documented approach guardrail transitions that corresponded to select crashworthy bridge railing systems.

Phase II of this project aimed at utilizing previously-designed bridge railing systems as a starting point for further development. The top priority railing system identified in Phase I was a timber railing with a curb system that could be redesigned to meet MASH 2016 TL-4 impact safety criteria. To begin the work on developing an updated version of this system, an in-depth analysis was performed on the most recent system of this type. This railing system, shown in Section 3.13 of the referenced report [8], was developed by MwRSF in the mid-1990s in collaboration with the USDA – FS – FPL [10-12]. At the time, MwRSF graduate student Michael Fowler created initial designs based upon information from other previously crash-tested systems, updated timber strength calculations, and computer simulation modeling using the BARRIER VII software [13-14]. BARRIER VII is a 2-dimensional, finite element analysis software that can be used to model vehicle crash events into various types of longitudinal barriers, such as guardrails and bridge railings. After the design and simulation efforts concluded, full-scale crash tests were run on both the bridge railing and approach guardrail transition systems. The two crash tests conducted on the bridge railing system were test nos. TRBR-1 and TRBR-2, both of which met the safety evaluation criteria for crash test nos. 4-12 and 4-11 from NCHRP Report No. 350, respectively [1]. The crash tests proved that the system met the NCHRP Report No. 350 TL-4 criteria, and final recommendations were made for the system. However, the computer simulations were never revisited to reanalyze the barrier model and conduct a calibration between the model and the actual physical crash tests.

To complete Task 1 of the Phase II research project, the research team began by gathering and reviewing information on similar systems and critical parameters, such as deck thickness, glulam panel size, and overhang length, through survey data, a literature review, and correspondence with the sponsor. The next goal was to develop a BARRIER VII bridge railing model that was calibrated to the crash tests run on the bridge railing system designed by Fowler [12]. This was achieved by reviewing the BARRIER VII model Fowler had originally used in his development effort and updating the basic geometry and material parameters within the model based on new information and considerations from the current research program. The model was deemed to be calibrated once the simulation results reasonably replicated the crash testing results from the TRBR test series. Once the model was calibrated, modifications were made to the structural components of the bridge railing system, and the associated model parameters were updated accordingly. Simulations were conducted with a model reflecting each modification with the goal of creating a system that would behave similarly to the full-scale system in the TRBR crash testing series, as there was no failures in those two tests. These simulations considered updated impact conditions and vehicle parameters established in MASH.

The process of calibrating the model to NCHRP Report No. 350 crash tests and then modifying the model to reflect changes necessary to meet MASH criteria had to be performed twice in this research effort. After initial calibration using an overall modeling scheme similar to that used by Fowler, the simulation provided system behavior comparable to what was observed in physical testing. The next step was to update the model to create a MASH crashworthy system. As part of this effort, a new BARRIER VII 10000S vehicle model had to be created, as will be further discussed. After investigation, it was determined that the modification of certain parameters when updating the system to meet MASH criteria caused a large amount of uncertainty in the accuracy of the model. The exact cause of this uncertainty is discussed in a later section of this study. Due to low confidence in the model's predictability, the research team decided to determine a modeling scheme that would be more representative of the actual bridge railing system. The model was recreated using the new modeling scheme and produced acceptable results in simulation once again. Simulations of MASH crash testing were conducted for the second time and utilized a BARRIER VII model that produced results that carried much more confidence. After making the necessary modifications to the system to achieve desired behaviors, additional simulations were performed to identify the critical impact points for crash testing with a pickup truck and a single-unit truck. The investigation and design processes are detailed in the following sections.

2.2 BARRIER VII Software

Developed in 1973 by Graham Powell at the University of California Berkeley [13-14], the BARRIER VII computer software has been utilized to simulate vehicle crash tests for five decades. Since its original development, the software has been updated to be able to simulate and evaluate barrier systems using refined mesh sizes with larger arrays of elements for beams, posts, and other element types.

BARRIER VII utilizes material and extensional geometric non-linearities to process solutions. Elements, such as beams and posts, are idealized with bilinear, elastic, perfectly-plastic properties when behaving flexurally and extensionally. If multiple members with different force versus deflection relationships are placed in parallel, strain-hardening effects can be introduced as well. The program uses the tangent stiffness method to process inelastic member behavior and midpoint constant acceleration numerical integration for incorporating dynamic loads [13-14].

In BARRIER VII, a barrier is modeled as a planar rigid body capable of deformations, while vehicles are given a prescribed shape, mass, and rotational inertia. The body of the vehicle is defined by nodes with nonlinear springs at each location that allow the body to deform based on a prescribed stiffness. The action of deformation for the vehicle is supposed to represent the crushing of sheet metal and plastic vehicle components, bottoming of these materials against the vehicle's frame, and eventually, unloading of the material as the vehicle disengages from the barrier. A BARRIER VII vehicle model also has inputs that can be changed to determine which points on the vehicle are capable of contacting each rail when multiple rails are present in a given system. In a double rail system, similar to what is being developed through this Phase II project, the vehicle is typically designated to apply most of the impact load to the upper rail, which is closer in alignment with its center of gravity (c.g.) height. The pickup truck and single-unit truck crashes have also demonstrated a tendency to climb up the lower curb rail. For these reasons, the vehicle

was modeled to only contact the upper rail in all impact simulations involving pickup truck and single-unit truck vehicles in this study.

Furthermore, vehicle models for idealized planar vehicles under NCHRP Report No. 350 were calibrated by MwRSF to accurately represent findings from vehicle crashes into an instrumented wall at TTI in 1989 [15]. From this study, the researchers determined vehicle impact forces and inertial properties. Based on this information and analysis of the vehicle deformations, vehicle crush stiffnesses and inertial properties were tuned and determined. This data was used for the original standard 2000P and 8000S vehicle models that were utilized for BARRIER VII simulation efforts. In the process of updating crash testing standards from NCHRP Report No. 350 to MASH, a model for the 2270P MASH pickup was also developed. This work was completed by researchers at MwRSF with the purpose of using the model to identify critical impact points on semi-rigid barriers [16]. The new pickup model contained modified dimensions, mass, and rotational inertia in comparison to the 2000P model. An updated model for the 10000S single-unit truck was not developed at that time, but a similar approach was taken through this research program to develop a basic model for the updated 10000S vehicle, which is later discussed. The 2-dimensional finite element models for the 2000P, 8000S, and 2270P vehicles can be seen in Figures A-1 through A-3 of Appendix A, along with the respective input file for each vehicle.

2.3 Initial BARRIER VII Model Calibration

2.3.1 Global Geometric Updates

Utilizing the models developed for the original timber railing with curb system, the research team created a bridge railing system to meet current crash testing standards, beginning with global geometric updates/calibrating the BARRIER VII model. Because the original BARRIER VII models were never reviewed to ensure reasonable replication of the results from the actual crash tests, this step was deemed the best place to start. All information regarding the simulations and the associated crash tests was acquired and reviewed. Calibration simulations were conducted utilizing the actual impact conditions of the full-scale crash tests performed on the bridge railing system in the 1990s to create a model that would reasonably replicate the barrier and 2-D vehicle behaviors observed in the full-scale crash testing. The BARRIER VII software's updated capabilities (i.e., expanded array sizes) let the team create a refined system model containing more nodes, and, therefore, a greater number of smaller beam elements to produce more refined results.

The original model created by Fowler, as shown in Figure A-4 of Appendix A, contained a surrogate approach guardrail transition, 15 bridge posts that were each attached to an upper rail and a curb rail, an anchorage post at the upstream end of the curb rail, and an anchorage post at the end of the bridge railing system, connected to both rails. This layout resulted in 11 transition posts, 15 bridge railing posts, one curb rail anchorage post, and one downstream anchorage post.

There were also a total of 117 nodes along the two rails. Nodes 1 through 14 represented the transition rail, even-numbered nodes from 14 through 116 represented the top rail, and odd-numbered nodes from 15 through 117 represented the curb rail. Bridge posts were spaced at 8 ft on center, with nodes in the first 10 bridge spans being spaced at 2 ft on center. In spans 11 through 15, nodes were spaced at 4 ft on center. Beam elements were modeled between consecutive nodes along each of the rails. The model contained timber strength properties for all bridge railing

members in the system, as it was built in the 1990s crash testing program. The upper rail and posts were modeled as DF Glulam Combination No. 2, while the curb rail was modeled as DF Glulam Combination No. 1, per recommendation from researchers in the original development [10-12]. The upper rail was an 8¾-in. deep by 13½-in. tall glulam beam.

The curb rail was a 6¾-in. tall by 12-in. deep glulam beam supported by glulam scupper blocks of the same size that were 54 in. long and centered on each post location. The posts were 8¾-in. wide by 10½-in. deep glulam timber sections [10-12]. A side-view schematic of the bridge railing system can be seen in Figure 2. The timber properties that were used to model the upper and curb rails of the system are provided in Table 1, and the properties of the posts are shown in Table 2 [12]. For post elements, the A- and B-axes are defined as the two primary axes extending longitudinally and laterally through the centroid of the post cross-section, respectively.

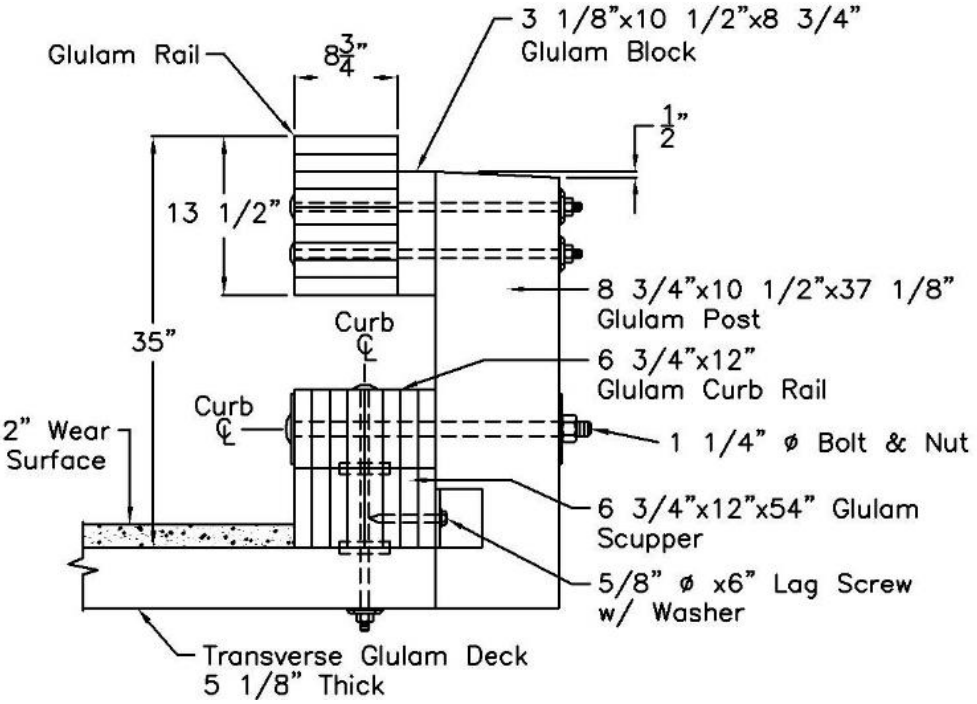

Figure 2. Side-View Schematic of NCHRP Report 350 TL-4 Glulam Timber Rail with Curb Bridge Railing [10-12]

Table 1. Original BARRIER VII Timber Rail Properties [12]

Member Type	**Member Size**	**Area (in.^{2})**	**Moment of Inertia (in.^{4})**	**Modulus of Elasticity (ksi)**	**Weight (lb/ft)**	**Nominal Tensile Yield Force (k)**	**Nominal Yield Moment (k-in.)**
Upper Rail	8¾"x13½" (Glulam)	118.1	753.7	1,400	41.0	236.2	1,098.4
Curb Rail	6¾"x12" (Glulam)	81.0	972.0	1,500	28.1	162.0	1,032.8

Table 2. Original BARRIER VII Timber Post Properties [12]

Member Type	Member Size	Top Node Height (in.)	Bottom Node Height (in.)	Stiffness k_A & k_B (k/in.)	Weight (lb)	Nominal Yield Moment (k-in.)	Failure Shear Force (k)	Failure Deflection (in.)
Bridge Post	8¾"x10½" (Glulam)	18.0	0.25	A-axis: 9.07 B-axis: 13.05	106.3	A-axis: 820.1 B-axis: 683.4	A-axis: 52.8 B-axis: 52.8	A-axis: 5.8 B-axis: 4.8

In the updated model used to calibrate the simulations with the full-scale crash testing results, an additional 8-ft bridge span was added, and the total number of nodes increased from 117 nodes to 369 nodes due to mesh refinement in each of the bridge spans. The extra span was added in order to model a system containing 16 bridge posts, as it was built for the full-scale crash testing program [11]. With the increased number of nodes, the elements in the first two bridge spans were each 1 ft long, elements in the third through eighth bridge spans were 6 in. long, and elements in the last eight bridge spans were 1 ft long. Elements in the third through eighth bridge spans were smaller in order to obtain more refined results in the critical area of the railings throughout impact simulations. All bridge railing posts were still spaced at 8 ft on center. The updated BARRIER VII model is shown in Figure 3.

With the changes to the general layout of the nodes and elements, simulations were then conducted with both the original and updated models utilizing the target impact conditions provided in NCHRP Report 350 for test nos. 4-11 and 4-12 [1], as well as with the actual impact conditions observed in test nos. TRBR-1 and TRBR-2 [10-12]. The ideal test conditions and the actual impact conditions are shown in Tables 3 and 4. This process was utilized in order to ensure that the models behaved similarly in terms of maximum deflections, based simply on the geometric changes that were made, so the material properties were not changed prior to performing this check. After comparison, the geometric updates provided similar simulation results. The comparison of the crash testing and simulation results can be seen in Tables 5 and 6, along with the maximum deflections observed in the appropriate full-scale crash test.

Table 3. NCHRP Report 350 2000P and TRBR-2 Impact Conditions

Criteria	Target Impact Conditions	Actual Impact Conditions
Vehicle Weight (lb)	4,410.0	4,393.8
Impact Velocity (mph)	62.1	61.6
Impact Angle (degrees)	25.0	27.4
Impact Severity (k-ft)	101.6	118.2

Table 4. NCHRP Report 350 8000S and TRBR-1 Impact Conditions

Criteria	Target Impact Conditions	Actual Impact Conditions
Vehicle Weight (lb)	17,637.0	17,637.0
Impact Velocity (mph)	49.7	46.5
Impact Angle (degrees)	15.0	16.0
Impact Severity (k-ft)	97.6	96.8

Table 5. 2000P Simulation Results with Geometrically Updated Model

Impact Conditions	Simulation Model or Test No.	Maximum Dynamic Deflection (in.)
Target Impact Conditions	Fowler	5.44
	Updated - Duren	5.35
Actual Impact Conditions	Fowler	8.12
	Updated – Duren	7.86
	Test No. TRBR-2	8.0

Table 6. 8000S Simulation Results with Geometrically Updated Model

Impact Conditions	Simulation Model or Test No.	Maximum Dynamic Deflection (in.)
Target Impact Conditions	Fowler	4.44
	Updated – Duren	4.56
Actual Impact Conditions	Fowler	5.48
	Updated – Duren	5.51
	Test No. TRBR-1	3.3

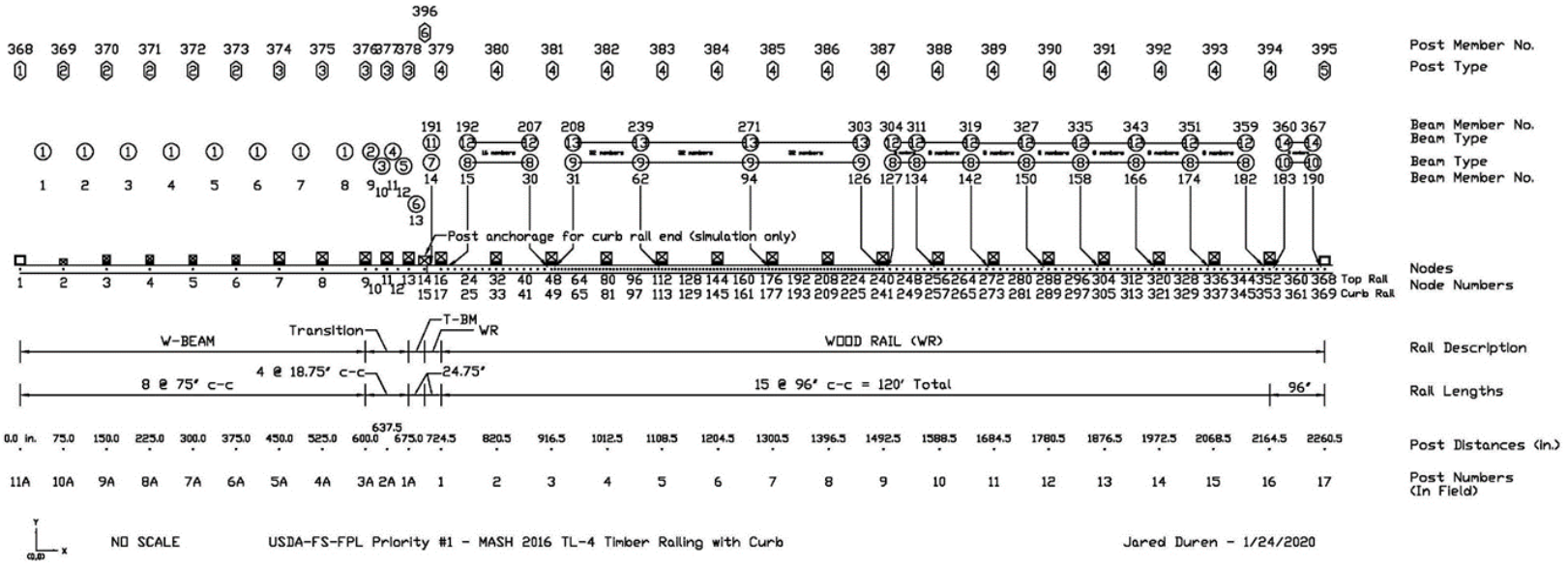

Figure 3. Updated BARRIER VII NCRHP Report 350 TL-4 Bridge Railing System Model

2.3.2 Material Parameter Updates

2.3.2.1 Post Modeling Scheme

After the model improved and was calibrated, the material properties for the bridge railing system components in Fowler's model were reviewed. For beam elements, the critical parameters included in a BARRIER VII model are the moment of inertia, cross-sectional area, element length, modulus of elasticity, weight per linear foot, tensile capacity, and moment capacity. For post elements in a BARRIER VII model, the key parameters are defined based on the two primary axes in which the post can be loaded and deflect. Figure 4 shows the orientation of these axes for a timber post in relation to the rail, as well as the typical behavior and failure mechanisms of a post in BARRIER VII. The key parameters include the heights of the rails that are attached to the posts, stiffnesses of the posts for elastic horizontal deflections along the two axes, the effective weight of the posts, yield moments about the two axes, failure shear strengths along the two axes, and deflection limits that will cause failure in each direction. In Figure 4, the first failure mechanism represents the post reaching its yield moment, M_A, due to the load, P_B, being applied at a height, H, and the post eventually fails at a specified deflection, Δ_B. The second failure mechanism occurs when the applied load, P_b, surpasses the shear capacity of the post, V_b, causing failure before moment yielding occurs.

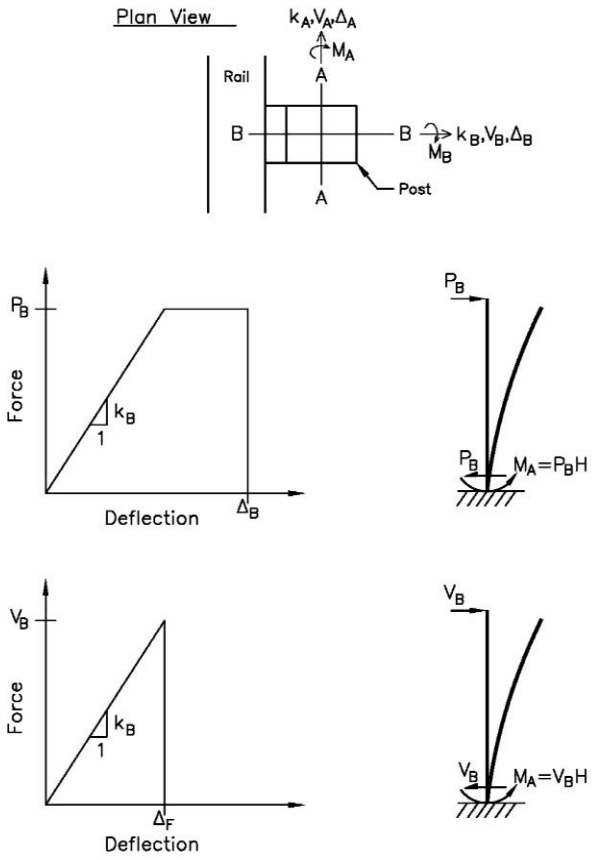

Figure 4. BARRIER VII Post Model and Failure Behavior

In the past, rails were modeled differently than they were physically built in order to encapsulate certain behaviors within a system. A chosen reference height or surrogate base height was created at a location other than the actual ground line or top of the deck, modifying the heights of the posts and locations of rails accordingly. Although the midheight of the curb rail was 10⅛ in. above the deck and the midheight of the upper rail was 28¼ in. above the deck, as denoted by the purple nodes in the left schematic of Figure 5, the post reference height was set at the midheight of the curb rail, which corresponded with the location of the horizontal-bolted connection and the red line in the right schematic of Figure 5. With this selection, the curb rail was modeled to be ¼ in. above the reference location, and the upper rail was modeled to be 18 in. above the reference location, as denoted by the blue nodes in the right schematic of Figure 5. The exact rationale behind this modeling scheme is unknown. However, after reviewing the crash testing footage, the post seemed to rotate about a point near this reference location, which may be the reason. This selection was deemed acceptable as it had historically been proven to provide successful railing design, and the same scheme was utilized in the initial efforts to validate the model using the actual crash test conditions.

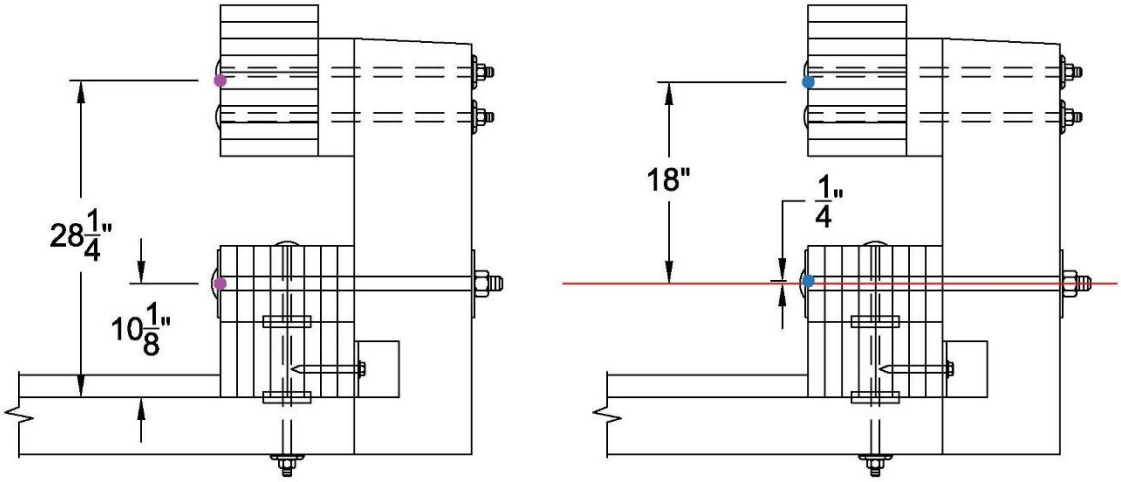

Figure 5. Original BARRIER VII Post Modeling Scheme

2.3.2.2 Determination of Timber Component Weights and Strengths

Both the *2018 National Design Specification (NDS) for Wood Construction* [9], along with the specification's supplementary documents [9, 17], and the AASHTO *LRFD Bridge Design Specification*, 9th Edition [18] were reviewed for current wood design procedures and equations for determining strengths. Each reference utilizes similar procedures to calculate timber strengths for bending, shear, compression parallel and perpendicular to the grain, and tension parallel to the grain. The general procedure includes identifying tabulated reference design values based on the type of wood being analyzed, and then modifying these values through multiplication using a series of factors based upon the in-use conditions of the element. The detailed procedure from each reference is outlined in Appendix B. An example calculation for each type of strength based on the members from the final design is also provided in Appendix B.

The *Manual for Engineered Wood Construction* also provides guidance on determining the weight of glulam materials [17]. Table M5.4-1 in the document includes weight factors that can be multiplied by the cross-sectional area of a section to determine the weight per linear foot of a specific type of timber. Weights for the components in the BARRIER VII model were assumed to be Douglas Fir-Larch with a specific gravity of 0.50, which is defined by a weight factor of 0.238 at a 15 percent moisture content.

The moment and tensile capacities are the critical structural parameters for a BARRIER VII model with a rail element. Through analysis using both references, it was determined that the AASHTO *LRFD Bridge Design Specification* provided slightly more conservative strengths than the NDS. For example, the AASHTO LRFD and NDS moment capacities for an 8¾-in. deep by 13½-in. tall DF Glulam Combination No. 2 beam loaded parallel to the wide face of laminations as the upper rail is loaded were calculated to be 805.24 k-in. and 870.30 k-in., respectively. The AASHTO LRFD and NDS tensile strengths for the same beam were calculated as 314.45 k and 339.61 k, respectively. Therefore, the strengths calculated using AASHTO LRFD were incorporated into the BARRIER VII model. For post models in BARRIER VII, the important structural parameters are the moment and shear capacities. Again, for the moment capacity of a post, AASTHO LRFD proved to be conservative in comparison to NDS, but for shear strength, AASHTO LRFD predicted higher strengths than NDS. For example, the AASHTO LRFD and NDS moment strengths for an 8¾-in. deep by 10½-in. wide DF Glulam Combination No. 2 post loaded perpendicular to the wide face of laminations, or M_A as shown in Figure 4, were calculated to be 682.43 k-in. and 752.11 k-in., respectively. The AASHTO LRFD and NDS shear strengths for the same post were calculated as 40.6 k and 31.0 k, respectively. These findings in relation to shear will be further discussed.

After all strengths and capacities were determined using updated procedures, these strengths and capacities were compared with Fowler's BARRIER VII input parameters for rail and post elements [12]. This comparison showed that the current bending capacities using both NDS and AASHTO LRFD were significantly lower than the capacities determined by Fowler.

An investigation was performed to determine the source of the differences noted above. This investigation determined that the capacities used by Fowler were likely not based on allowable design stresses in the wood members using the NDS and AASHTO LRFD procedures. Instead, the strengths were likely determined as a percentage of the modulus of rupture (MOR) of the wood. It has been common practice in the design of timber rails for barriers to use larger bending strengths, effectively allowing for an overstress condition under impact loading scenarios. Wood design strengths calculated by the AASHTO LRFD or NDS methods are based upon 5th percentile capacity, as observed from testing [19-20]. Designing for smaller bending capacities under impact loading conditions would lead to much larger railing components. Thus, the research team again considered using bending strengths above those provided by the design equations, but which would be less than documented and published MOR values. Further investigation helped to determine bending strengths near the mean, which would provide a more reasonable bending capacity for use in a bridge railing system.

Research performed by Moody et al. in the 1980s provided data showing that mean MOR strengths are approximately 1.5 times larger than 5th percentile strengths for glulam DF beams [21]. An average MOR for DF glulam beams was reported as 6,000 psi, with a 5th percentile MOR reported as 4,000 psi. This data resulted from the testing of DF Glulam Combination 24F-V4

beams with 4, 8, and 10 laminations. Many of the tests resulted in much larger MOR values as well, with some strengths above 8,000 psi. Later, research conducted by Green and Kretschmann discussed testing performed by Littleford in 1967 [22-23]. The data from Littleford's testing showed mean strengths for dry 6-in. by 12-in. sawn DF timbers were roughly 1.31 times the 5th percentile strength. The mean MOR was reported as 7,542 psi, while the 5th percentile MOR was reported as 5,750 psi. Data from the same study with wet DF timbers showed mean strengths 1.25 times the 5th percentile strength. The mean MOR for the wet timbers was reported as 6,127 psi, while the 5th percentile MOR was reported as 4,890 psi.

MwRSF has also performed research on a timber railing attached to a noisewall barrier for use in the state of Minnesota. Under NCHRP Report 350 provisions, an original design for shielding the noisewall barrier was developed and published in 2005 [24]. A redevelopment and design modification effort was used to update the system under the MASH impact safety criteria in 2019 [25]. In the follow-on research, timber bending stresses were calculated based on the application of static design loads and compared to the bending stresses as calculated using the standard NDS procedures. It was shown that the DF glulam timber beam in the original system was estimated to be overstressed by 39.6 percent when comparing the bending stress from design loads to the bending stress calculated with the NDS. The railing system performed favorably in the crash testing program and was put into service for several years.

In the efforts to update the system to meet MASH criteria, the size of the beam was increased to account for the increased impact severity and overall loading. A new comparison of the stresses was performed, and calculations showed the beam was overstressed by 23.4 percent in relation to the new loads and capacities that were calculated. Again, although the calculation showed the beam would be overstressed, the system performed favorably in the crash testing program and was deemed acceptable under MASH.

Based on the data found in the research studies by Moody et al., Green and Kretschmann, and Littleford, it was determined that applying an additional strength increase factor of 1.33 would further increase design bending capacities from a 5th percentile capacity to a mean or 50th percentile capacity. The investigation regarding the structural performance of the glulam beam in previous NCHRP Report 350 2000P and MASH 2270P crash tests at MwRSF provided further confidence that using an increase factor of 1.33 was reasonable for determining realistic design bending capacities for use in the BARRIER VII computer simulation model.

During the initial model updating phase, another concern arose over the calculated shear capacities of the posts, as stated previously. The calculated shear capacity of an 8¾-in. wide by 10½-in. deep post from AASHTO LRFD and NDS was determined to be 40.6 k and 31.0 k, respectively. Thus, AASHTO is considered to be less conservative than NDS for the calculation of shear capacity. These capacities were compared to the capacity used in the original BARRIER VII model of 52.8 k, and are only 76.9 percent and 58.7 percent of the modeled value, respectively. A higher shear failure limit is often used within a BARRIER VII model in order to obtain yielding and plastic behavior in the posts and, therefore, better represent the actual behavior of a railing system. If the shear limit is set higher than the force required for post yielding, then deflection will control the failure of the posts, as seen in the first failure scenario in Figure 4. Within the BARRIER VII computer program, the shear limit of a post is typically used for posts that are specifically meant to fail due to shear behavior, as shown in the second failure scenario in Figure 4 [14].

For the NCHRP Report 350 TL-4 bridge railing system evaluated with the TRBR test series there was no shear failure of the posts, and the connection hardware was configured to withstand the impact loading. The posts were modeled with a shear capacity that allowed the railing system to deform with the vertical supports yielding. Thus, the posts were governed by either the bending capacity of the lower curb rail and scupper blocks attached to the deck or the shear capacity of the vertical bolts connecting the curb and scuppers to the deck. The post behavior was not likely controlled by the calculation-based shear capacity of the 8½-in. by 10½-in. glulam post. For this reason, the shear capacity of the posts was increased to 55.0 k for use in the updated BARRIER VII model, as shear loading was not expected to exceed this value. This change allowed for the failure mechanism of the posts to be based on deflection after yielding instead of fracture due to reaching the shear limit. The simulation efforts discussed later in this study also proved that the shear forces carried by the posts were lower than the specified shear limits.

2.3.2.3 Determination of Timber Post Stiffnesses and Failure Deflections

The last major BARRIER VII input parameters were the post stiffnesses and failure deflection criteria. In the past, there have been many different studies to determine the capacities and stiffnesses of timber posts. As found in the literature review, all static and dynamic component tests were performed on sawn timber posts. No component test data was found for laterally-loaded, cantilevered, glulam timber posts, which were utilized in the original NCHRP Report 350 TL-4 glulam timber rail with curb bridge railing system.

For post tests on sawn sections, the bottom end of each post was placed in a fixed base or a cantilevered condition, often by insertion into a steel sleeve installed underground [26-28]. These tests provided MOR data, shear capacities, stiffnesses to yield or fracture, and dynamic post behaviors in both the lateral and longitudinal directions. For situations where test results were unavailable, such as for changes with the post size and load application height, the elastic, flexural stiffness relationship for a cantilevered post has often been used to determine the cantilevered stiffness of an alternative post. It should be noted that this relationship assumes only elastic behavior, and after a post reaches yielding, the stiffness calculated with this method would no longer be valid. The flexural stiffness is shown in Equation 1, where k represents the flexural stiffness of the post, E is the modulus of elasticity of the material, I is the moment of inertia of the selected post size, and L is the cantilevered length of the post, as measured between the ground and the load application height.

$$k = \frac{3EI}{L^3} \qquad \text{(Eq.) 1}$$

After analyzing the data from the aforementioned component tests, it was determined to utilize data from a MwRSF study in collaboration with the Nebraska Department of Roads (NDOR) [26]. This study focused on the performance of several different grades of wood posts. An average stiffness was determined from the data, and Equation 1 was then utilized to determine the flexural stiffness along each axis of the posts that were used in the NCHRP Report No. 350 TL-4 bridge railing system. After implementing the results into the BARRIER VII model with all of the other timber properties updated, it was determined that the stiffnesses provided by this method of analysis were too high to represent the actual behavior of the posts when deflecting along the B-axis. Because these stiffnesses were based upon cantilevered posts and the system is actually a composite system of multiple connections and components that all act together, they

were not truly representative of the behavior of the bridge railing. The stiffness is much more dependent on the combination of the deck, curb rail, and scupper block system than simply on a cantilevered post setup. For that reason, the post stiffness was modeled along the B-axis based on the deflection behavior observed in full-scale crash testing and the calculated moment capacity of the post using AASHTO LRFD and NDS. In test no. TRBR-2, which was the 2000P pickup truck test performed on the bridge railing system, the maximum observed dynamic deflection was 8.0 in., with a permanent set deflection of approximately 1.0 in. [10-12]. Based on the yield moment of the post and these deflections, a force versus deflection curve was produced and implemented into the BARRIER VII model. In full-scale crash testing with the pickup truck, an 8.0 in. backward lateral deflection was observed without post failure. Thus, it was determined to allow 10.0 in. of lateral barrier deflection before allowing the simulated posts to fail via reaching the deflection limit. The posts' deflection along the A-axis was limited to 4.0 in., as it was decided that deflections larger than this may cause adverse effects in the overall performance of the complete bridge railing system.

2.3.3 Initial Calibrated Model Simulation Results

Calibration of the model was mostly focused on replicating the crash test results involving the 2000P pickup as there was much more information available for this test. Gathering data on deflections and the overall deflected shape of the barrier throughout the 8000S single-unit truck test was not possible due to the box of the vehicle rolling onto the barrier system, obstructing camera views.

With this information, each of the previous modifications and updates were implemented into the model and a simulation was performed with the 2000P vehicle impacting the barrier at the centerline of post no. 5. The simulation results sufficiently replicated what was observed in full-scale crash testing based on maximum deflections and overall deflected shape. The updated timber parameters for the rails and posts can be seen in Tables 7 and 8, respectively. Table 9 and Figure 6 compare the results from test no. TRBR-2 and the BARRIER VII simulation. In Figure 6, the deflected shape of the bridge railing at the time of maximum dynamic deflection as observed from the full-scale crash test and simulated test are shown by the red and blue lines, respectively. The simulated vehicle is shown in pink.

Table 7. Updated BARRIER VII Timber Rail Properties

Member Type	Member Size	Area (in.^{2})	Moment of Inertia (in.^{4})	Modulus of Elasticity (ksi)	Weight (lb/ft)	Nominal Tensile Yield Force (k)	Nominal Yield Moment (k-in.)
Upper Rail	8¾"x13½" (Glulam)	118.1	753.7	1,600	28.6	314.5	1,070.5
Curb Rail	6¾"x12" (Glulam)	81.0	972.0	1,500	19.3	135.4	668.5

Table 8. Updated BARRIER VII Timber Post Properties

Member Type	Member Size	Top Node Height (in.)	Bottom Node Height (in.)	Stiffness k_A & k_B (k/in.)	Weight (lb)	Nominal Yield Moment (k-in.)	Failure Shear Force (k)	Failure Deflection (in.)
Bridge Post	8¾"x10½" (Glulam)	18.0	0.25	A-axis: 7.2 B-axis: 30.6	67.6	A-axis: 907.2 B-axis: 833.1	A-axis: 55.0 B-axis: 55.0	A-axis: 4.0 B-axis: 10.0

Table 9. Test No. TRBR-2 and Initial Calibrated 2000P Simulation Comparison

Impact Case	Maximum Dynamic Deflection (in.)	Parallel Time (sec)	Parallel Velocity (mph)	Exit Time (sec)	Exit Velocity (mph)
Test No. TRBR-2	8.0	0.238	41.0	0.437	38.7
Simulated Test	8.6	0.226	37.1	0.360	35.9
% Error	+7.5	-5.0	-9.5	-17.6	-7.2

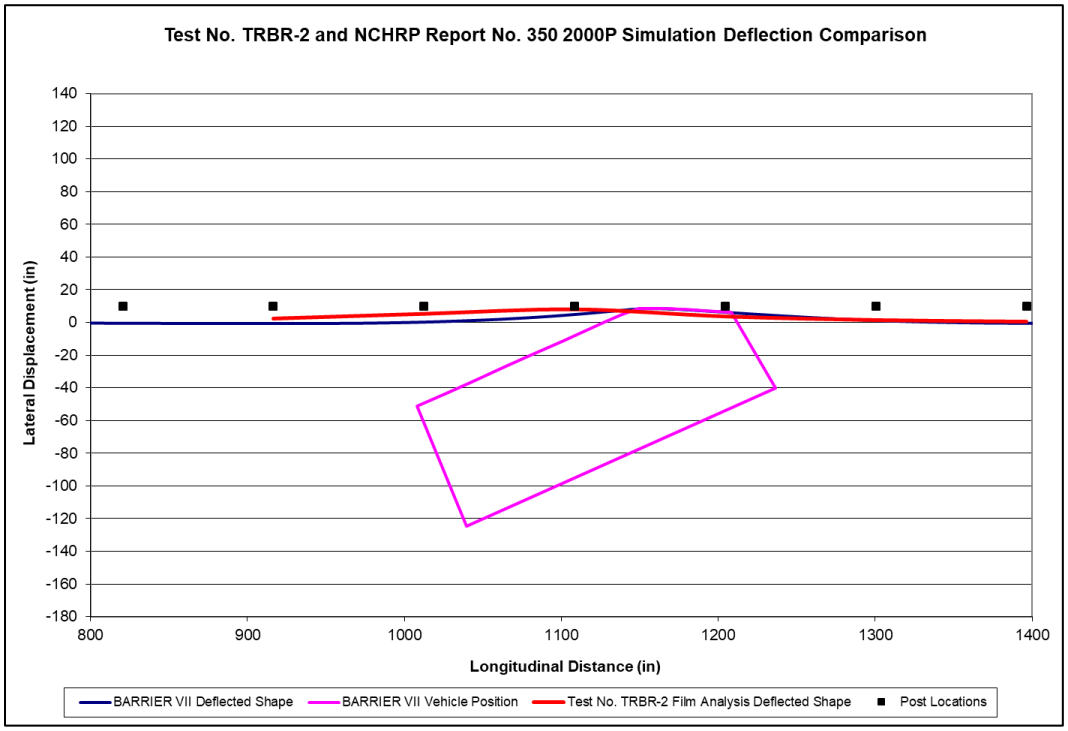

Figure 6. Test No. TRBR-2 and NCHRP Report 350 2000P Simulation Deflected Shape Comparison

A simulation was also conducted using the 8000S vehicle model impacting the barrier at midspan between post nos. 4 and 5. Table 10 shows a comparison of the results from test no. TRBR-1 and the BARRIER VII simulation, and Figure 7 shows the deflected shape of the barrier in simulation at the time of maximum dynamic deflection. Due to the lack of data regarding barrier deflections during the full-scale crash test, it is not possible to know the actual maximum dynamic deflection experienced by the system or to reasonably plot an overall deflected shape. It is believed that the maximum deflection was higher than the reported value, and thus, deflections observed in the simulation were expected to be larger as well. It should also be noted that during the full-scale crash test, the box of the vehicle rolled onto the barrier and remained in contact for an extended period of time as the vehicle continued to travel downstream. Because of this, the exit time from the crash test was reported as 1.522 seconds after impact. The BARRIER VII computer software cannot simulate this behavior as it is only a 2-D program. By not replicating the rolling behavior of the box, the exit times observed in the simulation are typically earlier in the event than what is observed in full-scale testing, as is the case for the comparison between the test no. TRBR-1 data and the 8000S simulation of the test.

After reviewing the data from these simulations on the updated model, it was determined that the model was calibrated reasonably well to the data from the full-scale crash tests. Thus, the research efforts could proceed into the next phase. With a calibrated model, the next step was to make component modifications.

Table 10. Test No. TRBR-1 and Initial Calibrated 8000S Simulation Comparison

Impact Case	**Maximum Dynamic Deflection (in.)**	**Parallel Time (sec)**	**Parallel Velocity (mph)**	**Exit Time (sec)**	**Exit Velocity (mph)**
Test No. TRBR-2	3.3	0.525	36.5	1.522	29.4
Simulated Test	6.9	0.390	35.1	0.675	34.5
% Error	**	-25.7%	+3.8%	**	**

** - Not calculated due to behaviors observed in full-scale crash testing, as previously discussed in this section.

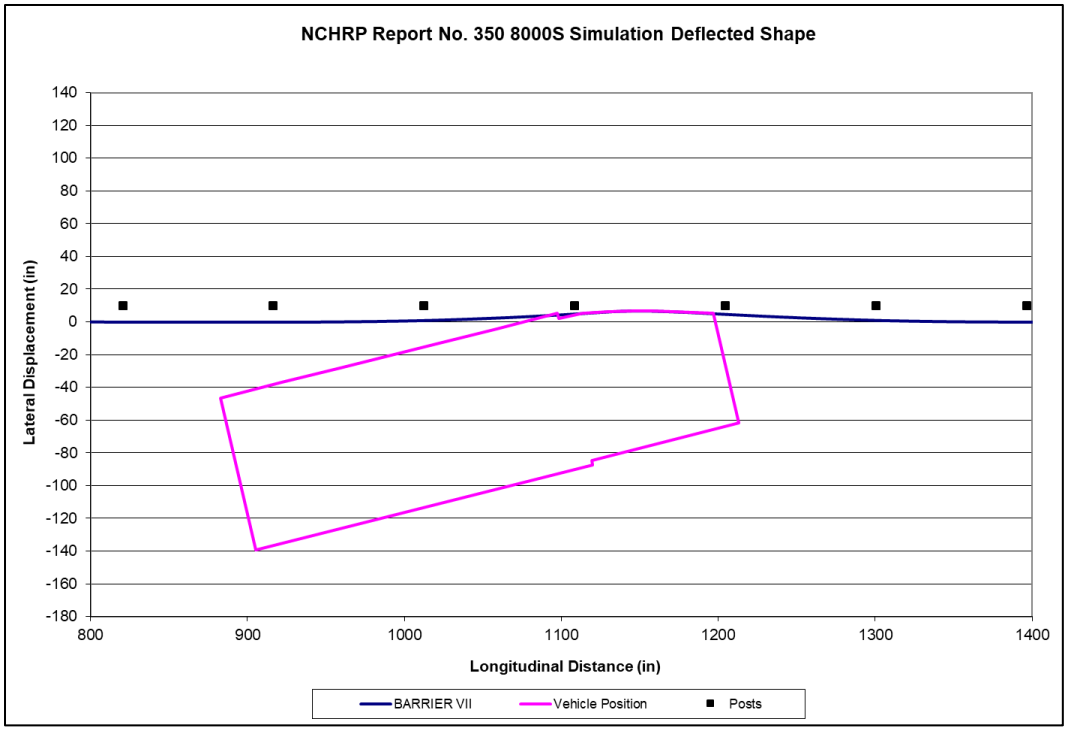

Figure 7. NCHRP Report 350 8000S Simulation Deflected Shape

2.4 Initial BARRIER VII Model Design Modifications for MASH TL-4 Bridge Railing System

2.4.1 MASH Vehicle Models

As previously noted, BARRIER VII vehicle models representing the NCHRP Report 350 2000P pickup truck and 8000S single-unit truck had previously been developed by MwRSF and calibrated to data obtained from researchers at TTI in the late 1980s [15]. A new model of the MASH 2270P pickup truck was also developed by researchers at MwRSF when updating impact safety guidelines from NCHRP Report 350 to MASH. This model used the original 2000P model as a baseline, and the vehicle weight, dimensions, and inertial properties were then modified to more closely represent modern pickup trucks. Based on these changes, along with other data gathered at the time, an updated rotational inertia for the vehicle was also estimated and implemented into the 2270P model.

Prior to this study, there had not been a model created to reflect the 10000S single-unit truck, as utilized for TL-4 testing under MASH. In line with this project's scope and approach, a 10000S vehicle model for use in BARRIER VII would be needed to obtain results and determine if updated versions of the TL-4 glulam bridge railing would be acceptable and ready for full-scale crash testing. A process similar to that followed in creating the 2270P model was performed to obtain a new single-unit truck model.

Creating a new model for the 10000S vehicle involved gathering data on three specific criteria: modern single-unit truck weights, dimensions, and rotational inertias. The vehicle weight

was determined based on information from MASH and a direct conversion of 10,000 kg to lb, resulting in a weight of 22,046 lb. Updating the vehicle's dimensions involved analyzing data from newer vintage single-unit trucks that have been used in crash tests from both TTI [29-31] and MwRSF [32-33], as well as current 10000S models used in LS-DYNA simulation. Based on the average and median dimensions of these vehicles, including the location of the c.g., a new geometric configuration was created for the vehicle. The weight supported by each axle was also examined from these tests, and wheel loads were redistributed within the model accordingly. The average, median, and modeled dimensions are shown in Table 11 and Figure 8. The geometric layout of the 10000S model is provided in Figure 9. The typical BARRIER VII input file for the 10000S vehicle model is shown in Appendix C.

Table 11. Average, Median, and Modeled 10000 Vehicle Dimensions

Value		Average (in.)	Median (in.)	Modeled (in.)
E	Wheel Base	206.4	206.0	206.0
M	Front track	80.1	80.0	80.0
AA	Rear Track	74.0	73.0	74.0
A	Front bumper width	94.4	95.0	94.0
T	Overall width	93.7	96.0	95.5
C	Overall length	323.0	330.5	320.0
V	Box Length	215.4	223.0	220.0
H	C.G. Horizontal Distance	129.4	131.7	130.0

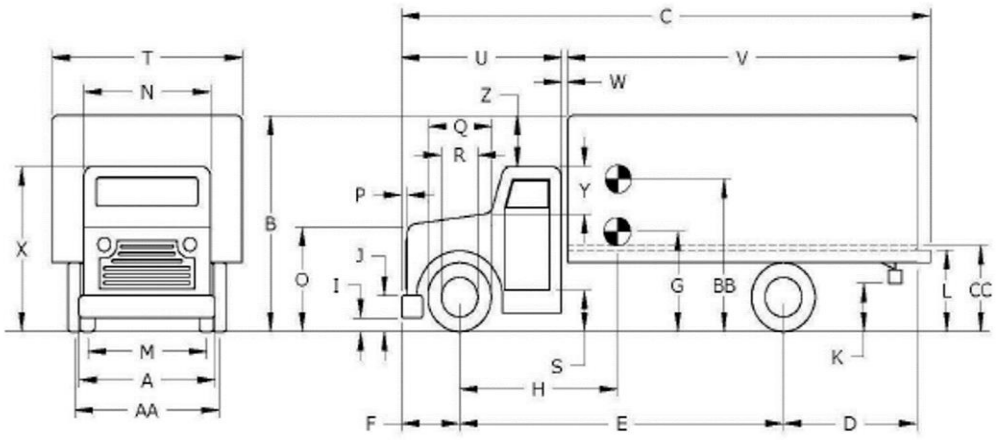

Figure 8. 10000S Vehicle Dimensions

The final information needed was rotational inertia for representative single-unit trucks. Sample values for the rotational inertia of this truck were found in a research study published by the University of Michigan Transportation Research Institute (UMTRI) in 1986 [34], as well as taken from the LS-DYNA single-unit truck model used by MwRSF. Both of these values were lower than the rotational inertia of the calibrated 8000S model, which should not be the case due

to the increase in mass and dimensions. The 8000S model utilized rotational inertia of 561,483.4 lb-in.-sec^2 in comparison to values between 315,000 and 480,000 lb-in.-sec2 for similar vehicles documented by UMTRI or 374,475.1 lb-in.-sec2 for the 10000S single-unit truck model in LS-DYNA.

Simulations with these values incorporated into the model also showed unexpected behaviors, displaying a need for a new method of determining the rotational inertia. An investigation showed that much of the information originally used to calibrate the 8000S model also came from the UMTRI report, but yet again, the rotational inertia of the 8000S vehicle model was set substantially higher than reported values [15]. This increase was incorporated in order to create an 8000S model that behaved in a similar manner to actual full-scale crash tests. For that reason, the modeled rotational inertia was increased, and a similar procedure was performed in order for the new 10000S model to be similarly accurate. The research team decided to scale the rotational inertia based on the increase in the weight when comparing the 8000S vehicle to the 10000S vehicle. The weight increased from 17,637 pounds to 22,046 pounds, corresponding to a 25 percent increase in weight, and therefore a 25 percent increase was applied to the rotational inertia of the modeled 8000S vehicle. Thus, the rotational inertia for the 8000S model was 561,483.4 lb-in.-sec^2, which was increased to 702,000.0 lb-in.-sec^2 for the 10000S model. Simulations with this value incorporated into the 10000S model on the calibrated bridge railing system showed vehicle behaviors similar to that observed for the 8000S model, but with larger forces and deflections, as would be anticipated. This increase led the team to conclude that the model was sufficient for use in conducting MASH simulations going forward.

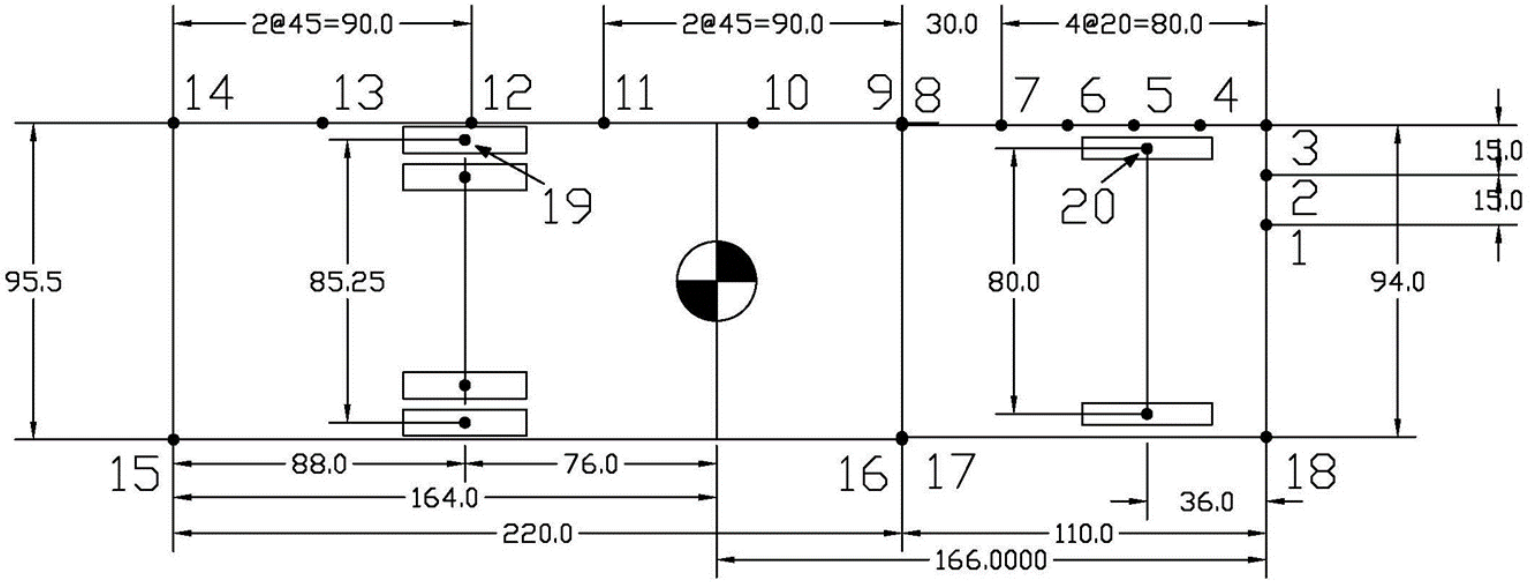

Figure 9. BARRIER VII 10000S Vehicle Model

2.4.2 MASH Simulations

With a barrier model that was calibrated and validated for the NCHRP Report 350 TL-4 bridge railing system and the TRBR crash tests, as well as vehicle models representative of the MASH 2270P and 10000S vehicles, efforts then began to update the bridge railing design to meet current MASH criteria. The first step in this process was to increase the overall height of the barrier. For a TL-4 system, a minimum height requirement of 36 in. was established based on successful single-unit truck crash testing performed on 36-in. tall barriers at TTI [35] and MwRSF [36-37]. For this research effort, it was necessary to account for an initial 2-in. thick overlay on top of the deck, as well as consider a second 2-in. thick overlay in the future. Thus, the top of the bridge railing needed to be increased to a height of 40 in. above the top of the bridge deck. This change would provide a 36-in. tall barrier in the future after both the initial wearing surface and future overlay were applied to the deck. This height increase was first incorporated into the model by simply increasing the height of the post while leaving all other components of the system the same. Several more iterations were also analyzed that included changes to the curb rail and scupper block sizes and their configurations, as well as where the reference height location was set. With each iteration, a new moment capacity and stiffness for the post were calculated and implemented into the model, and if the curb rail changed, the associated parameters were also changed.

After simulations were run with each iteration and results were reviewed by the research team, it was determined that the current process of making physical changes to the barrier system carried an extensive amount of uncertainty. This uncertainty was a product of the reference height that was originally chosen to model the previous system development. With each height increase or rail change, the point of rotation of the system would potentially change, which was believed to be the original basis of the reference height. It was thought that by changing the height of the reference location in the model, the new model would no longer correlate with the model that was calibrated to previous crash testing. It was also realized that with the curb rail only being modeled ¼ in. above the reference height and not being contacted by the vehicle, it did not play a large role in the behavior of the model. The force levels and moments experienced by the curb rail in the simulation were very minimal. This finding is not believed to be accurate when the full-scale bridge railing system was implemented in testing, as it is believed that the curb rail provides stiffness to the system and helps to distribute the load away from the impact point, especially into the deck. For these reasons, it was decided to return to the original model and reevaluate behaviors and parameters as observed in the full-scale crash testing program to determine a modeling scheme more representative of the system and capable of reflecting layout and design changes going forward.

2.5 Final BARRIER VII Model Calibration

2.5.1 Reference Height and Post Modeling Modifications

Following the determination that the initial model calibration effort resulted in excessive uncertainty when trying to update the bridge railing system to meet MASH criteria, new methods of modeling were examined. A modeling scheme was desired that would allow for geometric and material property changes to be applied consistently and uniformly for each design iteration. One logical approach was to model the bridge railing system as similarly as possible to the actual physical layout. This approach eventually utilized a reference height located at the top of the bridge

deck. This point would no longer be based on the behavior of the system, but would instead be based on the physical layout of the system. Again, using this location allowed for changes to be applied in a more controlled and uniform manner. Each rail was modeled at the midheight of the rail, and when parameters changed, the model would also change to match the components as they would physically be constructed.

The first step in the process of transforming the model using a reference height located at the top of the deck was to modify the heights for the upper and curb rails attached to the posts. With this change, the next step was to determine the stiffnesses of the modeled posts. As stated previously, the posts, rails, scuppers, and deck all act together to provide a combined system stiffness, which makes it difficult to quantify. Each component and connection involved in the railing system was examined, and an analysis was performed of the deflection behavior and final deformations of the original system during crash testing. It was determined that much of the post stiffness was a result of the curb rail, scupper block, and deck components, as they were directly connected to one another. Moving the reference height to the top of the deck was critical to this realization and the modeling going forward, as the model could utilize the strength of the curb rail more effectively by fully incorporating it into the system and allowing it to help transfer load.

With the curb rail and scupper components being a critical part of the posts' strength and stiffness, the research team utilized its experience with another prior railing system that was developed in 2009. In collaboration with the West Virginia Department of Transportation (WVDOT), MwRSF developed a MASH TL-1 crashworthy, low-height, curb-type glulam bridge railing for use on transverse, nail-laminated decks [5-6]. The system comprised an SYP Glulam Combination No. 48 curb rail that was placed on top of two Grade No. 1 SYP sawn timber scupper blocks. The railing system was connected to the bridge deck using four ¾-in. diameter ASTM A307 Grade A timber bolts, which was similar to the manner in which the curb and scupper components used for the TL-4 glulam timber rail with curb system were connected to the bridge deck. Details of this system can be found in the reference report [8], and a side-view schematic and images of the system are shown in Figures 10 and 11.

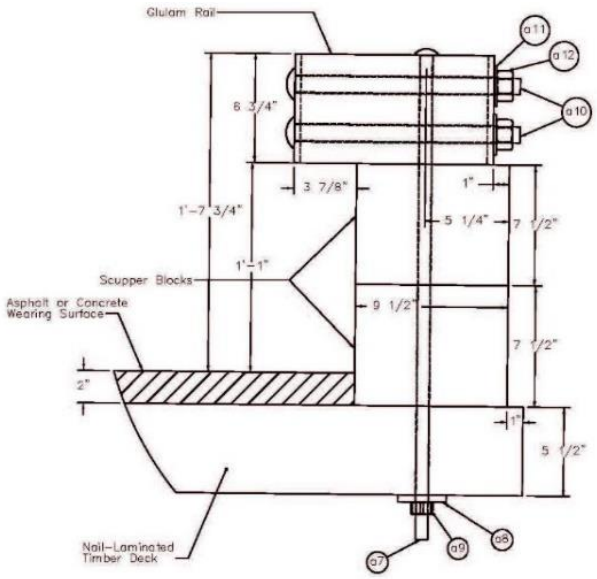

Figure 10. Schematic of Low-Height, Curb-Type, Glulam Bridge Railing [5-6]

Figure 11. Low-Height, Curb-Type, Glulam Bridge Railing [5-6]

As part of the development of this system, a series of static component tests were conducted. The purpose of these tests was to determine the capacities of the curb rail and scupper block system when different combinations of bolts, shear plates, and split rings were placed at the interfaces between the timber rail, timber scupper blocks, and timber deck. The testing setup, shown in Figure 12, consisted of a hydraulic ram attached to the back of a curb rail and scupper block system. The ram pulled the system backward, and the force and deflection levels were recorded using a load cell and string potentiometer, respectively. Force versus deflection plots were created and presented as part of the research on this system, showing that each hardware combination performed similarly. The test results are graphically depicted in Figure 13 [5-6]. Test nos. WVS-1 and WVS-4 utilized only bolts to connect the curb and scupper system to the deck. Test no. WVS-2 utilized bolts and split rings at each timber interface, and test no. WVS-3 utilized bolts and shear plates at each timber interface. Test no. WVS-5 utilized bolts and split rings only at the interface between the bottom scupper and the deck. The similarity in behavior and observation of extra damage to the deck when shear plates or split rings were utilized led the research team to detail the full-scale bridge railing system with only the timber bolts as connection hardware. Because of the similarities between the WVDOT curb-type system and the curb and scupper portion of the TL-4 system, the data from these static component tests served as the starting point in determining the stiffness of the combined post system incorporated into the TL-4 glulam timber rail with curb bridge railing system.

When analyzing the force versus deflection plots related to the TL-1 curb rail system, it was evident that a bilinear behavior existed before reaching a plastic behavior and failure. The first stiffness occurred from 0 in. of deflection up to roughly 2¾ in. of deflection. The second stiffness of the system occurred from 2¾ in. of deflection through roughly 15 in. of deflection. After 15 in. of deflection, the system seemed to behave in a plastic manner with force versus deflection curves leveling off.

Figure 12. WVDOT Static Testing Setup [5-6]

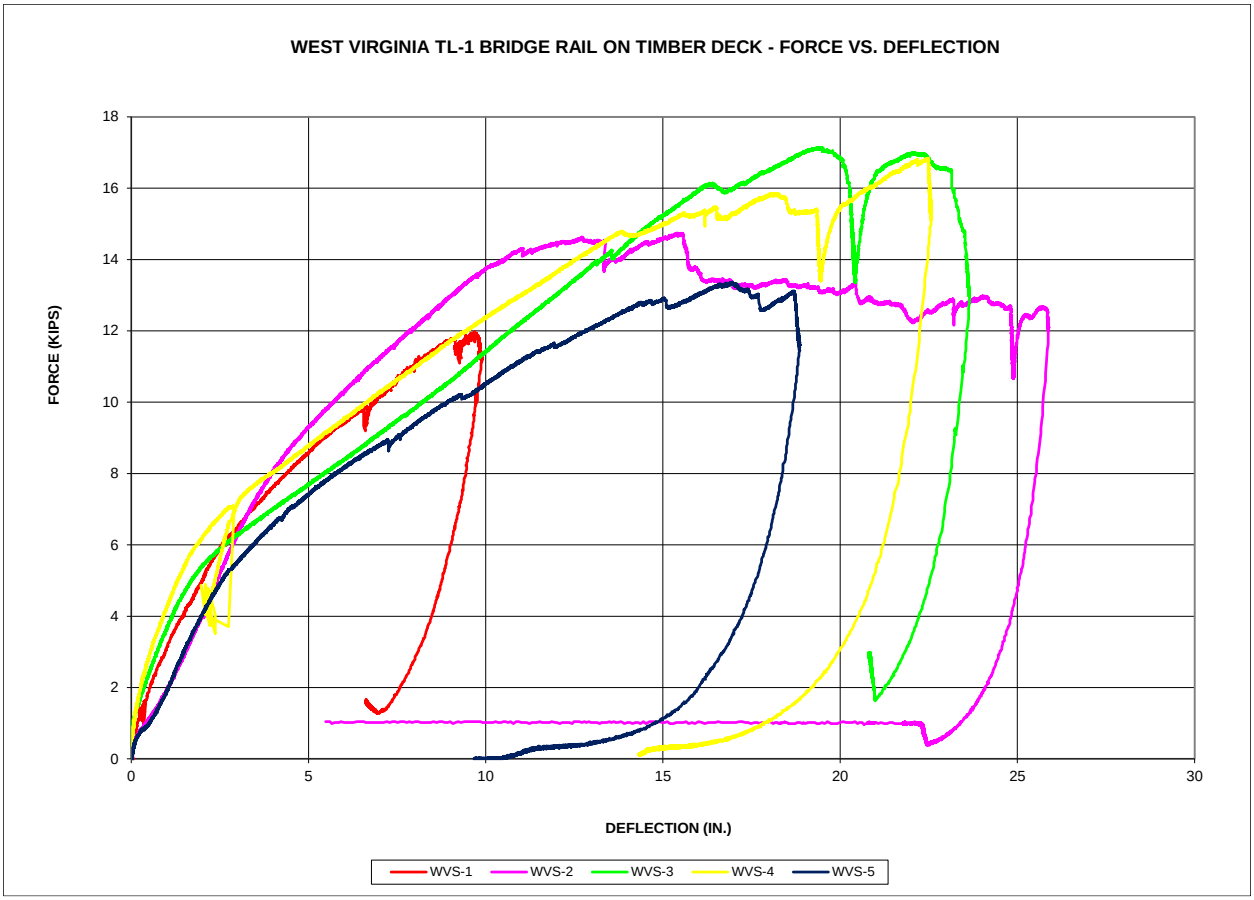

Figure 13. Force vs. Deflection for WVDOT TL-1 Static Testing [5-6]

In the past, posts have typically been modeled in BARRIER VII with a single post element at each post location that behaved in an elastic, perfectly-plastic manner. However, it is possible to model two post elements at each post location in order to obtain a composite, bilinear stiffness behavior, as shown in Figure 14. The first post at each location was given an elastic, perfectly-plastic, force versus deflection behavior with stiffness k_1, while the second post at each location was given a different elastic, perfectly-plastic, force versus deflection behavior with stiffness k_2, which was less than stiffness k_1. The deflection at which the second post yielded was also larger than the yield deflection of the first post type. With both post types located at each post location, the two posts acted in parallel, creating an initial stiffness, k_3, which is the sum of k_1 and k_2. When the deflection of the composite post system reaches the yield deflection of the first post type, δ_1, the overall stiffness becomes the stiffness of the second post type only, k_2, for deflections between δ_1 and δ_2. This behavior occurs because the first post type no longer applies any additional resistance, even as deflections increase. After further deflection, the second post type reaches yielding at δ_2, and the stiffness of the combined post at that location then becomes 0 k/in. Eventually, the composite post reaches a deflection at which both posts are set to fail, and at this point, the post is removed from the BARRIER VII model by distributing the forces that were carried by the post into the rest of the system over the next 10 time steps equally [14].

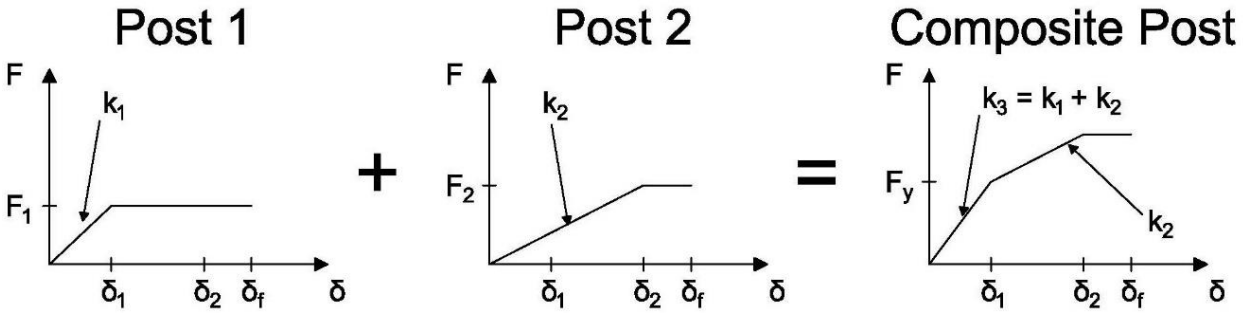

Figure 14. BARRIER VII Dual Post Superposition Behavior for Stiffness Model

The composite post modeling scheme was utilized for the TL-4 timber rail with curb system in order to replicate the general stiffness behavior observed by the TL-1 curb rail and scupper system. To ensure this modeling scheme produced accurate results when implemented into BARRIER VII, simulations were conducted using a model with a single post at each location that contained equivalent energy dissipation before failure. The simulation results with each modeling scheme proved to provide nearly equivalent results in terms of maximum deflections and deflected shape. Thus, the composite post modeling scheme was utilized going forward.

Beginning with a bilinear stiffness model fit to the data from the TL-1 static testing program, a series of equations was then used to modify the curve to represent the combined post system modeled for the TL-4 system. The model for the TL-1 force versus deflection behavior was overlaid with the static test results in Figure 15. Note that the final plastic behavior occurred after approximately 15 in. of deflection. The TL-1 stiffness model was created to only be bilinear and not the plastic behavior beyond 15 in. since the BARRIER VII model was configured to incorporate post failure due to a deflection limit being reached before deflections of 15 in.

The TL-1 static testing was performed on a transverse, nail-laminated timber deck that was 5½ in. thick with a 4-ft 2-in. wide overhang, as measured from the centerline of the exterior girder.

The scuppers were fabricated with 8-in. by 10-in. SYP Grade No. 1 sawn timber, and the curb rail was a 6¾-in. tall by 12⅜-in. deep SYP Combination No. 48 glulam beam, each of which were 23 in. long. Impact height was taken as the midheight of the curb rail, located 18⅜ in. above the top of the deck. The curb rail and scuppers were connected to the deck using four ¾-in. diameter ASTM A307 timber bolts. A new stiffness model for the TL-4 system was determined based on using (1) an increased impact height located at the midheight of the upper rail, 28¼ in. above the top of the deck, (2) scupper blocks and a curb rail that were 6¾ in. tall by 12 in. deep with the scupper blocks being 54 in. long, and (3) a transverse, glulam timber deck that was 5⅛ in. thick with a 2-ft wide overhang. The scupper blocks and curb rail were attached to the deck using six ¾-in. diameter ASTM A307 timber bolts for the TL-4 system.

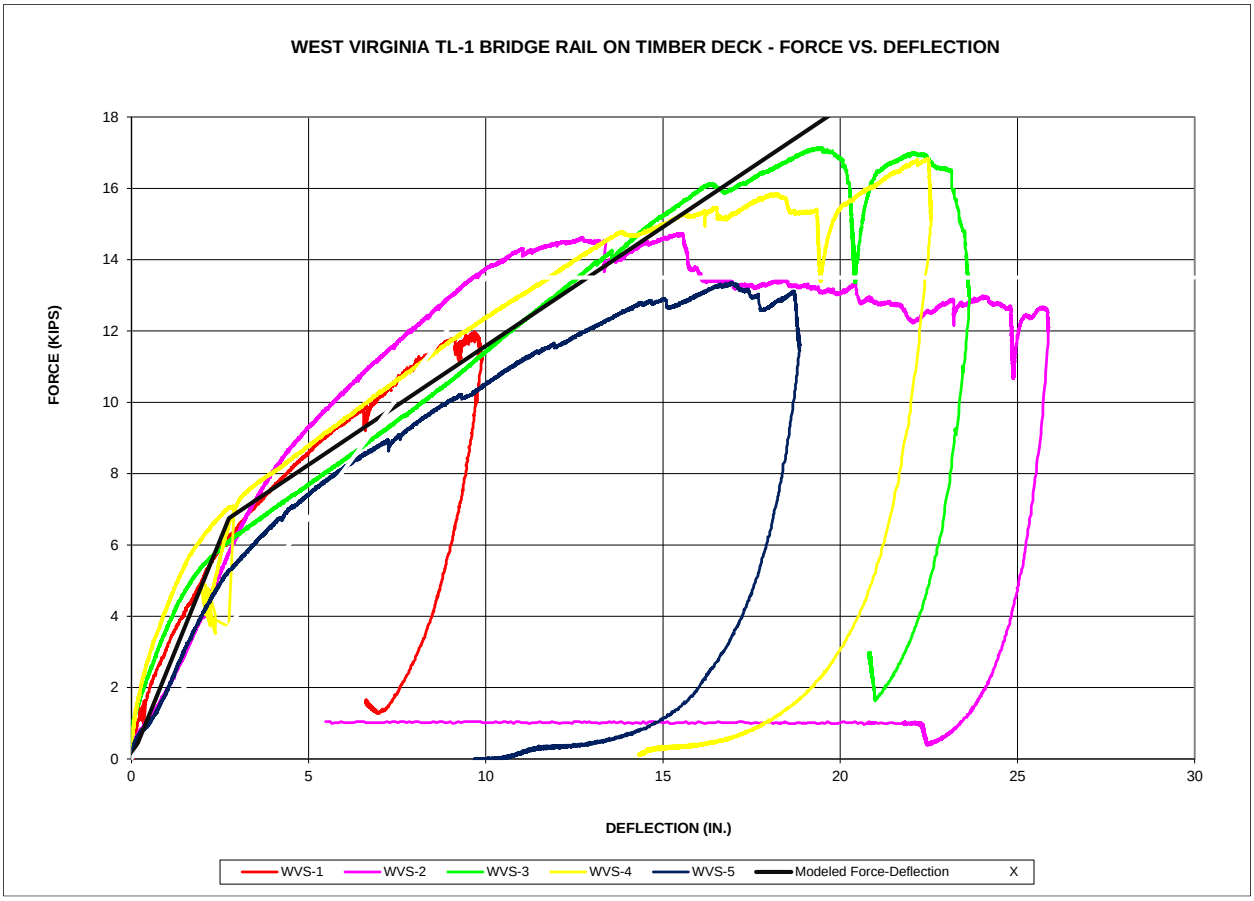

Figure 15. TL-1 Stiffness Model with WVDOT TL-1 Static Testing Results

For each difference between the TL-1 system used in static testing and the TL-4 system that needed to be modeled, a standardized modification was performed to the force-deflection plot in a step-by-step process. These differences include a change in load application height, a change in curb and scupper layout and configuration, and a change in the deck configuration. The data from the modeled TL-1 stiffness was implemented into the following equations and the final results represented the stiffness input into the BARRIER VII model.

2.5.1.1 Load Application Height Modifications

For changes in load application height, two modification equations were applied to determine an updated force versus deflection behavior, and thus, an updated post stiffness. The first equation, Eq. 2, was used to change the deflections at which the post yields and was determined by examining a post when the rotation angle of the post is held constant with corresponding the height changes. The second equation, Eq. 3, was used to change the force required to yield the post and was determined by assuming that the applied moment remains the same in order to yield but the load application height changes. These relations can be visualized for a post or curb and scupper system in Figure 16, and the equations are as follows, where H_n is the height of load application, δ_n is the deflection of the post at height H_n under a particular rotation of the post, and F_n is the force applied to create a particular moment. Performing these transformations for a load application height increase from 18⅜ in. to 28¼ in. resulted in the force versus deflection relationships detailed in Tables 12 and 13. The data from Tables 12 and 13 are plotted as the black and green lines, respectively, to show the change in behavior in Figure 17.

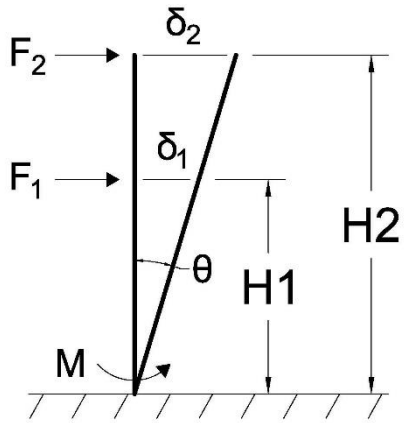

Figure 16. Visual of Forces and Deflections for Stiffness Calculations

$$\frac{\delta_1}{H_1} = \frac{\delta_2}{H_2} \quad \rightarrow \quad \delta_2 = \delta_1 \frac{H_2}{H_1} \qquad \text{Eq. 2}$$

$$F_1 H_1 = F_2 H_2 \quad \rightarrow \quad F_2 = F_1 \frac{H_1}{H_2} \qquad \text{Eq. 3}$$

Table 12. Initial TL-1 Modeled Post Stiffness Data

Deflection (in.)	Force (k)	Total Stiffness (k/in.)
0.00	0.00	-
2.75	6.75	2.45
20.00	18.25	0.67

Table 13. Post Stiffness Data – Modified for Load Application Height Change from 18⅜ in. to 28¼ in.

Deflection (in.)	Force (k)	Total Stiffness (k/in.)
0.00	0.00	-
4.23	4.39	1.04
30.75	11.87	0.28

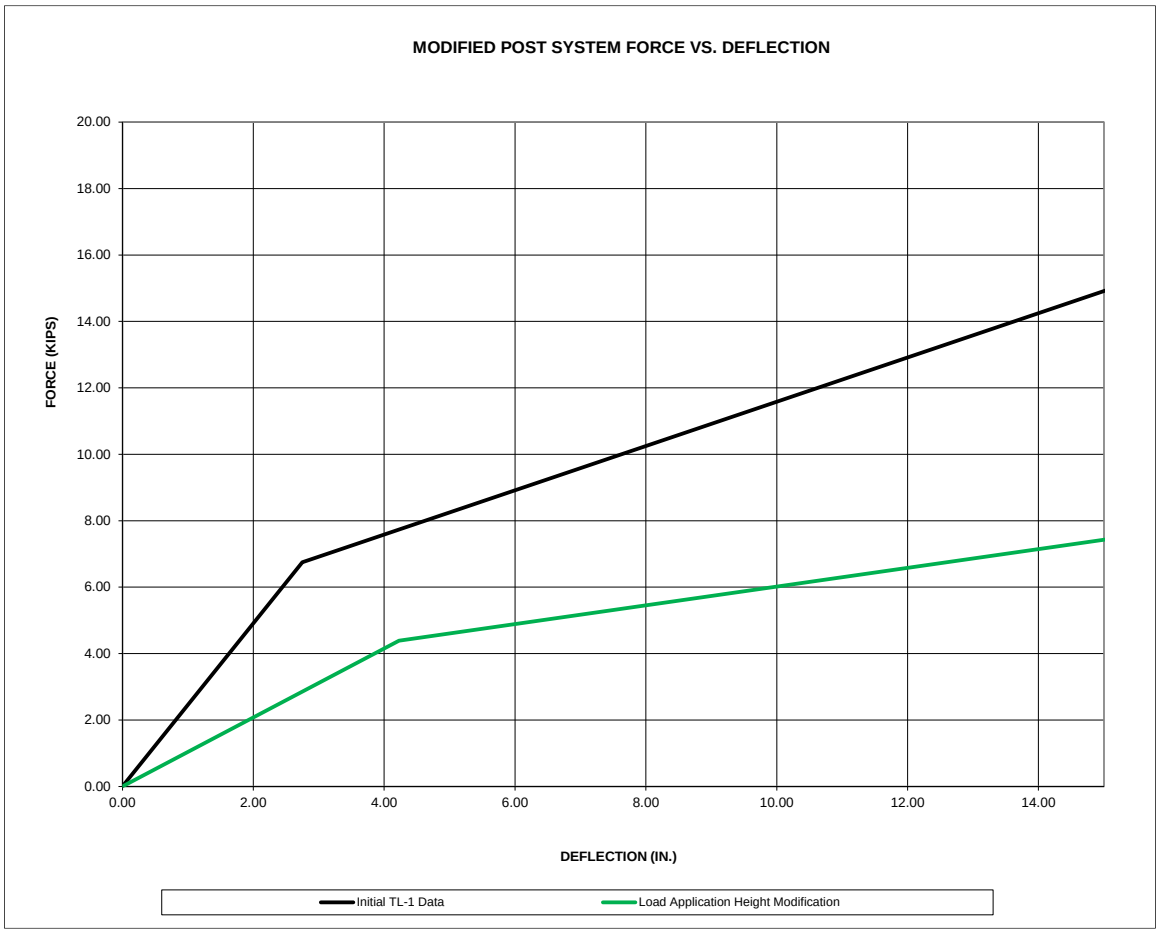

Figure 17. Force vs. Deflection - Initial TL-1 Data to Modifications for Load Application Height Change from 18⅜ in. to 28¼ in.

2.5.1.2 Curb and Scupper Strength Modifications

For changes in the curb rail and scupper block layout, a single modification equation was applied to determine an updated force versus deflection behavior, and thus, an updated post stiffness. Equation 5 modifies the force required to yield the post system and was determined by examining the moment capacity of the curb and scupper layout. As the components of the curb and scupper system became larger, the moment capacity and flexural stiffness of the overall system increased accordingly. The equation used to modify the force required for yielding of the post is

as follows, where *H* is the load application height, F_n is the force at which the post yields, and M_n is the moment capacity of the scupper and curb layout.

$$F_1H = M_1 \; and \; F_2H = M_2 \quad \rightarrow \quad \frac{F_1}{M_1} = \frac{F_2}{M_2} \qquad \text{Eq. 4}$$

$$\frac{F_1}{M_1} = \frac{F_2}{M_2} \quad \rightarrow \quad F_2 = F_1\frac{M_2}{M_1} \qquad \text{Eq. 5}$$

The behavior of a curb rail and scupper block system was investigated to determine a reasonable means to calculate the moment capacity of the layout. The bolted timber rail and scupper system behaves as a post with cantilevered end conditions. In testing, as a lateral force was applied to the structure, the curb rail and scupper blocks deflected backward, and eventually the front of the lower scupper block lost contact with the deck surface due to wood crush and bending of the vertical connecting bolts. The deformation of the scupper and bolts as a result of static test no. WVS-1 is shown in Figure 18. The scupper blocks and curb rail remained planar relative to each other and deflected backward, as can be seen in Figure 19. It was evident from this behavior that crushing of the wood on the back side of the scupper and extension of the connection bolts were critical behaviors and must be considered for calculation of the moment capacity for this type of combined post system. This capacity was dependent upon the scupper's strength in compression perpendicular to grain and the tensile strength of the connecting bolts. It should also be noted, that depending on the type of timber used for the scupper blocks and the deck, the compressive strength of the weaker material will govern the timber crushing behavior.

Through the review of the data, it was realized that this behavior was similar to a reinforced-concrete beam subjected to bending, in which the concrete carries the compressive load, and the steel reinforcement carries the tensile load. For this case, the wood carries the compressive load and the steel bolts carry the tensile load. After observing this behavior, it was determined that typical equations for calculating the moment capacity of a reinforced concrete beam should be investigated for use with a timber curb rail and scupper block system.

Figure 18. Test No. WVS-1 Scupper Block and Bolt Deformation [5-6]

Figure 19. Deflected State in Static Test No. WVS-4 on WVDOT TL-1 Low-Height, Curb-Type, Glulam Bridge Railing [5-6]

Through investigation and analysis, it was determined that the compressive stress versus strain relationships for concrete and timber are relatively similar. However, the compressive strength perpendicular to the grain for timber is significantly less than the compressive strength of typical concrete. The typical stress versus strain curves for concrete and timber are shown in Figures 20 and 21, respectively. Because of this similar behavior, it was deemed appropriate to utilize the equations typically used to determine the moment capacity of a reinforced concrete beam to determine the moment capacity of a timber scupper and curb system, as used in the TL-1 and TL-4 bridge railing systems. After review, the Whitney Stress Block Theory was used to determine these bending capacities, which assumes a uniform compressive stress that is equal to 85 percent of the compressive strength of the material that spans a percentage of the compression zone [38]. This relationship is shown in Figure 22, where d is the distance between the tension reinforcement and the extreme compressive fiber, c is the distance from the extreme compressive fiber to the neutral axis, a is a percentage of the distance from the extreme compressive fiber, β_1 is a factor that is dependent upon the compressive strength of the material, and f'_c is the compressive strength of the material. A value of 0.85 is used for β_1 when analyzing concrete that has a compressive strength less than or equal to 4,000 psi. Almost all timber, and specifically DF and SYP, will have a compressive strength perpendicular to grain that is much less than this value, so the β_1 value was taken as 0.85 for all calculations, meaning that the equivalent stress block spanned 85 percent of the distance from the extreme compressive fiber in the timber to the neutral axis.

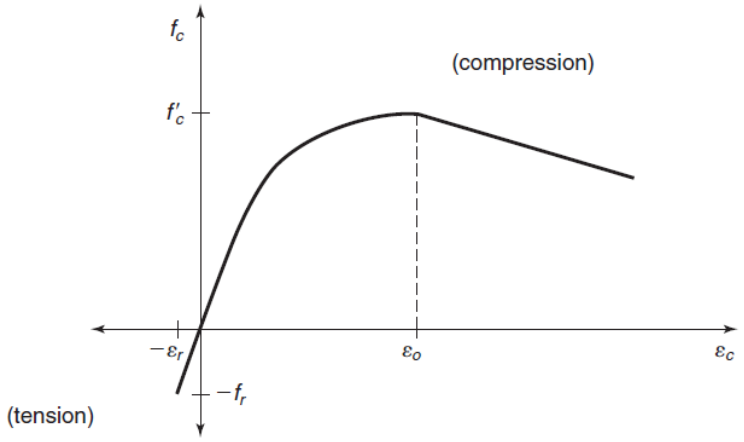

Figure 20. Typical Stress-Strain Curve for Concrete [38]

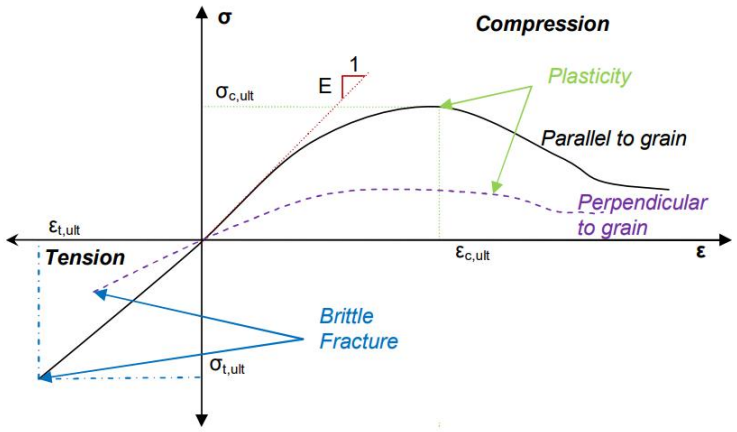

Figure 21. Typical Stress-Strain Curve for Timber [39]

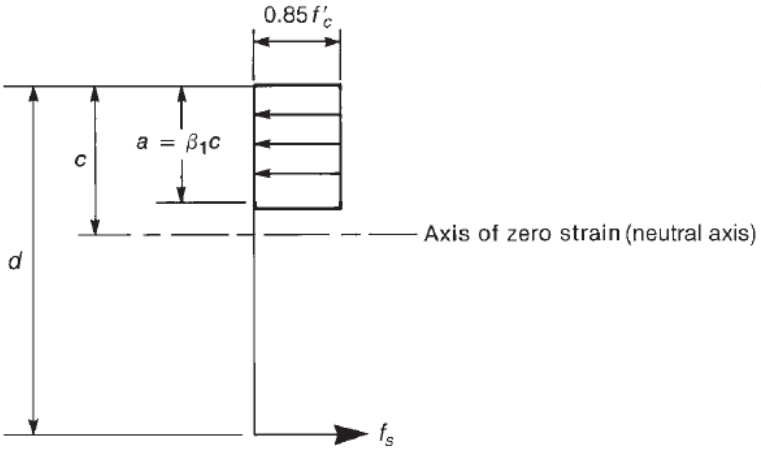

Figure 22. Whitney Stress Block [38]

With this information, one can then assume the tensile (*T*) and compressive (*C*) forces to be equal and work through Equations 6 through 10 to determine moment capacity, where f'_c is replaced by the compressive strength of the timber perpendicular to grain, *b* is the length of the scupper, *a* is the length of the equivalent stress block, A_s is the area of the steel bolts used in the connection, f_y is the tensile strength of the bolts, M_n is the nominal moment capacity of the scupper and curb system, and *d* is the distance between the bolts and the extreme compressive fiber in the timber. Also, based on research into ASTM A307 Grade A bolts, as are used for this connection, the material has no defined yield strength. Specifications only provide a nominal tensile strength for the material of 60 ksi [40]. In some designs, a yield strength of 45 ksi has been utilized, but this selection has been believed to be very conservative for yielding in ASTM A307 bolts [41]. Based on observations in the TL-1 static testing program and historically published information, the concern for rupture of the bolts was minimal due to the amount of deformation observed without any failure. As a result, calculations were performed using two yield strengths – 60 ksi and 45 ksi – to bracket the capacity in the simulation effort. Both yield strength values provided conservative simulations and in an effort to be aggressive in the design of the curb and scupper system, the minimum tensile strength of the bolts, 60 ksi, was utilized for f_y in place of a tensile yield strength going forward. The equations utilized are as follows:

$$C = T \qquad \text{Eq. 6}$$

$$0.85 f'_c b a = A_s f_y \qquad \text{Eq. 7}$$

$$a = \frac{A_s f_y}{0.85 f'_c b} \qquad \text{Eq. 8}$$

$$M_n = A_s f_y \left(d - \frac{a}{2}\right) \qquad \text{Eq. 9}$$

$$M_r = \varphi M_n, where\ \varphi = 1.0\ for\ impact\ loading \qquad \text{Eq. 10}$$

The moment capacities calculated using this method, M_r, were then implemented into Equation 4, as previously presented, to determine the change in force versus deflection behavior that accompanied changes in the curb and scupper layout. The moment capacity of the TL-1 and TL-4 combined curb, scupper, and bolt systems were calculated as 191.5 k-in. and 720.0 k-in., respectively.

Starting with the data from Table 13, performing these transformations for the change in the curb and scupper systems resulted in the force versus deflection relationship detailed in Table 14. The data from Tables 12 through 14 are plotted to show the change in behavior in Figure 23. The blue line represents the data in Table 14, the force versus deflection behavior of a post system as modified to incorporate the size change of the curb rail and scupper block components. It is evident that this change in the curb and scupper components increased the overall stiffness of the combined post system, as expected.

Table 14. Post Stiffness Data – Modified for Curb and Scupper Changes

Deflection (in.)	Force (k)	Total Stiffness (k/in.)
0.00	0.00	-
4.23	16.51	3.90
30.75	44.63	1.06

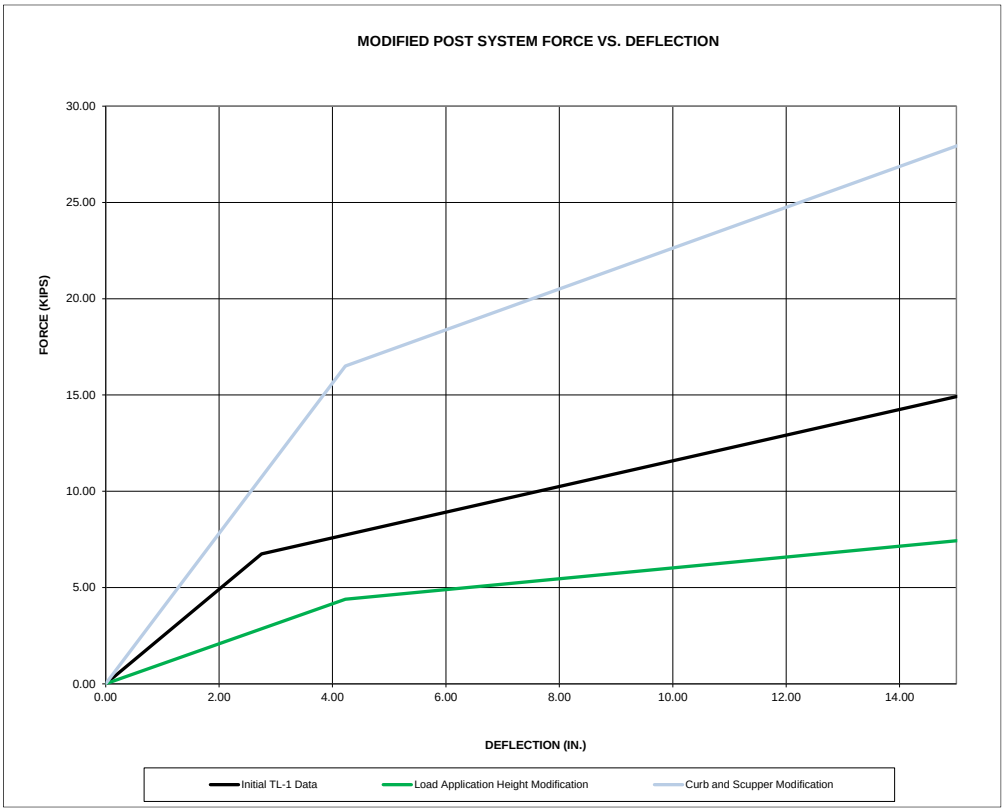

Figure 23. Force vs. Deflection - Initial TL-1 Data to Modifications for Curb and Scupper Changes

2.5.1.3 Deck Configuration Modifications

The last modifications to the stiffness model for the TL-4 combined post system were the result of the differences in the decks, including different timber types, thickness, and overhang length. These modifications assume small angles of rotation, θ, and a rigid post member in order to only account for deck changes in this step. The angle of rotation of the deck can be calculated using Equation 11 by assuming the deck is a cantilevered beam loaded by a moment that is the result of the lateral load, F, applied at a height, H, to the post. Equation 12 was then derived from Equation 11, and ratios using this equation determined Equation 13. The first modification equation, Equation 13, was applied to modify the deflections at which the posts yield and was determined based upon applying the same moment to the system. The second modification equation, Equation 14, was used to change the forces at which the posts will yield and was determined based upon subjecting the deck to the same amount of rotation. These equations are as

follows, where θ is the rotation angle of the deck, M is the moment applied to the deck as a result of the force F applied at a height H on the barrier, L is the length of the overhang, E is the elastic modulus of the timber deck, I is the moment of inertia of the deck based on loading width and deck thickness, and δ is the deflection of the posts at height H. Each of the variables can be seen in relation to the post and deck in Figure 24, and values for E, I, and L relating to each deck type are provided in Table 15.

$$\theta = \frac{ML}{EI} = \frac{FHL}{EI} = \frac{\delta}{H} \quad \text{Eq. 11}$$

$$\delta = \frac{FH^2L}{EI} \quad \text{Eq. 12}$$

$$\frac{\delta_1}{\frac{FH^2L_1}{E_1I_1}} = \frac{\delta_2}{\frac{FH^2L_2}{E_2I_2}} \quad \rightarrow \quad \delta_2 = \delta_1 \frac{L_2E_1I_1}{L_1E_2I_2} \quad \text{Eq. 13}$$

$$\theta_1 = \theta_2 \quad \rightarrow \quad \frac{F_1HL_1}{E_1I_1} = \frac{F_2HL_2}{E_2I_2} \quad \rightarrow \quad F_2 = F_1 \frac{L_1E_2I_2}{L_2E_1I_1} \quad \text{Eq. 14}$$

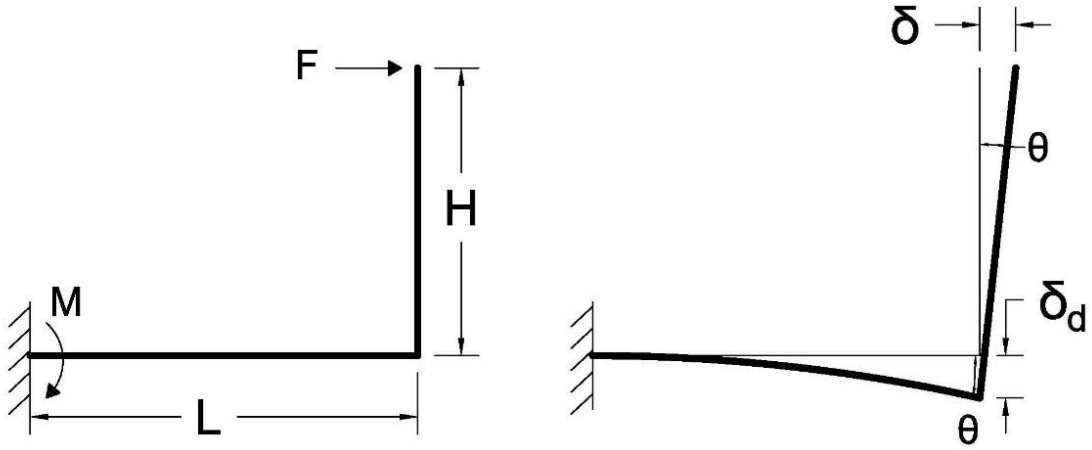

Figure 24. Timber Deck Behavior Due to Lateral Post Loading

Table 15. Timber Deck Properties

Deck Type	Modulus of Elasticity, E (ksi)	Moment of Inertia, I, (in.^{4})	Overhang Length, L (in.)
Transverse, Nail-Laminated	1,500	998.25	50.0
Transverse, Glulam	1,600	1,076.9	24.0

Starting with the data from Table 14, performing these transformations based upon the deck changes resulted in the force versus deflection relationship detailed in Table 16. The data from Tables 12 through 14 and Table 16 are plotted to show the change in behavior in Figure 25.

The red line represents the data in Table 16, the force versus deflection behavior of a post system as modified to incorporate changes in the deck. The transformation included a change in the overhang length from 4 ft – 2 in. to 2 ft, a change in deck material from Grade No. 1 SYP dimensional lumber to DF Glulam Combination No. 2 deck panels, and a change in deck thickness from 5½ in. to 5⅛ in. The dashed maroon line represents the post's force versus deflection behavior after being capped by the force causing yielding of the curb and scupper system, as further discussed in the next section.

Table 16. Post Stiffness Data – Modified for Deck Changes from Transverse, Nail-Laminated Timber Deck to Transverse, Glulam Timber Deck

Deflection (in.)	Force (k)	Total Stiffness (k/in.)
0.00	0.00	-
1.76	39.57	22.44
12.83	106.99	6.09

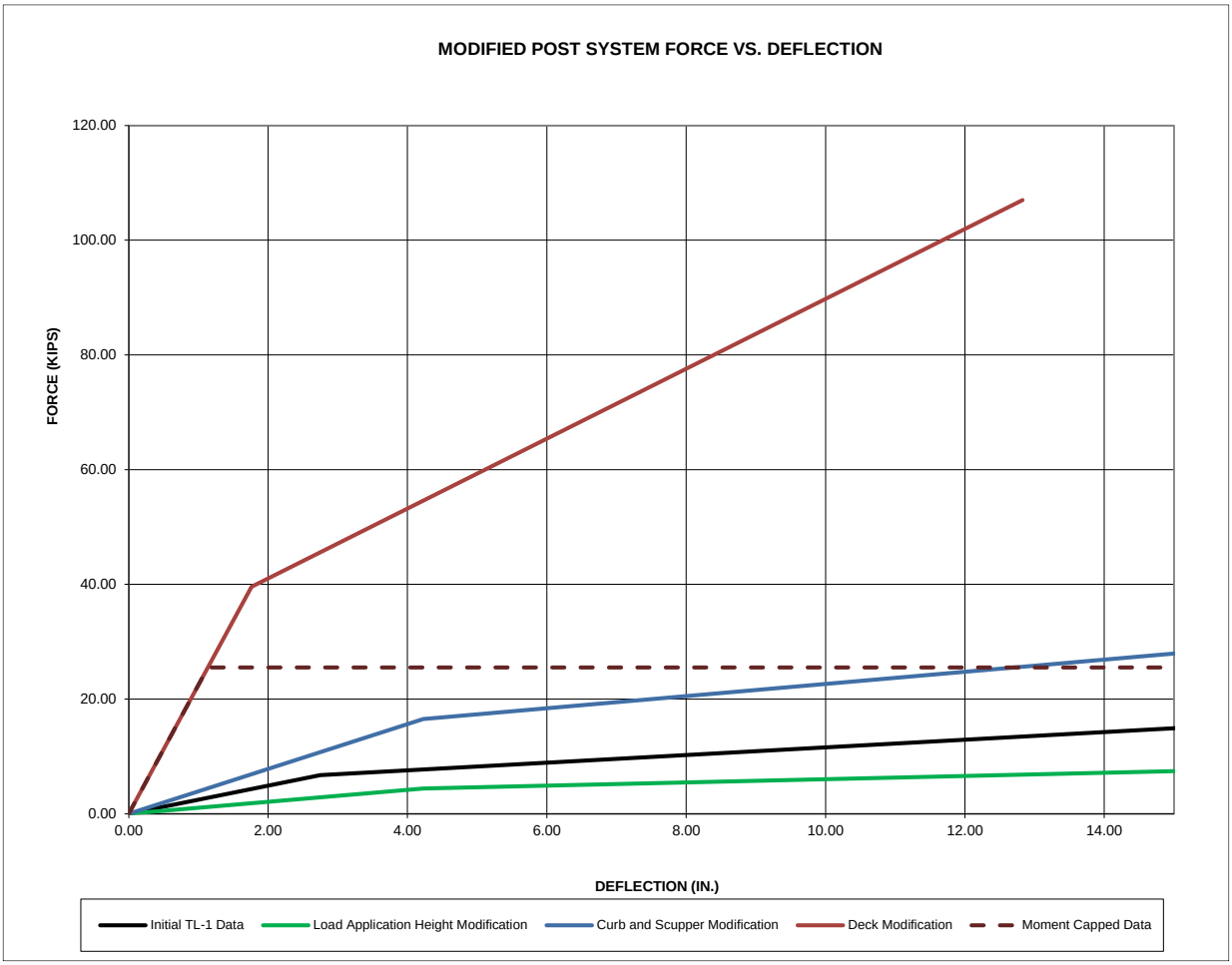

Figure 25. Force vs. Deflection - Initial TL-1 Data to Modifications for Deck Changes from Transverse, Nail-Laminated Timber Deck to Transverse, Glulam Timber Deck

2.5.2 Results of Post Modeling Modifications

In Sections 2.5.1.1 through 2.5.1.3, a new stiffness model and BARRIER VII simulation configuration were created using information from a TL-1 curb rail and scupper block system that was then adjusted for (1) a new load application height, (2) a more robust curb rail and scupper block configuration, and (3) use on transverse, glulam timber decks instead of transverse, nail-laminated timber decks. All three modifications pertained to details reflected with the layout of the TL-4 glulam timber rail with curb bridge railing system. The final stiffness values were considered for the BARRIER VII model. In this process, the research team realized that based on the scheme used to model the TL-4 post system, the moment capacity of the post was dependent upon the capacity of the curb rail and scupper block portion of the post, as well as the post that connected the curb rail and the upper rail.

Next, the moment capacity of each timber bridge railing post was input into the BARRIER VII model as the moment capacity was calculated using the typical concrete beam equations discussed above, for a result of 720.0 k-in. For this modeling scheme, the stiffness model capped the peak force using the moment capacity of the curb and scupper system by dividing the moment capacity by the load application height of 28¼ in. This selection resulted in a yield force of 25.5 k. In order to verify that this scheme was reasonable, the moment and shear capacities of the glulam bridge post were compared to the anticipated loads transmitted through the posts and imparted to the curb rail and scupper block system. As mentioned previously, the posts had a moment capacity of 907.2 k-in. and shear capacity of 40.6 k, as calculated using AAHSTO LRFD procedures. The shear load that would yield the curb and scupper system was 25.5 k, which was less than the post's shear capacity of 40.6 k. The peak moment imparted on the post was calculated by multiplying the applied load, 25.5 k, by the distance between the load application height and the horizontal bolt that connected the post to the curb rail, 18⅛ in. This selection resulted in a peak moment of 462.2 k-in., which again is less than the bending capacity of the post at 907.2 k-in.

Although the TL-4 system had a higher load application height, the increased capacity of the scupper and curb system along with the changes in the deck produced a final stiffness that was larger than what was originally modeled from the TL-1 system. The force versus deflection plot modeled from the original TL-1 data and the final force versus deflection plot used to model the posts in the calibrated bridge railing system model are provided in Figure 26. All timber parameters for the rails and posts are provided in Tables 17 and 18. A typical computer simulation input data file for the TL-4 glulam timber rail with curb bridge railing system with a 2000P vehicle is also shown in Appendix D.

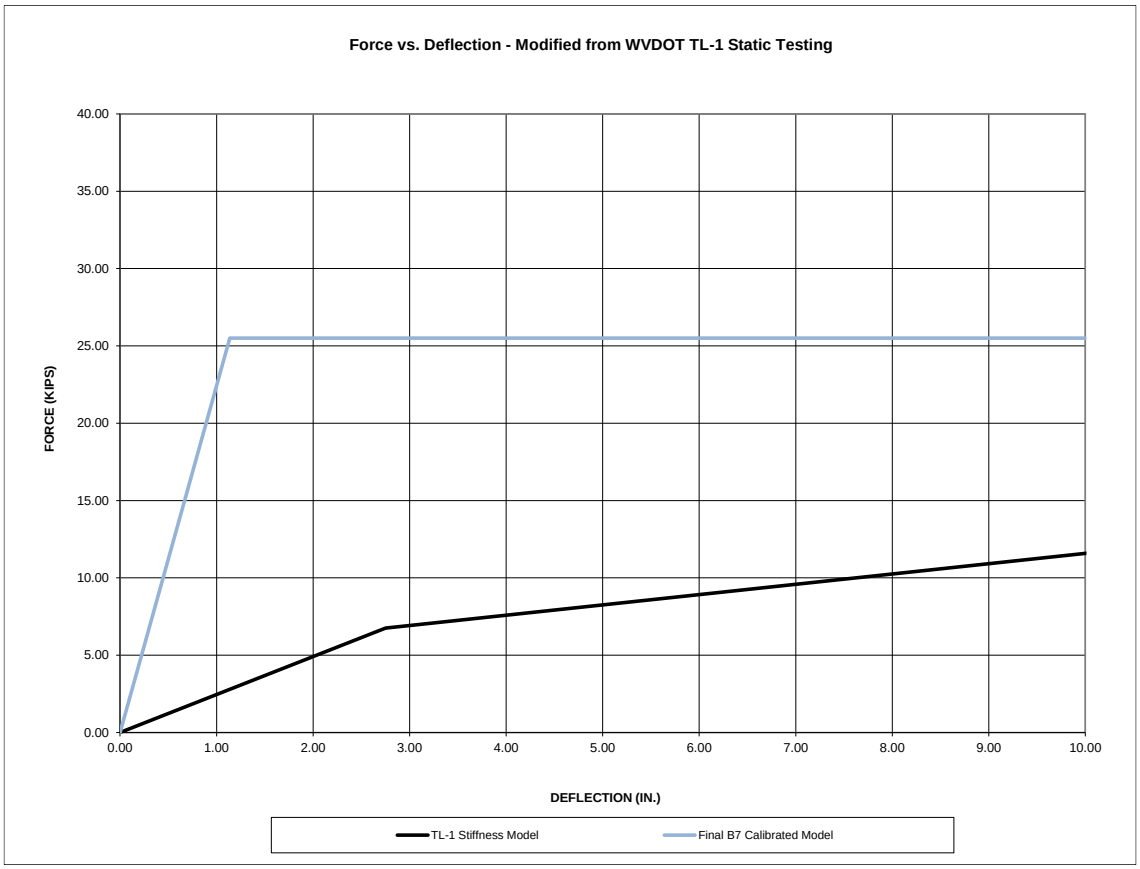

Figure 26. Force vs. Deflection Plot for Post Stiffnesses in Calibrated Model

Table 17. BARRIER VII Timber Rail Properties for Calibrated Model

Member Type	Member Size	Area ($in.^2$)	Moment of Inertia ($in.^4$)	Modulus of Elasticity (ksi)	Weight (lb/ft)	Nominal Tensile Yield Force (k)	Nominal Yield Moment (k-in.)
Upper Rail	8¾"x13½" (Glulam)	118.1	753.7	1,600	28.6	314.5	1,070.5
Curb Rail	6¾"x12" (Glulam)	81.0	972.0	1,500	19.3	135.4	668.5

Table 18. BARRIER VII Timber Post Properties for Calibrated Model

Member Type	Member Size	Top Node Height (in.)	Bottom Node Height (in.)	Stiffness k_A & k_B (k/in.)	Weight (lb)	Nominal Yield Moment (k-in.)	Failure Shear Force (k)	Failure Deflection (in.)
Bridge Post	8¾"x10½" (Glulam)	28.25	10.125	A-axis: 22.44 B-axis: 30.6	67.6	A-axis: 720.0 B-axis: 833.1	A-axis: 55.0 B-axis: 55.0	A-axis: 4.0 B-axis: 10.0

2.5.3 Final Calibrated Model Simulation Results

To determine if the simulation model was calibrated after using the new modeling scheme, previously discussed several behaviors were examined: the maximum dynamic deflection and overall deflected shape of the rail, the time and speed of the vehicle when it became parallel to the system, and the time and speed of the vehicle when the vehicle exited the system. The 2000P and 8000S simulation results and a comparison to data from the corresponding full-scale crash tests is discussed below.

After analysis of the available data from the TRBR test series, simulation with the pickup truck was shown to be the most critical since the full-scale crash test with the single-unit truck, test no. TRBR-1, the box of the truck rolled over the vertical plane created by the bridge railing, blocking the view of the posts and upper rail from video camera views for a substantial period of time. For this reason, the reported maximum deflection was believed to be too small, but a more accurate value was unable to be determined. For the pickup truck test, test no. TRBR-2, there was also a small period of time when the pickup crossed the vertical plane created by the bridge railing. However, most deflections were still documented, providing greater confidence in the available data.

For test no. TRBR-2, the pickup truck impacted the system at an angle of 27.4 degrees and a speed of 61.6 mph. The maximum dynamic deflection was 8.0 in. The vehicle became parallel to the system 0.238 seconds after impact and traveled at approximately 41.0 mph. The vehicle exited the system traveling 38.7 mph, 0.437 seconds after the initial impact. When using the same impact conditions in the BARRIER VII simulation model, the maximum dynamic deflection was determined to be 10.0 in. The vehicle became parallel to the system 0.243 seconds after impact and was traveling at a speed of 39.4 mph. In the simulation, the vehicle exited the system 0.350 seconds after impact, traveling at a speed of 37.2 mph.

For test no. TRBR-1, the single-unit truck impacted the system at an angle of 16.0 degrees and a speed of 46.5 mph. The maximum reported dynamic deflection was 3.3 in. This is not believed to be the actual maximum dynamic deflection experienced by the railing system as the truck box blocked the view of the posts and upper rail from the overhead video camera for a period of time. The vehicle became parallel to the system 0.525 seconds after impact and traveled at approximately 36.5 mph. The vehicle exited the system 1.522 seconds after impact, traveling at a speed of 27.3 mph. The actual exit time was expected to be much later than the simulated exit times due to the box of the vehicle rolling and leaning on the top of the upper rail, thus remaining in contact for an extended period of time. BARRIER VII is a 2-D computer simulation program that cannot account for vehicular roll, and therefore it cannot simulate this 3-D vehicle behavior. Using the same impact conditions in the BARRIER VII simulation model, the maximum dynamic deflection was 6.9 in. The vehicle became parallel to the system 0.421 seconds after impact and traveled at a speed of 36.3 mph. In the simulation, the vehicle exited the system 0.730 seconds after impact, traveling at a speed of 34.2 mph.

Comparisons of the physical crash test results and simulated test results for the 2000P and 8000S vehicles are provided in Tables 19 and 20, respectively. The simulation results were deemed acceptable for the 2000P vehicle. The simulation results for the 8000S vehicle did not compare well for maximum dynamic deflection or exit time due to vehicle roll. However, the discrepancy in dynamic deflections was not concerning as there was missing data from the higher deflection

period of the physical test. As mentioned previously, the calibration effort mostly focused on the comparison of results for the pickup truck test due to the reliability of the available data from test no. TRBR-2. Note that the deflected barrier shapes at the time of maximum deflection as observed in test no. TRBR-2 and simulation are provided in Figure 27. The deflected shape at the time of maximum dynamic deflection in simulation with the 8000S vehicle is provided in Figure 28.

The 2000P simulation results provided a maximum dynamic deflection that was overestimated by 2 in., a parallel time that occurred 0.005 seconds later, and a parallel velocity that was 1.6 mph slower than in the full-scale crash test. The exit time of the 2000P vehicle was 0.087 seconds earlier in the simulation, but the vehicle was traveling 1.5 mph slower than what was observed in full-scale crash testing at the exit time. With these results, it was evident that the vehicle was being redirected and slowed down by the system in a manner similar to how the full-scale bridge railing system reacted. Since the simulation overestimated deflections, the model was conservative for predicting system failure if controlled by deflection limit criteria. Although the location of maximum deflection was slightly farther downstream in simulation than observed in full-scale testing, as shown in Figure 27, the overall length of the deflected barrier was relatively similar. In both testing and simulation, approximately three spans were dynamically deflected due to impact, which further indicated that the model was appropriate for continued use into the next phases of the project.

Table 19. Test No. TRBR-2 and Final 2000P Simulation Results

Impact Case	**Maximum Dynamic Deflection (in.)**	**Parallel Time (sec)**	**Parallel Velocity (mph)**	**Exit Time (sec)**	**Exit Velocity (mph)**
Test No. TRBR-2	8.0	0.238	41.0	0.437	38.7
Test Simulation	10.0	0.243	39.4	0.350	37.2
% Error	+25.0%	+2.1%	-3.9%	-19.9%	-3.9%

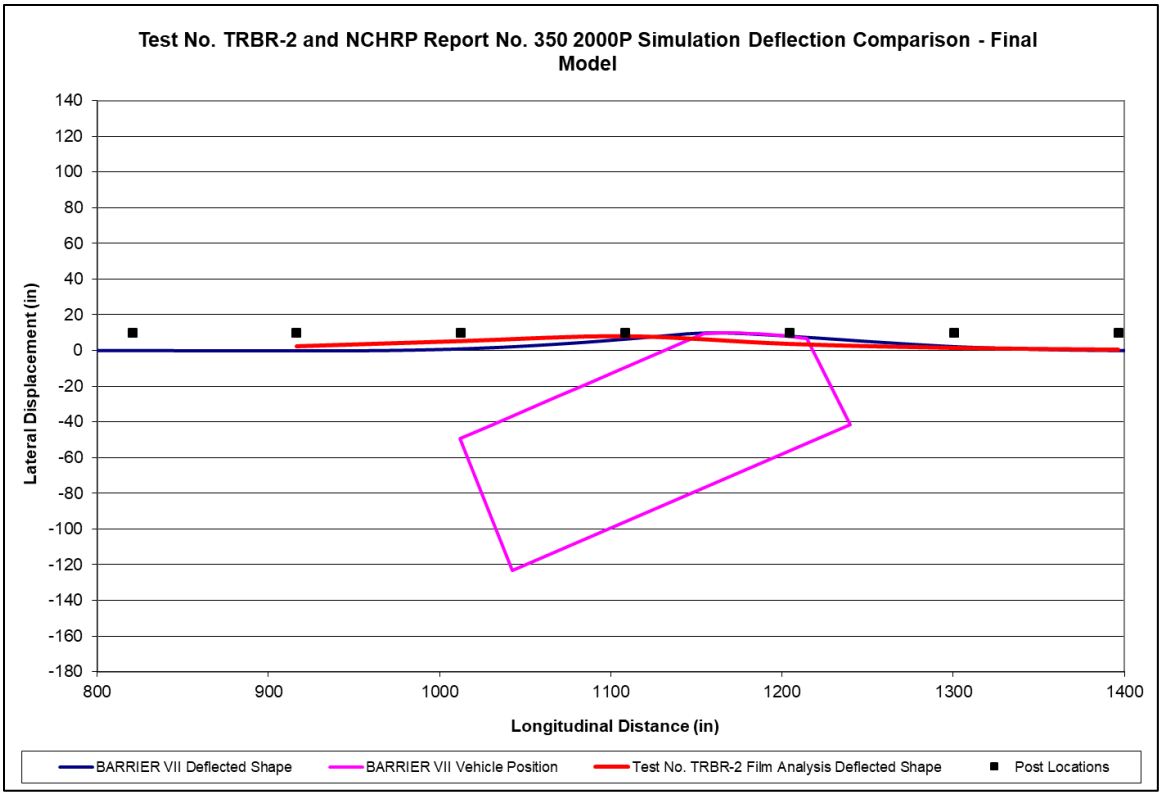

Figure 27. Test No. TRBR-2 and NCHRP Report No. 350 2000P Simulation Deflected Shape Comparison – Final Model

Table 20. Test No. TRBR-1 and Final 8000S Simulation Results

Impact Case	Maximum Dynamic Deflection (in.)	Parallel Time (sec)	Parallel Velocity (mph)	Exit Time (sec)	Exit Velocity (mph)
Test No. TRBR-1	3.3	0.525	36.5	1.522	27.3
Test Simulation	6.9	0.421	36.3	0.730	34.2
% Error	**	-19.8%	-0.5%	**	**

** - Not calculated due to behaviors observed in full-scale crash testing, as previously discussed in this section.

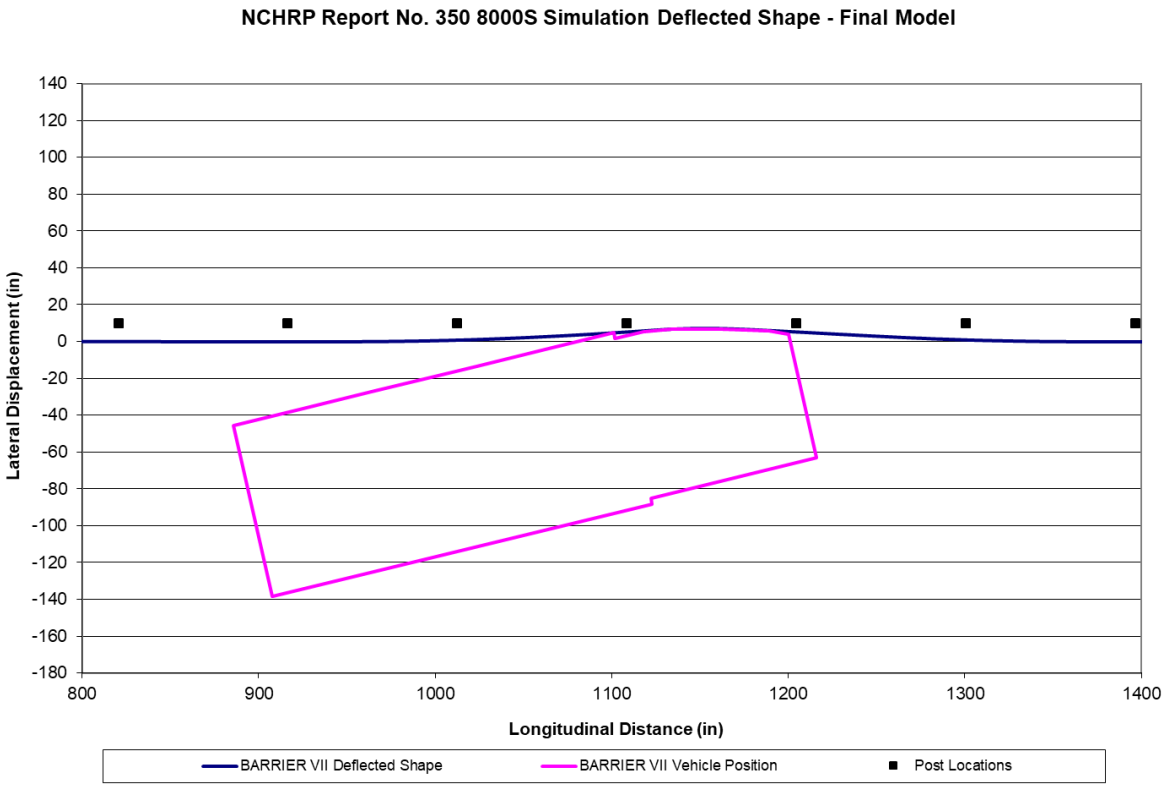

Figure 28. NCHRP Report 350 8000S Simulation Deflected Shape – Final Model

2.6 BARRIER VII Model Design Modifications for MASH TL-4 Bridge Railing System

2.6.1 Design Modification Process

After re-evaluating and modifying the procedures for modeling the different components in BARRIER VII based on a reference height set at the top of the deck, the research team was ready to begin making the necessary changes to create a system that could be deemed MASH crashworthy. The top of the deck is a clearly defined location that will remain constant through each iteration, thus eliminating the need to move the reference height location to match a certain behavior as design modifications were made to the system. This simple fact provided confidence that the model accurately reflected the physical characteristics of the bridge railing system and would continue to do so as components were modified in order to meet updated standards.

The goal of this effort was to modify the NCHRP Report 350 system in a step-by-step process, eventually obtaining an updated design that would meet MASH impact safety criteria. This process was performed by conducting crash test simulations with MASH vehicles using the BARRIER VII computer simulation program on a bridge railing system model containing updated parameters reflecting each modification. Analysis of the results after each simulation was used to determine if the system would adequately meet MASH impact safety criteria. This process would be repeated until enough reasonable changes were made to the system to conclude that the bridge railing system could meet MASH TL-4 requirements.

The design modifications included an overall height increase to accommodate larger single-unit truck vehicles found on the road today and in MASH, as well as future roadway overlays while also limiting the size of openings between rails to avoid snagging on vertical posts. The opening between rails were limited by incorporating a taller curb and scupper system into the overall bridge railing design. This height increase also utilized a larger curb rail, increasing overall strength, which will be discussed. The connection mechanism between the curb rail, scupper blocks, and deck was also modified to increase the strength and stiffness of the bridge railing posts. The final design modification implemented into the system was utilizing a larger upper rail. Each of these modifications were made with the purpose of providing enough strength to avoid failure, redirecting the impacting vehicle in a safe manner, and limiting the system's dynamic deflections. The results of these modifications are discussed in the following sections.

The maximum dynamic deflection of any portion of the system was desired to be less than 10.0 in. based on the observed behavior of the NCHRP Report 350 TL-4 bridge railing system sustaining 8 in. of deflection without failure. Allowing up to 10.0 in. of deflection was deemed the limit as the research team was unsure how the system would react if subjected to further deflection. Along with limiting deflections, the number of elements reaching yield and the amount of time spent in a yielded state, according to simulation, were analyzed. Due to a larger number of elements yielding and remaining in this state for an extended period of time even when the maximum dynamic deflection in a simulation was less than 10.0 in., further modifications were made to strengthen the members of the bridge railing system. These modifications included the addition of extra bolts in the connection between the curb rail, scupper blocks, and deck, and increasing the size of the upper rail. These modifications and the corresponding simulation results are discussed in Sections 2.6.4.2 and 2.6.5, respectively.

2.6.2 General Height Modifications and Simulations

The first design modification performed to update the NCHRP Report 350 system to meet MASH criteria was to increase the overall height of the barrier. To create a 36-in. tall barrier after both overlays were in place, the top height of the railing needed to be 40 in. above the top of the deck. Increasing the barrier height to 40 in. made the updated system 5 in. taller than the system developed under NCHRP Report 350 criteria, and moved the midheight of the upper rail from 28¼ in. above the deck to 33¼ in. above the deck.

The change in loading height of the upper rail caused the need for the stiffness of the posts to be modified once again using the method laid out in Section 2.5.1.1 of this study. The force versus deflection behavior of the posts based on this height change is detailed in Table 21, including the stiffnesses input into the BARRIER VII model for each post type of the composite post system. In reference to the discussion in Section 2.5.1 on the use of a two post system in BARRIER VII, the stiffness of the first post type was 4.92 k/in. This post yielded after 2.08 in. of deflection. The second post type had a stiffness of 1.84 k/in. and yielded after 8.33 in. of deflection. Figure 29 shows the modified force versus deflection behaviors as well. The red line indicates the behavior of the post system after all previous modifications had been made for the NCHRP Report 350 system. The blue line indicates the behavior as it was detailed in the calibrated system model, capped due to the moment capacity of the curb and scupper system. The green line, most of which is hidden under the black line, indicates the behavior of the post system after modifications due to a height increase from 28¼ in. to 33¼ in. The black line indicates the post behavior that was

modeled for this scenario was again capped due to the moment capacity of the curb and scupper system.

Table 21. Post Stiffness Data after Height Increase from 28¼ in. to 33¼ in.

Deflection (in.)	Force (k)	Total Stiffness (k/in.)	Post 1 Stiffness (k/in.)	Post 2 Stiffness (k/in.)
0.00	0.00	-	-	-
2.08	14.03	6.76	4.92	1.84
8.33	25.50	1.84	-	1.84
15.00	25.50	0.00	0.00	0.00

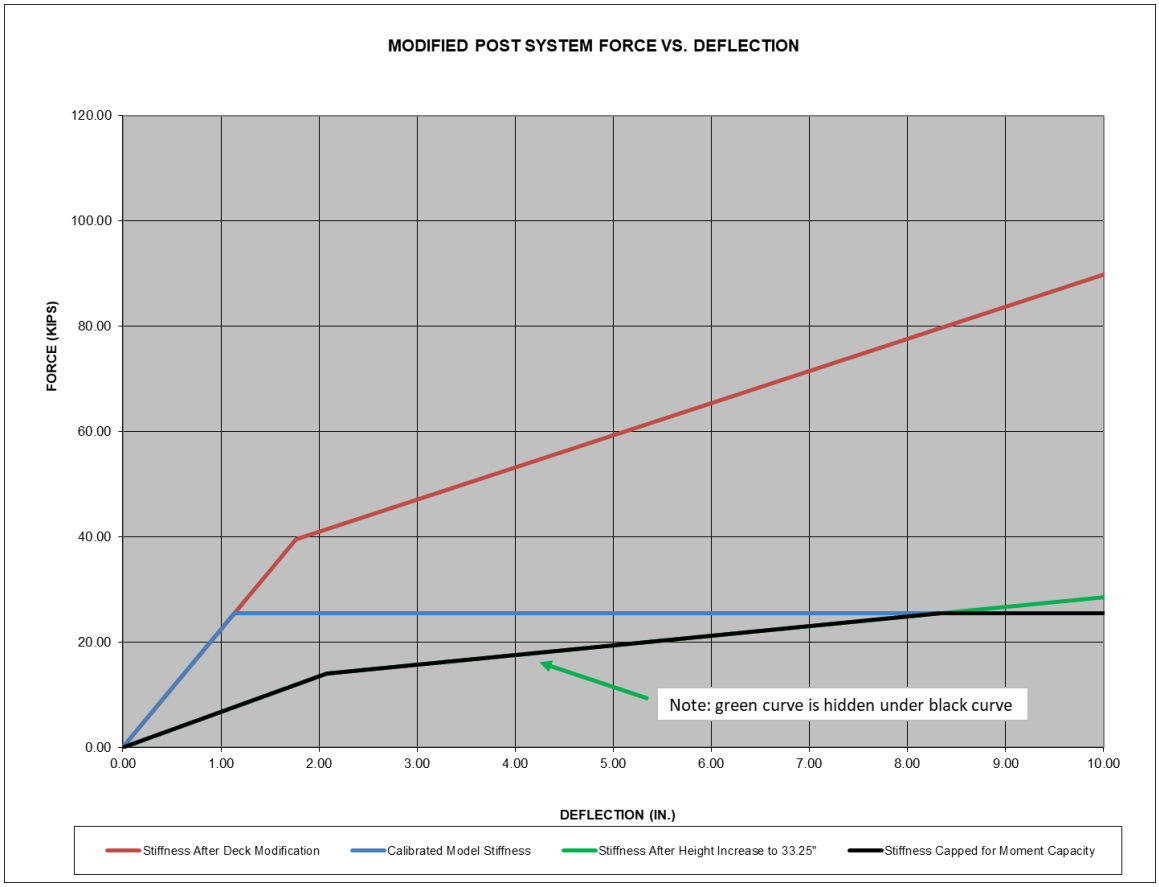

Figure 29. Force vs. Deflection Behavior for MASH TL-4 System Configuration after Height Increase from 28¼ in. to 33¼ in.

Simulations with only this height change incorporated and all other component sizes remaining the same resulted in deflections that were considered unacceptably large at 11.54 in. and 13.72 in. when impacted by the 2270P and 10000S vehicles, respectively. The simulations also resulted in post failure at two post locations due to reaching the maximum deflection limit of 10.0 in. when impacted by each vehicle.

2.6.3 Curb Rail Height and Size Modifications and Simulations

2.6.3.1 Vertical Rail Opening Heights and Post Setback

Based on past research efforts, the size of vertical openings between rails or between a rail and the deck should also be limited in order to prevent vehicle components from snagging on posts or other system components. The larger an opening is, the further the front face of the post or other component must be in order to avoid snagging and additional risk to occupants. AASHTO LRFD presents a discussion on the snag potential for several bridge railing designs [18]. Crash tests conducted under NCHRP Report 230 criteria were used to determine the threat of snagging based on different geometric parameters. The data was used to detail the potential risk of snag based on post shape and setback, as shown in Figure 30. The post setback distance versus the ratio of rail contact width to height can also be used to determine post setback criteria, as detailed in Figure 31. The ratio of rail height to width is determined by taking the surface area of the front face of the bridge railing divided by the overall height of the system.

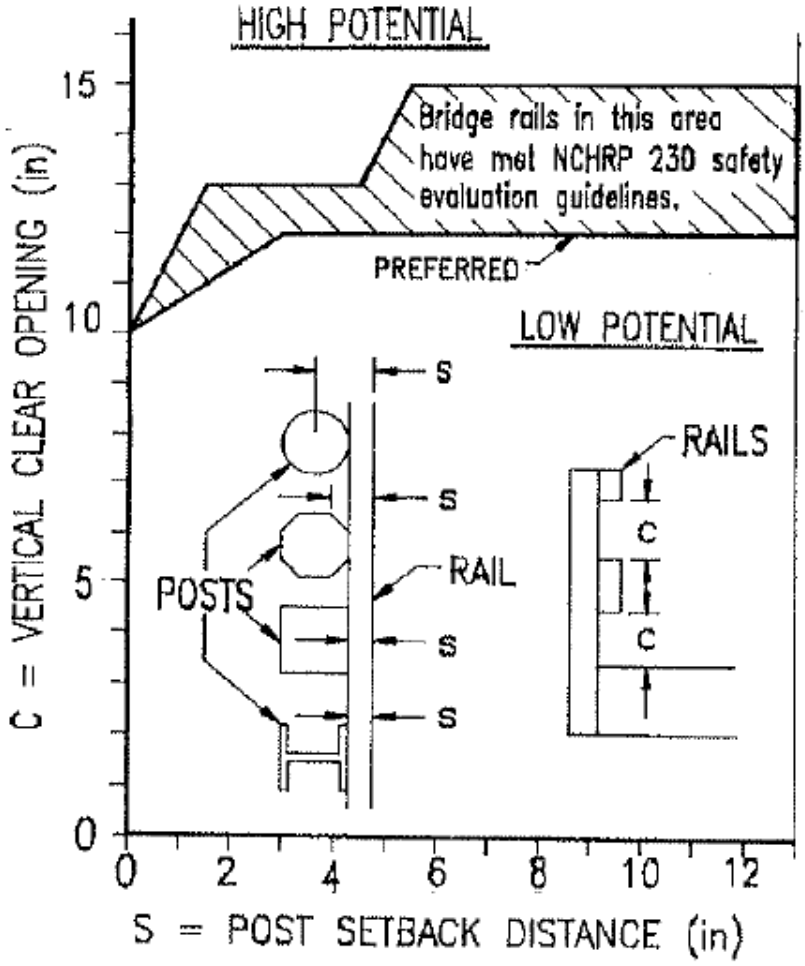

Figure 30. Snag Potential Based on Ratio of Vertical Clear Opening and Post Setback [18]

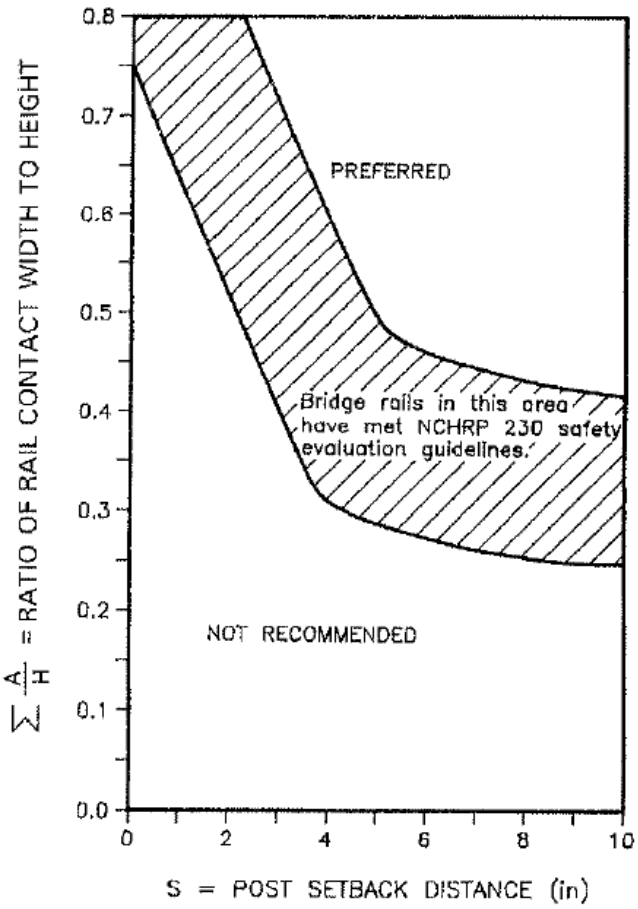

Figure 31. Snag Potential Based on Ratio of Contact Width to Height and Post Setback [18]

Additional research conducted by MwRSF in the effort to develop a new open concrete bridge railing system led to further recommended post setback distances for different opening heights. Table 22 defines the recommended post setbacks determined in this previous research effort [42]. Additional information from MwRSF researchers is shown in Table 23 regarding typical front bumper structural component heights [33]. In the TL-4 system with only the height of the upper rail increased, the opening between the rails became 13 in. The posts were set back 12 in. from the front of the rails, which technically aligns with the data in Table 22, but when the heights of the bumper structural components were plotted in front of the TL-4 system with an increased overall height, as seen in Figure 32, there was still concern about the 1100C and 2270P vehicles intruding through the opening and contacting the posts. In the figure, the railing is shown with a single 2-in. thick overlay on the left, and two 2-in. thick overlays on the right. The bumper heights are plotted relative to the top of the highest overlay in each case. For this reason, the next iteration in updating the system was to increase the height of the curb rail, thus reducing the opening between the two rails.

Table 22. Recommended Vertical Openings and Post Setbacks [42]

Vertical Opening (in.)	Minimum Post Setback (in.)
8	0
9	2
10	4
11	4
12	4
13	5
14	6

Table 23. Typical Front Bumper Structural Component Heights [33]

Vehicle Type	Bumper Bottom Edge Height (in.)	Bumper Top Edge Height (in.)
Small Car (1100C)	16.25	20.125
Pickup Truck (2270P)	18.375	24.375
Single-Unit Truck (1000S)	23.125	33.5

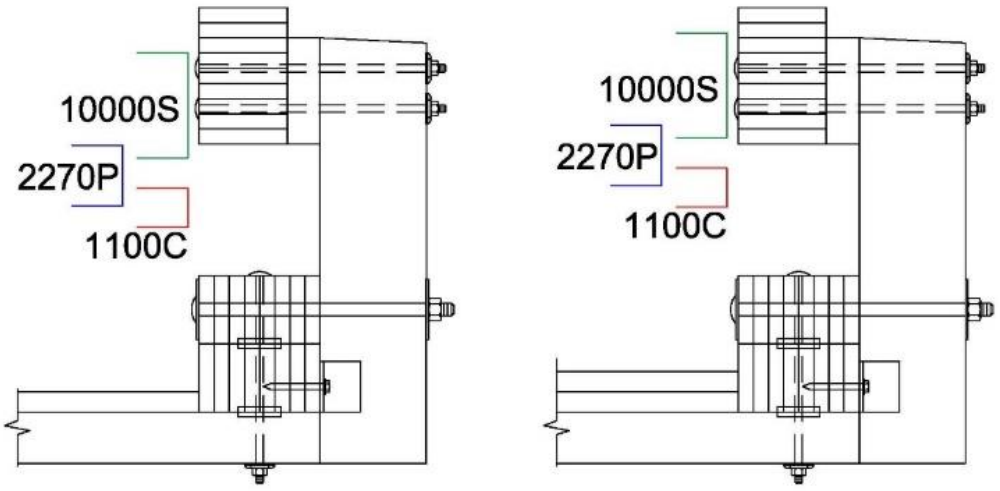

Figure 32. MASH TL-4 System Configuration after General Height Modification and Typical MASH Vehicle Bumper Heights

2.6.3.2 Curb Rail Modification Results

In order to increase the height of the curb rail, information on standard glulam sizes was gathered and different curb rail and scupper block configurations were created from these standard sizes and examined in relation to the resulting openings. Combinations were specifically created using 5⅛-in., 6¾-in., and 8¾-in. glulam sections. The final configuration that provided satisfactory openings and also increased the strength of the system utilized two 5⅛-in. tall scupper blocks with

an 8¾-in. tall curb rail. Increasing the size of the curb rail also increased the moment capacity of the rail by 30.0 percent, from 668.5 k-in. to 869.3 k-in. This new configuration is shown in Figure 33. In the figure, the system is again shown with a single 2-in. thick overlay on the left and two 2-in. thick overlays on the right, with all heights plotted in respect to the top of the highest overlay. The new scupper and curb layout left an opening between the upper and curb rails of only 7½ in. and a maximum opening between the top of the overlay and the bottom of the curb rail of 8¼ in. With this new configuration, simulated maximum deflections were slightly smaller than with the previous iteration, but still deemed to be too large at 11.26 in. and 13.35 in. for the pickup truck and single-unit truck simulations, respectively. The pickup truck simulation also resulted in post failure at one post location, while the single-unit truck simulation resulted in post failure at two post locations.

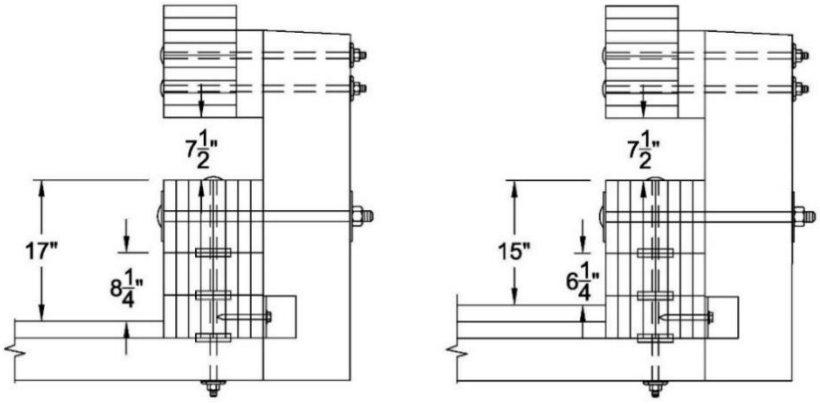

Figure 33. MASH TL-4 System Configuration after Curb Rail Modifications

2.6.4 Curb and Scupper to Deck Connection Modifications and Simulations

2.6.4.1 Bolt Placement

After increasing the height and size of the curb rail, the next two changes included modifications to the bolting configuration between the curb and scupper system to the deck. Because of the methodology used to determine post strength and stiffness, which is strongly based upon the strength of the curb and scupper system, moving the vertical bolts to create a larger moment arm between the compression force in the scupper blocks and the tension force carried by the bolts would greatly increase the overall strength of the system and reduce deflections. Adding more bolts was also implemented to create more steel area to carry the tension and provide further strength increases and deflection reductions. In each case, the bolts that were utilized were still ¾-in. diameter ASTM A307 bolts with 4-in. shear plates at each timber interface.

The third iteration utilized the same number of bolts, but the bolts were moved 2 in. closer to the front face of the curb rail and scupper blocks. This configuration is shown in Figure 34.

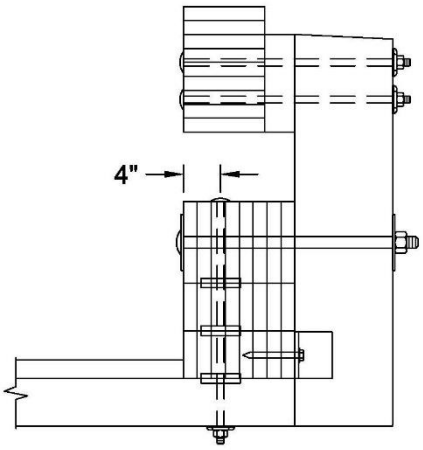

Figure 34. MASH TL-4 System Configuration after Movement of Vertical Bolt Location

To ensure that moving the bolts forward was geometrically acceptable, spacing and edge distance requirements as set forth in the 2018 NDS were examined. The center of the bolts and shear plates would be located 4 in. from the front face, and when loaded from impact, would need to provide strength perpendicular to the grain of the wood. For bolts and shear plates, edge requirements are determined for both the loaded edge and the unloaded edge. In the case of impact loading, the distance to the loaded edge would be the distance from the front of the curb or scupper to the centerline of the bolt or shear plate. The unloaded edge would then be the distance from the centerline of the bolt or shear plate to the back of the curb or scupper. For bolts, the edge distance requirement for the loaded edge is four times the diameter of the bolt, or 3 in., and for the unloaded edge the requirement is one and a half times the diameter of the bolt, or 1⅛ in. The bolts must be spaced at one and a half times the diameter of the bolt, or 1⅛ in. For 4 -in. shear plates, the loaded edge distance must be at least 3¾ in. and the unloaded edge distance must be a minimum of 2¾ in. The shear plates must be spaced at 5 in. For both bolts and shear plates, the actual loaded edge distance would be 4 in., the unloaded edge distance would be 8 in., and spacing would be 6 in., therefore, all of the requirements were met.

Moving the bolts forward once again causes a modification to the stiffness of the post system. To account for this change in the strength of the curb and scupper system, the method detailed in Section 2.5.1.2 of this study was followed. Through this process, the moment capacity of the curb and scupper system increased from 720.0 k-in. to 1,038.0 k-in., and the resulting changes to the post stiffnesses are detailed in Table 24. In reference to the discussion in Section 2.5.1 on the use of a two post system in BARRIER VII, the stiffness of the first post type was 7.10 k/in. This post yielded after 2.08 in. of deflection. The second post type had a stiffness of 2.65 k/in. and yielded after 6.23 in. of deflection. Figure 35 shows the modified force versus deflection behaviors. The green line indicates the behavior of the post system after modifications due to the initial increase in height to meet MASH criteria. The black line indicates the post behavior as it was modeled for simulation after increasing the overall height of the system, and the curb rail and scupper configuration. The blue line indicates the post behavior after modification due to the change in the location of the vertical bolts connecting the curb and scupper blocks to the deck. The red line indicates the post behavior that was modeled for this scenario, again capped due to the moment capacity of the curb and scupper system.

Table 24. Post Stiffness Data after Movement of Vertical Bolt Location

Deflection (in.)	Force (k)	Total Stiffness (k/in.)	Post 1 Stiffness (k/in.)	Post 2 Stiffness (k/in.)
0.00	0.00	-	-	-
2.08	20.22	9.74	7.10	2.65
6.23	31.20	2.65	-	2.65
15.00	31.20	0.00	0.00	0.00

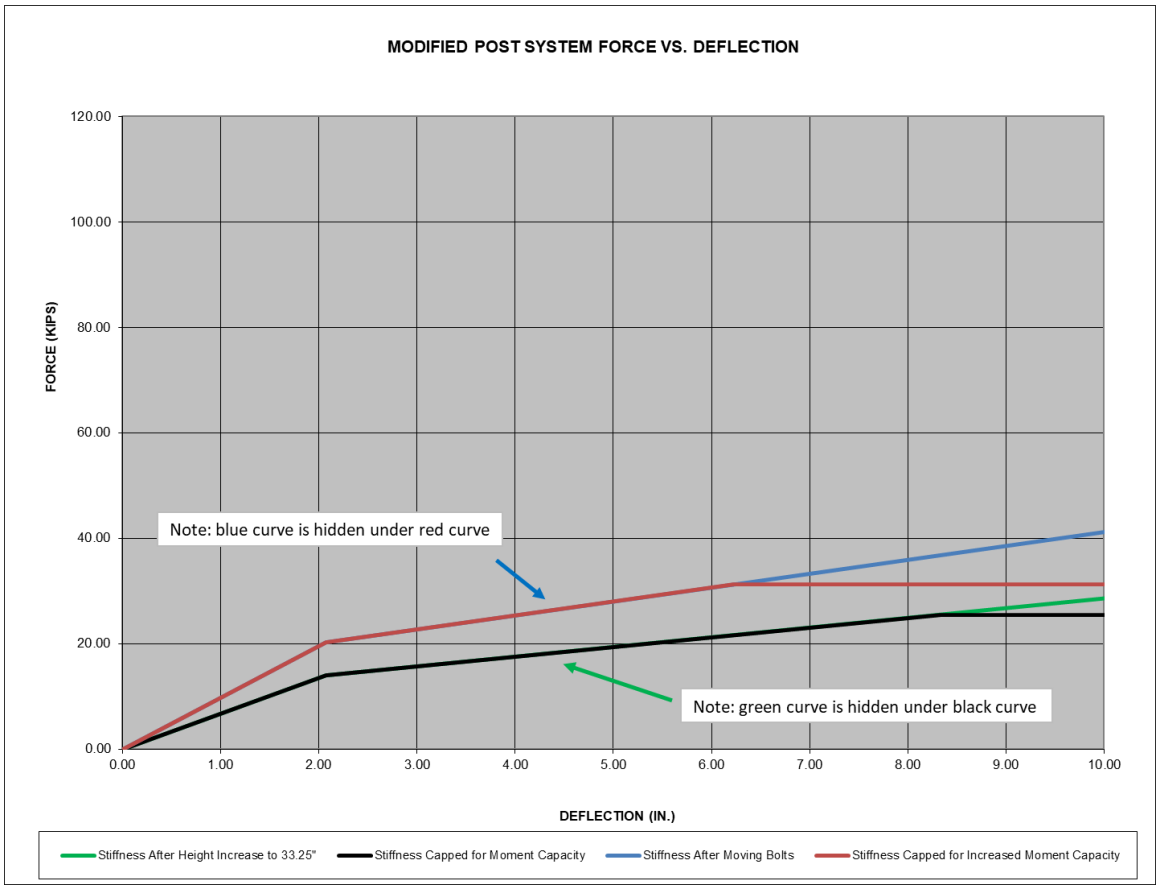

Figure 35. Force vs. Deflection Behavior after Movement of Vertical Bolt Location

Simulation with the updated parameters based on moving the vertical bolts forward produced more favorable results than previous iterations. However, they were still deemed unacceptable, and further deflection reduction was desired. The maximum deflections from the simulations were determined to be 9.30 in. and 10.31 in. for the pickup truck and single-unit truck, respectively. No post failure was observed in these simulations.

2.6.4.2 Number of Bolts

The next iteration in updating the MASH TL-4 design included further changes to the curb and scupper portion of the system by adding two additional vertical bolts connecting the curb and scupper blocks to the deck. This new configuration can be seen in Figure 36.

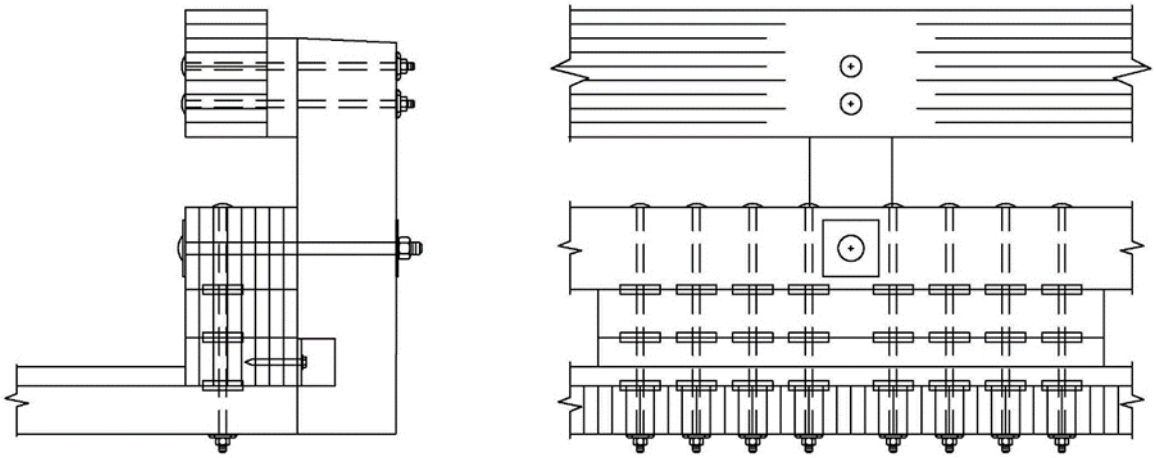

Figure 36. MASH TL-4 System Configuration after Addition of Two Vertical Bolts

Adding two bolts caused further modification to the stiffness of the post system. To account for this change in the strength of the curb and scupper system, the method detailed in Section 2.5.1.2 of this study was followed once again. Through this process, the moment capacity of the curb and scupper system increased from 1,038.0 k-in. to 1,279.9 k-in., and the resulting changes to the post stiffnesses are detailed in Table 25. In reference to the discussion in Section 2.5.1 on the use of a two post system in BARRIER VII, the stiffness of the first post type was 8.75 k/in. This post yielded after 2.08 in. of deflection. The second post type had a stiffness of 3.26 k/in. and yielded after 2.79 in. of deflection. Figure 37 shows the modified force versus deflection behaviors as well. The blue line indicates the post behavior after modification due to the change in the location of the vertical bolts connecting the curb and scupper blocks to the deck. The red line indicates the post behavior as it was modeled for the third MASH iteration. The green line indicates the behavior of the post system after modifications due to the increased number of bolts. The black line indicates the post behavior as it was modeled for this scenario, capped for the new moment capacity of the curb and scupper system.

Table 25. Post Stiffness Data after Addition of Two Vertical Bolts

Deflection (in.)	Force (k)	Total Stiffness (k/in.)	Post 1 Stiffness (k/in.)	Post 2 Stiffness (k/in.)
0.00	0.00	-	-	-
2.08	24.93	12.01	8.75	3.26
2.79	27.25	3.26	-	3.26
15.00	27.25	0.00	0.00	0.00

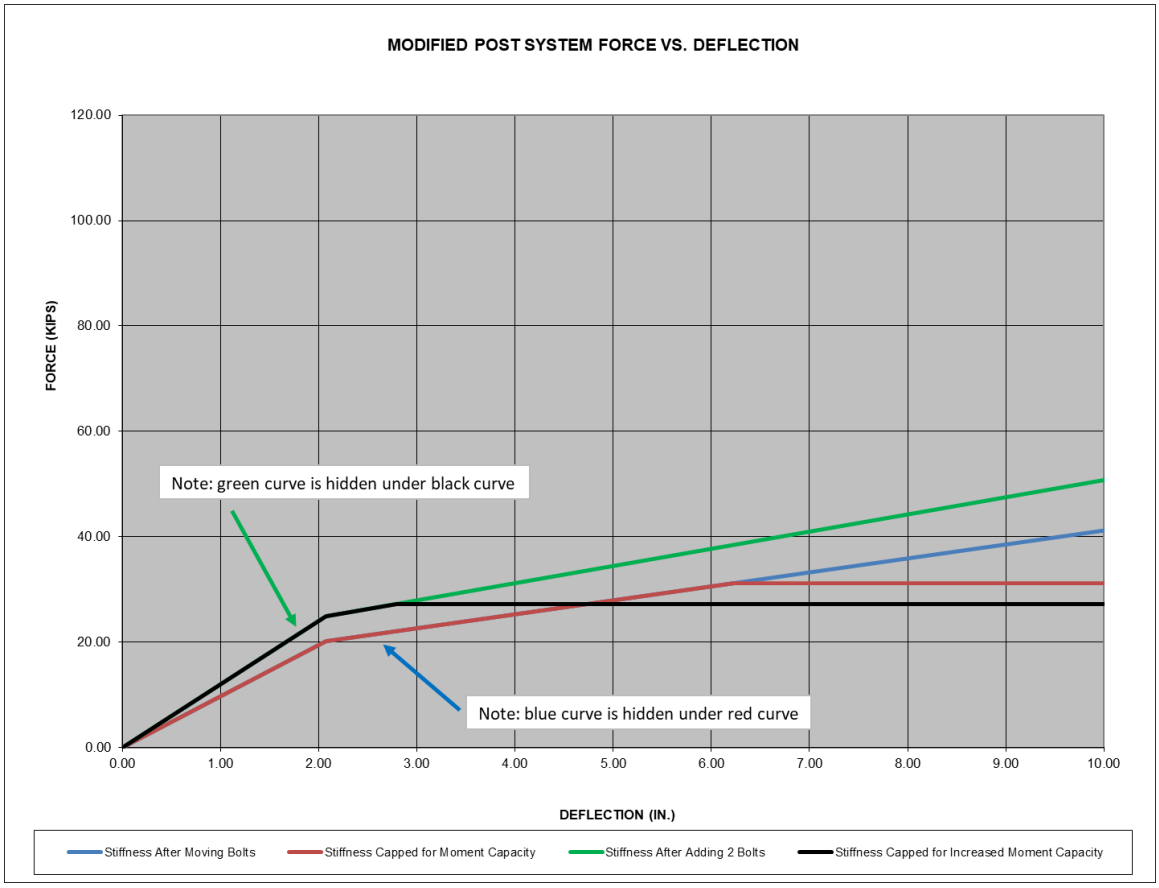

Figure 37. Force vs. Deflection Behavior after Addition of Two Vertical Bolts

The inclusion of the additional bolts further increased the strength of the system and reduced the maximum deflections experienced by the system to 8.33 in. and 9.03 in. for the pickup truck and single-unit truck simulations, respectively. Again, these simulations resulted in no post failure. These deflection values were near the end goal of obtaining deflections of less than 10.0 in., but due to a substantial amount of yielding of the upper rail, curb rail, and post elements in simulation, additional measures were taken to further reduce deflections and ensure adequacy with less yielding.

2.6.5 Upper Rail Size Modifications and Simulations

In what was reasoned to be the final iteration of upgrading the components of the system to meet MASH criteria, a larger upper rail was implemented. In order to provide more strength in bending and further distribute loads, the next deepest standard glulam section size was implemented. This replaced the original 8¾-in. deep by 13½-in. tall rail with a 10¾-in. deep by 13½-in. tall rail. This size increase reflected a 46.5 percent increase in the moment capacity of the beam from 1,070.5 k-in. to 1,568.6 k-in. The new beam was also the same size of glulam beam utilized for the rub rail in the noise wall system developed by MwRSF in 2019 that performed successfully in full-scale testing [25].

The additional strength provided by the larger rail reduced the maximum dynamic deflections to 7.22 in. and 7.77 in. for the pickup truck and single-unit truck simulations, respectively. The final system configuration can be seen in Figure 38. With these deflections dropping below the maximum deflections observed in crash testing of the original NCHRP Report 350 system, the deflection behavior of the system was deemed acceptable and additional analysis into other portions of the simulated system was needed to determine if the design could be considered acceptable overall.

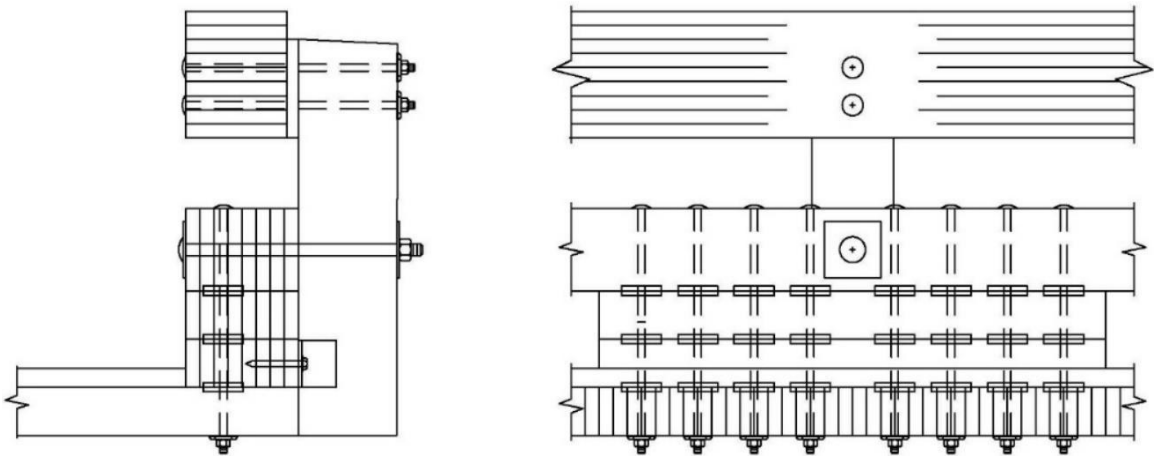

Figure 38. Final MASH TL-4 System Configuration

Each of the BARRIER VII output files were examined to determine the overall system behavior in terms of yielding or failure of any members and compared to previous testing. When examining the simulation results from the NCHRP Report 350 calibrated model, it was determined that 9 upper rail elements, 2 curb rail elements, and 3 posts all reached their specified yielding point due to impact from the pickup truck model. Because this test had a higher impact severity and larger deflections than the 8000S single-unit truck test, this data was used for comparison with simulations run on the new model. With the final iteration of the updated system, the 2270P pickup truck impact caused a maximum of 10 upper rail elements, 2 curb rail elements, and 1 post to reach yielding. Simulation of the 10000S single-unit truck impact on the updated system caused a maximum of 13 upper rail elements, 2 curb rail elements, and 2 posts to reach yielding. This information is tabulated in Table 26. The results obtained from the simulation of test no. TRBR-2 in comparison to the damage that was actually observed in the test gave the research team confidence that the amount of simulated yielding occurring under the MASH test simulations was acceptable. The damage to the bridge railing system in test no. TRBR-1 mainly consisted of gouging of the rail from vehicle components such as the bumper and wheels, and there was little to no damage observed from bending failure. With the similarities in the number of elements yielding in each of the simulations, the updated railing system would be expected to behave similarly and have minimal damage caused by bending when subjected to full-scale testing in the near future. For this reason, as well as from the examination of deflections, this design was determined to be acceptable and final considerations could be made in order to proceed to the next phase of this research project.

Table 26. Number of Yielded Elements in Simulation

Element Type to Reach Yield	Calibrated NCHRP 350 Pickup Truck Simulation	MASH 2270P Pickup Truck Simulation	MASH 10000S Single-Unit Truck Simulation
Upper Rail	9	10	13
Curb Rail	2	2	2
Post	3	1	2

The final updated BARRIER VII model for the MASH TL-4 glulam timber rail with curb bridge railing system and a generic approach guardrail transition system is shown in Figure 39. Tables 27 and 28 show the timber parameters for the components of the final bridge railing system. A typical computer simulation input data file for the bridge railing system with a 2270P vehicle is provided in Appendix E.

Table 27. BARRIER VII Timber Rail Properties for Final MASH TL-4 Model

Member Type	Member Size	Area ($in.^2$)	Moment of Inertia ($in.^4$)	Modulus of Elasticity (ksi)	Weight (lb/ft)	Nominal Tensile Yield Force (k)	Nominal Yield Moment (k-in.)
Upper Rail	10¾"x13½" (Glulam)	145.1	1397.6	1,600	34.5	383.6	1,568.6
Curb Rail	8¾"x12" (Glulam)	105.0	1,260.0	1,500	25.0	192.4	869.3

Table 28. BARRIER VII Timber Post Properties for Final MASH TL-4 Model

Member Type	Member Size	Top Node Height (in.)	Bottom Node Height (in.)	Stiffness k_A & k_B (k/in.)	Weight (lb)	Nominal Yield Moment (k-in.)	Failure Shear Force (k)	Failure Deflection (in.)
Bridge Post Type 1	8¾"x10½" (Glulam)	33.25	14.625	A-axis: 8.75 B-axis: 9.38	39.3	A-axis: 605.15 B-axis: 416.5	A-axis: 30.0 B-axis: 30.0	A-axis: 4.0 B-axis: 10.0
Bridge Post Type 2	8¾"x10½" (Glulam)	33.25	14.625	A-axis: 3.26 B-axis: 9.38	39.3	A-axis: 676.38 B-axis: 416.5	A-axis: 30.0 B-axis: 30.0	A-axis: 4.0 B-axis: 10.0

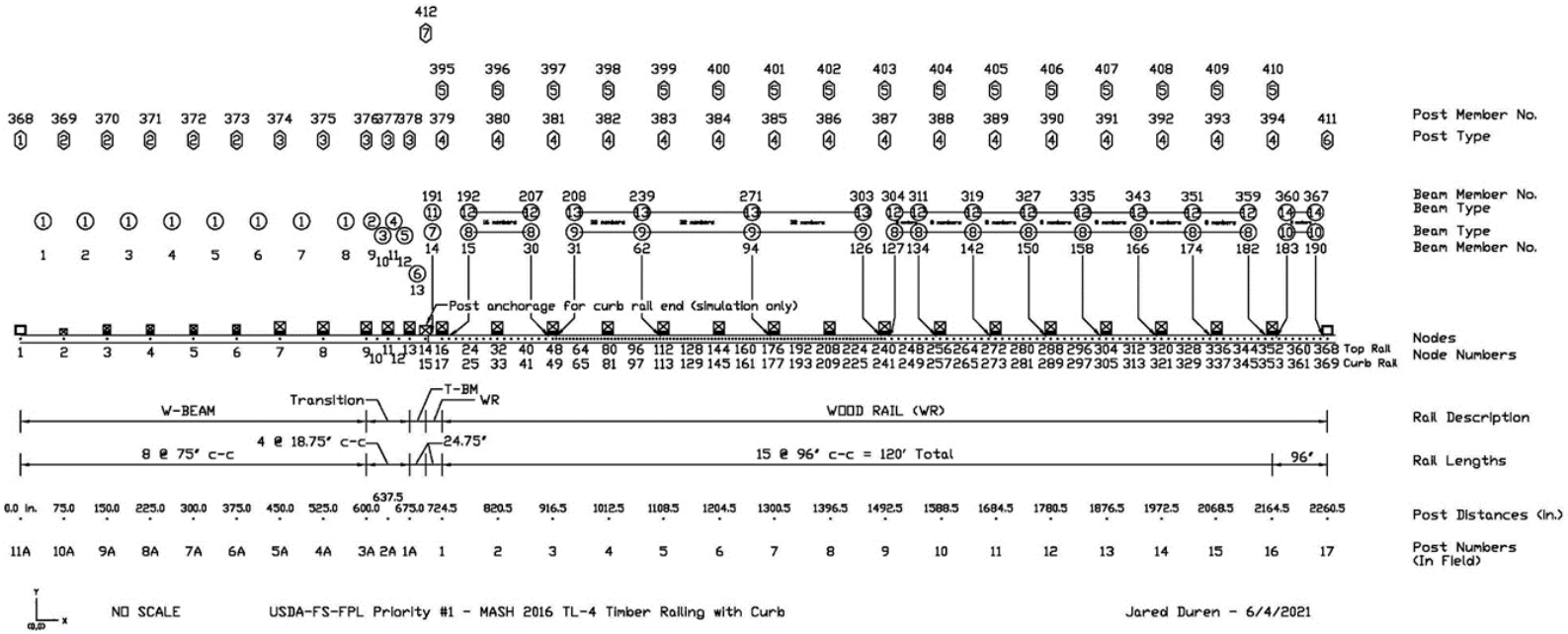

Figure 39. Final MASH TL-4 BARRIER VII Model

2.7 Critical Impact Point Study

Following the completion of updates to create a barrier model that was sufficient to handle MASH loading, a series of additional simulations was run with the model. In each of these simulations, the impact point of the vehicle was moved and the results were analyzed. This process was performed by moving the impact point downstream in 1-ft increments, starting at bridge post 4 and ending at bridge post 7, using both the 2270P and 10000S vehicle models. The bridge railing system model can be seen in Figure 39 for reference. These were determined to be the critical regions for impact in order to observe the behavior of the bridge railing itself and not substantially include the surrogate approach guardrail transition or the anchorage system at the far downstream end. In the region between post nos. 4 and 7, the beam elements were also smaller, as described earlier, allowing more detailed information on the performance of the bridge railing. The data from each of these simulations was then compared in an effort to identify the critical impact point for each vehicle. Specifically, the data that was gathered included the maximum deflection experienced by the bridge railing, the maximum tensile force in the railing, the number of post, upper rail, and curb rail elements that reached yield, and the lateral and longitudinal forces exerted on the rail from the impact.

2.7.1 2270P Critical Impact Point

The data gathered from each simulation with the 2270P vehicle was compiled into Table 29 and compared to determine ranges for each critical piece of information. In this table, the two largest values in each column, including duplicates, are highlighted in yellow for visual recognition of maximum values.

For simulations run with the 2270P vehicle, the largest maximum deflection was 7.29 in., and three additional simulations returned a maximum deflection of 7.28 in. These deflections occurred when the vehicle impacted at the centerline of post 4, and 1 ft upstream from post nos. 5, 6, and 7, respectively. The lowest maximum deflection observed in simulation occurred when impacting 3 ft downstream from post nos. 5 or 6, and was measured at 6.27 in. The largest maximum tensile force in the rail was measured to be 58.49 k when the vehicle impacted the system 1 ft upstream from post 6, and the lowest maximum tensile force was the result of impact 3 ft downstream from post 4 with a magnitude of 36.81 k. Each simulation resulted in a single post element reaching yield, a range of 5 to 10 upper rail elements reaching yield, and a range of 0 to 2 curb rail elements reaching yield. The lateral impact forces, calculated based on the weight of the vehicle and 50-msec average accelerations of the vehicle in the global coordinate system, ranged from 75.90 k to 76.94 k ranges for the lateral and longitudinal impact forces did not vary much, as would be expected, so this data was not a major factor in determining critical impact point.

With each set of data compared side by side, the critical impact point based on these simulations was concluded to be 4 ft upstream from post no. 7. In Table 29, the first three columns of data for this simulation are highlighted in green. At this location, the maximum deflection was measured to be 6.44 in., the maximum tensile force was 42.78 k, 1 post element, 9 upper rail elements, and 2 curb rail elements each reached yielding. The maximum lateral force imparted on the barrier was determined to be 76.18 k, and the maximum longitudinal force was determined to be 38.01 k. The plot of the impact loads versus time for simulation at this impact point is provided

in Figure 40. Comparison of the results for impact simulation 4 ft downstream from post no. 6 with the absolute maximum observed in each category of data proved to be the worst case scenario in obtaining a critical combination of large deflections, tensile forces, and element yielding according to the simulations. For glulam rail with curb bridge railing systems, splices have typically been installed at post locations, so according to BARRIER VII simulation and MASH criteria, a splice shall be located at post no. 7 with impact occurring approximately 4 ft upstream from this location when full-scale testing is performed with the 2270P vehicle.

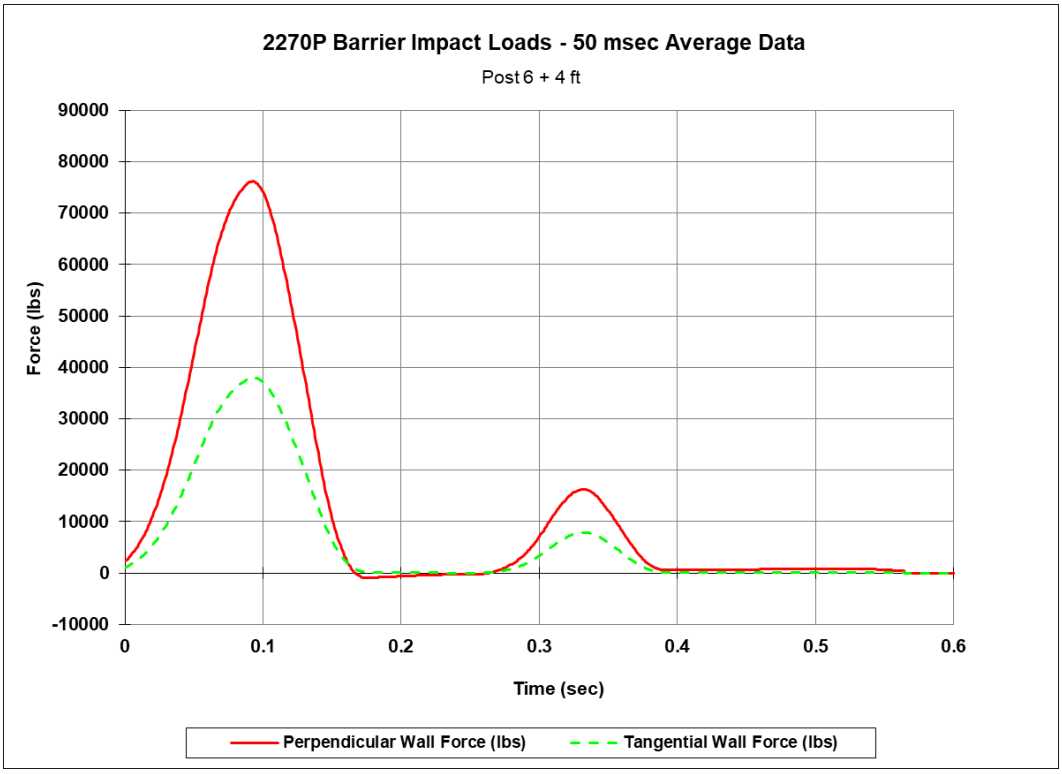

Figure 40. Impact Force vs. Time for 2270P Simulation

Through analysis of the data provided in Table 29, it was recognized that performing crash testing utilizing alternate points of impact may be viable as there are multiple impact points that resulted in similar simulation results. For example, if the critical impact point was chosen to replicate 2270P simulation no. 20 from Table 29, located 3 ft downstream from post no. 6, one would expect to observe slightly less deflection and tensile force in the rail, but according to simulation, a slightly longer portion of the upper rail would reach yielding. It was also apparent that impacting the system 3 or 4 ft downstream from post no. 5 would provide very similar results as impacting the system 3 or 4 ft downstream from post no. 6. With the understanding that multiple impact points could be chosen and provide similar results, it is still recommended to impact the system 4 ft downstream from post no. 6. If additional information becomes available through future research efforts that would suggest an alternate impact location, further analysis will need to be performed.

Table 29. Critical Impact Point Data for 2270P Simulations

Run	Vehicle	Impact Node	Max Defl. (in.)	Max Force (k)	Posts Yielded	Upper Rails Yielded	Curb Rails Yielded	Lateral Load (Global)	Longitudinal Load (Global)
1	2270P	80	7.29	55.86	1	7	0	76.29	39.30
2	2270P	84	7.02	49.44	1	6	2	76.09	39.11
3	2270P	88	6.69	43.09	1	5	2	76.69	39.09
4	2270P	92	6.28	36.81	1	10	2	76.91	38.66
5	2270P	96	6.44	41.88	1	9	2	76.16	38.00
6	2270P	100	6.70	48.10	1	7	2	75.96	38.17
7	2270P	104	7.02	55.03	1	8	0	75.90	38.53
8	2270P	108	7.28	57.90	1	7	0	76.10	39.10
9	2270P	112	7.22	55.81	1	6	0	76.10	39.25
10	2270P	116	7.01	50.12	1	6	2	76.09	39.10
11	2270P	120	6.68	43.56	1	5	2	76.71	39.09
12	2270P	124	6.27	37.15	1	10	2	76.92	38.66
13	2270P	128	6.44	42.35	1	9	2	76.17	38.00
14	2270P	132	6.69	48.57	1	7	2	76.05	38.21
15	2270P	136	7.02	55.61	1	8	0	75.93	38.54
16	2270P	140	7.28	58.49	1	7	0	76.12	39.11
17	2270P	144	7.22	56.44	1	7	0	76.10	39.17
18	2270P	148	7.01	50.62	1	6	2	76.10	39.10
19	2270P	152	6.68	44.00	1	5	2	76.72	39.09
20	2270P	156	6.27	37.38	1	10	2	76.94	38.67
21	2270P	160	6.44	42.78	1	9	2	76.18	38.01
22	2270P	164	6.69	49.03	1	7	2	76.06	38.21
23	2270P	168	7.02	56.12	1	8	0	75.95	38.54
24	2270P	172	7.28	59.01	1	7	0	76.14	39.11
25	2270P	176	7.22	56.98	1	7	0	76.12	39.18

2.7.2 10000S Critical Impact Point

The data gathered from each simulation with the 10000S vehicle was compiled into Table 30 and compared to determine ranges for each critical piece of information. In this table, the two largest values in each column, including duplicates, are highlighted in yellow for visual recognition of maximum values.

For simulations run with the 10000S vehicle, the largest maximum deflection was determined to be 8.05 in. This deflection occurred in three simulations, when the vehicle impacted 2 ft downstream from post nos. 4, 5, and 6. The lowest maximum deflection observed in simulation occurred when impacting 1 ft upstream from post no. 7 and was measured at 7.29 in. The largest maximum tensile force in the rail was measured to be 76.26 k when the vehicle impacted the system 3 ft downstream from post no. 6, and the lowest maximum tensile force was the result of impact 1 ft downstream from post no. 5 with a magnitude of 58.07 k. Each simulation resulted in a either 1 or 2 post elements reaching yield, a range of 8 to 13 upper rail elements reaching yield, and a range of 0 to 2 curb rail elements reaching yield. The lateral impact forces, calculated based on the weight of the vehicle and 50-msec average accelerations of the vehicle in the global coordinate system, ranged from 84.18 k to 85.71 k. The longitudinal impact forces, calculated in the same manner, ranged from 61.88 k to 64.57 k. Again, the ranges for the lateral and longitudinal impact forces did not vary much, as would be expected, so this data was not a major factor in decision of the critical impact point.

With each set of data compared side by side, the critical impact point based on these simulations was concluded to be 3 ft downstream from post no. 7. In Table 30, the first three columns of data for this simulation are highlighted in green. At this location, the maximum deflection was measured to be 7.92 in., the maximum tensile force was 76.26 k, 2 post elements, 10 upper rail elements, and no curb rail elements reached yielding. The maximum lateral force imparted on the barrier was determined to be 85.15 k, and the maximum longitudinal force was determined to be 63.95 k. The plot of the impact loads versus time for simulation at this impact point is provided in Figure 41. It is recognized that the impact force versus time plots from BARRIER VII do not exactly correlate with plots created from actual crash test data from single-unit truck impacts. In full-scale crash testing, a larger load is applied to the barrier due to tail slap of the vehicle and not the initial impact of the front end of the vehicle. BARRIER VII is not able to encapsulate this behavior, but the maximum force level is still in accordance with design loading conditions. Comparison of the results for the impact simulation 3 ft downstream from post no. 6 with the absolute maximum observed in each category of data proved to be the worst case scenario in obtaining a critical combination of large deflections, tensile forces, and element yielding according to the simulations. For glulam rail with curb bridge railing systems, splices have typically been installed at post locations, so according to BARRIER VII simulation and MASH criteria, a splice shall be located at post no. 7 with impact occurring 5 ft upstream from this location when full-scale testing is performed with the 10000S vehicle.

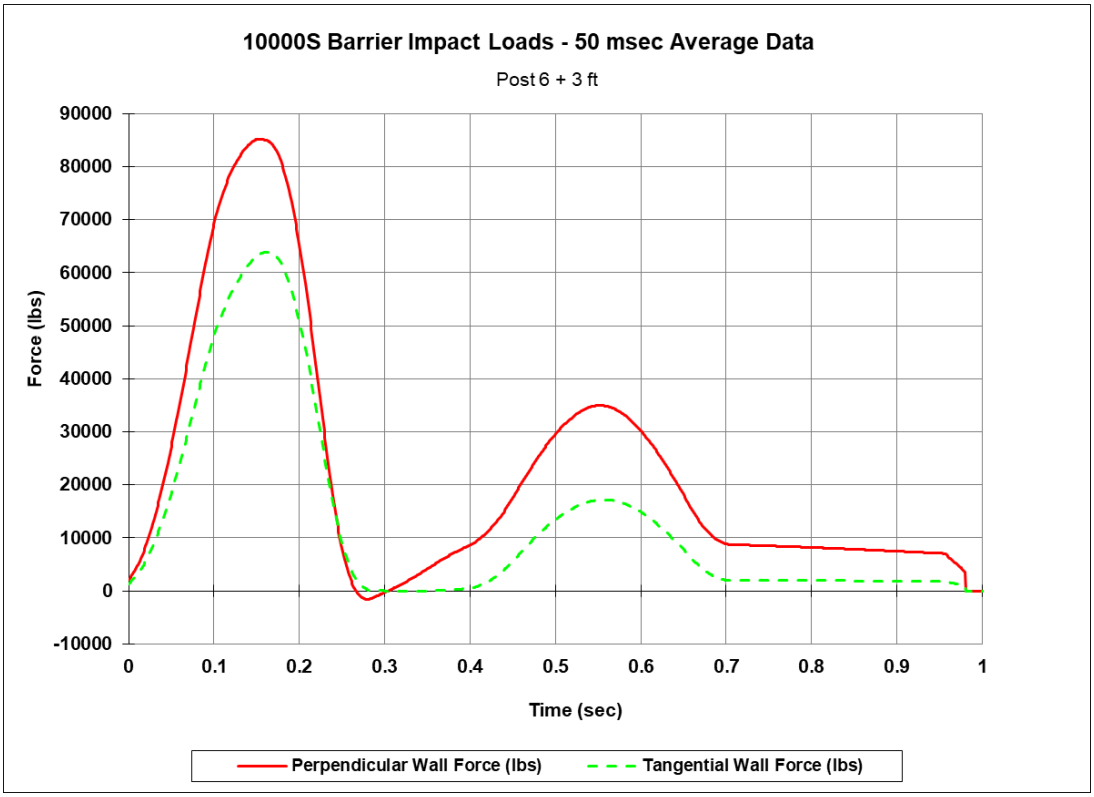

Figure 41. Impact Force vs. Time for 10000S Simulation

Through analysis of the data provided in Table 30, it was recognized that performing crash testing utilizing alternate points of impact may be viable as there are multiple impact points that resulted in similar simulation results. For example, if the critical impact point was chosen to replicate 10000S simulation no. 19 from Table 30, located 2 ft downstream from post no. 6, one would expect to observe slightly more deflection, but the tensile force in the rail and the length of the upper rail which reaches yield would be expected to be lower. It was also apparent that impacting the system 2 or 3 ft downstream from post no. 5 would provide very similar results as impacting the system 2 or 3 ft downstream from post no. 6. With the understanding that multiple impact points could be chosen and provide similar results, it is still recommended to impact the system 3 ft downstream from post no. 6. If additional information becomes available through future research efforts that would suggest an alternate impact location, further analysis will need to be performed.

Table 30. Critical Impact Point Data for 10000S Simulations

Run	Vehicle	Impact Node	Max Defl. (in.)	Max Force (k)	Posts Yielded	Upper Rails Yielded	Curb Rails Yielded	Lateral Load (Global)	Longitudinal Load (Global)
1	10000S	80	7.56	59.28	1	13	2	84.43	62.20
2	10000S	84	7.90	67.06	1	13	2	84.18	61.90
3	10000S	88	8.05	73.98	2	9	2	84.47	63.07
4	10000S	92	7.94	75.04	2	10	0	84.99	63.88
5	10000S	96	7.77	73.12	2	9	0	85.57	64.50
6	10000S	100	7.61	68.54	1	8	2	85.70	64.57
7	10000S	104	7.46	63.32	1	12	2	85.67	64.17
8	10000S	108	7.30	58.07	1	13	2	84.93	63.06
9	10000S	112	7.54	59.49	1	12	2	84.45	62.19
10	10000S	116	7.89	67.61	1	13	2	84.25	61.94
11	10000S	120	8.05	74.83	2	9	2	84.48	63.05
12	10000S	124	7.92	75.58	2	10	0	85.15	63.96
13	10000S	128	7.76	73.75	2	9	0	85.57	64.49
14	10000S	132	7.61	69.09	1	8	2	85.71	64.57
15	10000S	136	7.47	64.07	1	13	2	85.59	64.12
16	10000S	140	7.30	58.53	1	13	2	84.95	63.07
17	10000S	144	7.54	60.04	1	12	2	84.49	62.22
18	10000S	148	7.89	68.18	1	13	2	84.24	61.88
19	10000S	152	8.05	75.50	2	9	2	84.54	63.09
20	10000S	156	7.92	76.26	2	10	0	85.15	63.95
21	10000S	160	7.76	74.27	2	9	0	85.59	64.50
22	10000S	164	7.61	69.50	1	8	2	85.67	64.52
23	10000S	168	7.47	64.43	1	13	2	85.52	64.04
24	10000S	172	7.29	58.90	1	13	2	84.98	63.09
25	10000S	176	7.54	60.51	1	13	2	84.44	62.16

3 SUMMARY, CONCLUSIONS, AND FUTURE RESEARCH

3.1 Summary and Conclusions

Through these research efforts, an updated design configuration for a MASH 2016 TL-4 crashworthy glulam timber rail with curb bridge railing system was developed. In the process of developing this bridge railing system, a thorough review of similar systems developed under previous crash testing standards was performed. The most recent iteration of this type of system, developed by MwRSF in the 1990s under NCHRP Report 350, served as an initial basis for this further development.

In order to create a new system deemed acceptable under MASH criteria, simulation using BARRIER VII software was performed with models originally developed for the NCHRP Report 350 system. The goal was to calibrate the models to the data obtained through full-scale crash testing that was performed at the time. With a calibrated model, the components of the system could then be modified and simulations could be performed with MASH vehicles to help predict the behavior of the system. Once a model was developed that would perform satisfactorily in simulation, final designs could be detailed and further component and full-scale crash testing could be performed to ensure adequacy of the system.

To begin, the original models were examined piece by piece and general updates were made to utilize the increased capacities of BARRIER VII. These updates included the incorporation of smaller elements in order to produce more accurate and detailed results, as well as the refinement of timber properties, as calculated through updated design procedures according to 2018 NDS and AASHTO LRFD. After extensive investigation and updating of the model, the research team believed to have built a calibrated model that reasonably replicated that original crash testing results. Simulation with updated MASH vehicles and further modifications to the system were then made to attempt to develop a system that would be MASH crashworthy. In this process, uncertainties were recognized due to certain modeling schemes that were used, and a new calibration effort began based on a new method of modeling.

New efforts were made to develop a calibrated model and proceed with further development. Through changing the modeling scheme and applying modifications to post stiffnesses and strengths based on data from previous research, a second calibrated model was created and used going forward. To then update the system to meet MASH criteria, height increases were applied to both the upper and curb rails; the curb and scupper block configuration, including the bolts connecting the system to the deck, was changed; and eventually, a larger upper rail was implemented. Through these changes, a system was developed that performed satisfactorily in simulation based on overall behavior. This included information in regard to the vehicle being slowed down and redirected, acceptable deformations of the bridge railing, and acceptable forces and yielding of elements in the system. Following the development of this model, additional research efforts were made in order to identify the critical impact point when performing crash testing using both the 2270P and 10000S vehicles.

The final bridge railing design utilizes all glulam components. The upper rail is to be a 10¾-in. deep by 13½-in. tall glulam beam, while the curb rail should be an 8¾-in. tall by 12-in. deep glulam beam. The curb rail will be placed on two scupper blocks that each measure 5⅛ in. tall by 12 in. deep. The posts are to be 8¾ in. wide by 10½ in. deep. Connection hardware and

splices are yet to be designed, but in order to obtain adequate strength as modeled, a minimum of eight ¾-in. diameter ASTM A307 timber bolts should be used in the vertical connection between the curb and scupper system and the deck. With each of these components incorporated into the BARRIER VII model, the critical impact point for the 2270P vehicle was determined to be 4 ft upstream from post no. 7, and the critical impact point for the 10000S vehicle was determined to be 5 ft upstream from post no. 7. In testing, there should be a splice located at post no. 7 based on guidelines from MASH 2016. Simulation of these impact scenarios predicts a maximum deflection of approximately 6.44 in. and 7.92 in. for the 2270P pickup truck and 10000S single-unit truck impacts, respectively.

3.2 Future Research

Going forward, continued research will be performed in order to complete Phase IIb of this project. This research study is expected to cover the following tasks and subtasks.

Task 0 – Project Planning and Management, Client Correspondence, and Project Updates

Task 1 – Bridge Railing System - Background, Analysis, Design, Computer Simulation, and CAD Details

- Subtask 1 – Using electronic survey, direct communications, literature, and USDA-FS-FPL expertise, identify critical deck types and determine ranges for critical parameters (deck thickness, cantilevered deck overhang, panel width and length) for selected timber decks (i.e., longitudinal glulam timber deck, transverse glulam timber deck, and any alternative deck options to be considered). Obtain feedback from external stakeholders as needed. In this study (i.e., Phase IIa), 35% this subtask was completed, and the remaining 65% will be completed in Phase IIb.

- Subtask 2 – Develop a baseline BARRIER VII computer simulation model for use in an impact investigation and calibration effort of the NCHRP 350 TL-4 Glulam timber rail with curb bridge railing system. Simulate crashes under test designation nos. 4-11 and 4-12 but using actual crash conditions. Compare simulated performance to physical crash results. Modify and refine material parameters and structural model as needed. If deemed appropriate, consider impacts at varied locations along railing system. 100% of this subtask was completed in Phase IIa.

- Subtask 3 – Conduct computer simulation of MASH 2016 TL-4 crashes into existing bridge railing configuration with test designation nos. 4-11 and 4-12. Use target MASH impact conditions for simulation effort. Evaluate suitability of existing design under MASH crash tests. As needed, modify system configuration to meet loading from pickup truck and single-unit truck impact events. Modify the BARRIER VII model to incorporate additional design revisions. Consider impacts at varied locations along railing system. 100% of this subtask was completed in Phase IIa.

- Subtask 4 – Investigate design modifications for accommodating a future 2-in. thick, asphalt overlay placed on top of the deck and initial 2-in. thick asphalt wearing surface. Use target MASH impact conditions for simulation effort. Modify the BARRIER VII model to incorporate additional design revisions. Consider impacts at varied locations along railing system to determine critical impact point. It should be noted that 60% of this task was completed in this study and the remaining 40% will be completed in Phase IIb of the project.

- Subtask 5 – Determine final design with recommendations. Complete preliminary bridge railing configuration and prepare 3-D Solidworks model and 2-D plans for bridge railing system with sizes, preservative treatment, and material specifications for all components (i.e., upper glulam rail, lower glulam rail, glulam scuppers, glulam spacer blocks, and all structural steel connection hardware). If desired, seek feedback from external stakeholders. Modify system configuration as needed. Document Task 1 findings in an ongoing research report.

Task 2 – Approach Guardrail Transition System - Background, Analysis, Design, Dynamic Bogie Testing, Computer Simulation, and CAD Details

- Subtask 6 – Develop a baseline BARRIER VII computer simulation model for use in an impact investigation and calibration effort of the NCHRP 350 TL-4 thrie-beam rail and timber curb transition to the glulam timber rail with curb bridge railing system. Simulate crashes under test designation no. 3-21 but using actual crash conditions. Compare simulated performance to physical crash results. Modify and refine material parameters and structural model as needed. If deemed appropriate, consider impacts at varied locations along railing system near bridge railing end.

- Subtask 7 – Conduct a literature review on post-soil resistance for standard steel posts and wood posts using existing dynamic component testing data. Review larger steel transition posts (e.g., W6x15 (W152x22.3)) embedded in soil and wood posts of multiple cross-sections and embedment depths located adjacent to the bridge rail and evaluate the force vs. deflection and energy vs. deflection behavior of posts during rotation through soil. Evaluate the dynamic impact behavior of various sizes of wood posts and identify equivalent wood posts for the W6x9 (W152x13.4) and W6x15 (W152x22.3) steel post sizes used in the Midwest Guardrail System (MGS) approach guardrail transitions. Identify wood posts equivalent to the W6x15 (W152x22.3) steel post in terms of post-soil resistances and a reduced propensity to fracture compared to smaller post cross-sections.

- Subtask 8 – Identify and develop test setup, test plan, and test matrix for the bogie testing program. Prepare 3-D Solidworks model and 2-D plans for the bogie testing program with all construction materials and specifications. Conduct three (3) bogie tests on two wood post groups in soil to evaluate each of the post group behaviors and understand how closely-spaced wood posts interact with each other through the granular soil media. Document the three bogie tests with onboard sensors, videos, and photographs. Analyze and evaluate all data collected through dynamic

component testing and make comparisons between tests. All tests will be conducted with critical wood post sizes, embedments, and spacings identified in Subtask 7. The bogie tests will be conducted according to MwRSF's list of accredited testing services granted by the A2LA laboratory accreditation body (A2LA Cert. No. 2937.01).

- Subtask 9 – Conduct computer simulation of MASH 2016 TL-3 crashes into existing thrie-beam rail and timber curb transition to bridge railing configuration with test designation no. 3-21. Use target MASH impact conditions for simulation effort. Evaluate suitability of existing design to MASH crash tests. As needed, modify system configuration to meet loading from pickup truck impact events. Modify the BARRIER VII model to incorporate additional design revisions. Consider impacts at varied locations along railing system near bridge railing end.

- Subtask 10 – Modify thrie-beam rail and timber curb transition system to include an upstream stiffness transition to Midwest Guardrail System (MGS). Investigate design modifications for accommodating a future 2-in. thick, asphalt overlay placed on top of the roadway. Use target MASH impact conditions for simulation effort. Modify the BARRIER VII model to incorporate additional design revisions. Consider impacts at varied locations along railing system to determine critical impact point.

- Subtask 11 – Determine final design with recommendations. Complete preliminary transition configuration and prepare 3-D Solidworks model and 2-D plans for thrie-beam rail and timber curb transition with upstream stiffness transition to MGS with sizes, preservative treatment, and material specifications for all components (i.e., lower glulam rail, glulam/sawn guardrail spacer blocks, thrie-beam and W-beam rails, end anchorage hardware, and all structural steel connection hardware). If desired, seek feedback from external stakeholders. Modify system configuration as needed. Document Task 2 findings in an ongoing research report.

Task 3 – Timber Deck System - Dynamic Component Testing

- Subtask 12 – Identify and develop test setup, test plan, deck configurations, surrogate post and deck attachment, surrogate substructure, and test matrix for dynamic component testing program. Prepare 3-D Solidworks model and 2-D plans for dynamic component testing program with all construction materials, including preservative treatment and material specifications. Determine requirements for any special instrumentation of bridge railing components.

- Subtask 13 – Prepare site at MwRSF's Outdoor Proving Grounds. Acquire timber posts, timber post-to-deck attachment hardware, timber spacer blocks, timber deck panels, and steel connection hardware for use in the dynamic component testing program. Acquire, fabricate, and install substructure system for supporting and anchoring deck panels with posts and post-to-deck attachment hardware.

- Subtask 14 – Install several timber systems on surrogate substructures and conduct six (6) instrumented, dynamic component tests. Document the component tests with videos and photographs. Remove systems, restore test site, and dispose of debris. Use electronic instrumentation on system components as needed.

- Subtask 15 – Analyze test results and make comparisons between tests and deck systems. Determine the critical timber deck system with recommendations for use in the full-scale crash testing and evaluation program. If desired, seek feedback from external stakeholders. Document Task 3 findings in an ongoing research report.

4 REFERENCES

1. Ross, H.E., Sicking, D.L., Zimmer, R.A., and Michie, J.D., *Recommended Procedures for the Safety Performance Evaluation of Highway Features*, National Cooperative Highway Research Program (NCHRP) Report 350, Transportation Research Board, Washington, D.C., 1993.

2. *Guide Specifications for Bridge Railings*, American Association of State Highway and Transportation Officials (AASHTO), Washington, D.C., 1989.

3. *Manual for Assessing Safety Hardware (MASH)*, American Association of State Highway and Transportation Officials (AASHTO), Washington, D.C., 2009.

4. *Manual for Assessing Safety Hardware (MASH), Second Edition*, American Association of State Highway and Transportation Officials (AASHTO), Washington, D.C., 2016.

5. Rosenbaugh, S.K., Benner, C.D., Faller, R.K., Bielenberg, R.W., Reid, J.D., and Sicking, D.L., *Development of a TL-1 Timber, Curb-Type, Bridge Railing for Use on Transverse, Nail-Laminated, Timber Bridges*, Final Report to the West Virginia Department of Transportation, Transportation Research Report No. TRP-03-211-09, Midwest Roadside Safety Facility, University of Nebraska-Lincoln, Lincoln, Nebraska, May 6, 2009.

6. Mongiardini, M, Rosenbaugh, S.K., Faller, R.K., Reid, J.D., Bielenberg, R.W., and Sicking, D.L., *Design and Testing of Two Bridge Railings for Transverse, Nail-Laminated, Timber Deck Bridges*, Paper No. 11-2936, Transportation Research Record No. 2262, Journal of the Transportation Research Board, TRB AFB20 Committee on Roadside Safety Design, Transportation Research Board, Washington D.C., January 2011.

7. Williams, W.F., *W-Beam Bridge Rail for Temporary Timber Deck Bridge Installations*, Memorandum, TM-405160-40, Texas A&M Transportation Institute, College Station, TX. August 2013.

8. Duren, J.T., and Faller, R.K., *Crash-Tested Bridge Railings and Transitions for Wood Bridges – Phase I*, Final Report to the United States Department of Agriculture-Forest Service-Forest Products Laboratory, Transportation Report No. TRP-03-429-20-R1, Midwest Roadside Safety Facility, University of Nebraska-Lincoln, Lincoln, Nebraska, July 2020.

9. *National Design Specification Supplement*, 2018 Edition, Third Electronic Version, ANSI/AWC NDS-2018, American Wood Council, April 2019.

10. Faller, R.K., and Rosson, B.T., *Development of a Flexible Bridge Railing for Longitudinal Timber Decks*, Draft Report to the United Sates Department of Agriculture-Forest Service-Forest Products Laboratory, Transportation Report No. TRP-03-62-96, Midwest Roadside Safety Facility, University of Nebraska-Lincoln, Lincoln, Nebraska, June 1997.

11. Faller, R.K., Rosson, B.T., and Fowler, M.D., *Top-Mounted W-Beam Bridge Railing for Longitudinal Glulam Timber Decks Located on Low-Volume Roads*, Draft Report to the United Sates Department of Agriculture-Forest Service-Forest Products Laboratory, Transportation Report No. TRP-03-61-96, Midwest Roadside Safety Facility, University of Nebraska-Lincoln, September 1996.

12. Fowler, M.D., *Design and Testing of a Test Level 4 Bridge Railing for Transverse Glulam Timber Deck Bridges*, Study, University of Nebraska – Lincoln, May 1997.

13. Powell, G.H., *Computer Evaluation of Automobile Barrier Systems*, Report No. FHWA-RD-73-73, FHWA, August 1970.

14. Powell, G.H., *BARRIER VII: A Computer Program for Evaluation of Automobile Barrier Systems*, Report No. FHWA-RD-73-51, FHWA, U.S. Department of Transportation, April 1973.

15. Beason, W.L., Hirsch, T.J., and Campise, W.L., *Measurement of Heavy Vehicle Impact Forces and Inertia Properties*, Report No. FHWA-RD-89-120, Submitted to the Office of Safety and Traffic Operations R&D, Federal Highway Administration, Texas Trasportation Institute, Texas A&M University, May 1989.

16. Sicking, D.L., Mak, K.K., Rohde, J.R., and Reid, J.D., *Recommended Procedures for the Safety Performance Evaluation of Highway Features*, NCHRP Project No. 22-14(2), National Cooperative Highway Research Program, February 2007.

17. *Manual for Engineered Wood Construction*, 2018 Edition, First Web Version, ANSI/AWC NDS-2018, American Wood Council, September 2018.

18. *AASHTO LRFD Bridge Design Specifications, 9th Edition*, American Association of State Highway and Transportation Officials (AASHTO), Washington, D.C., 2020.

19. Bender, D. and Woeste, F., *Effect of Variability on Lumber Design Values*, Frame Building News, August 2012. <http://www.constructionmagnet.com/wp-content/uploads/0812-RT-Lumber-Design.pdf> Last accessed July 8, 2021.

20. *ASTM Standard D1990-19 Standard Practice for Establishing Allowable Properties for Visually-Graded Dimension Lumber from In-Grade Tests of Full-Size Specimens*, Revised 2019, ASTM International, West Conshohocken, Pennsylvania. DOI: https://doi.org/10.1520/D1990-19

21. Moody, R., Falk, R., and Williamson, T., *Strength of Glulam Beams – Volume Effects*, Proceedings of the 1990 International Timber Engineering Conference, Tokyo, October 1990.

22. Green, D.W., and Kretschmann, D.E., *Properties and Grading of Southern Pine Timbers*, Forest Products Journal, Vol. 47, No. 9, Madison, Wisconsin, September 1997.

23. Littleford, T.W., *A Comparison of Flexural Strength-Stiffness Relationships for Clear Wood and Structural Grades of Lumber*, Info. Rep. VP-X-30, Forestry Branch, Forest Products Laboratory, Vancouver, British Columbia, 1967.

24. Polivka, K.A., Rohde, J.R., Faller, R.K., Holloway, J.C., and Sicking, D.L., *Design and Evaluation of Minnesota's Timber Rub-Rail Noise Barriers*, Report No. TRP-03-156-05, Midwest Roadside Safety Facility, University of Nebraska-Lincoln, Lincoln, Nebraska, March 8, 2005.

25. Schmidt, J.D., Asselin, N., Faller, R.K., Fallet, W.G., Holloway, J.C., and Lechtenberg, K.A., *Evaluation of the Minnesota Noise Wall and Rubrail System*, Report No. TRP-03-396-19, Midwest Roadside Safety Facility, University of Nebraska-Lincoln, Lincoln, Nebraska, January 31, 2019.

26. Reid, J.D., Letter to Yvonne D. Murray, *NDOR Post Testing 1995*, Midwest Roadside Safety Facility, University of Nebraska-Lincoln, Lincoln, Nebraska, June 27, 2000.

27. Calcote, L.R., *Development of a Cost-Effectiveness Model for Guardrail Selection*, Vol. I, Report No. FHWA-RD-78-74, Southwest Research Institute, San Antonio, Texas, January, 1980.

28. Gatchell, C.J., and Michie, J.D., *Pendulum Impact Tests of Wooden and Steel Highway Guardrail Posts*, Research Paper NE-311, U.S. Department of Agriculture, Forest Servive, Northeastern Forest Experiment Station, Upper Darby, Pennsylvania, 1974.

29. Sheikh, N.M., Bligh, R.P., and Menges, W.L., *Determination of Minimum Height and Lateral Design Load for MASH Test Level 4 Bridge Rails*, Report No. FHWA/TX-12/9-1002-5, Texas A&M Transportation Institute, College Station, Texas, December 2011.

30. Bligh, R.P., Menges, W.L., and Kuhn, D.L., *MASH Evaluation of TxDOT Roadside Safety Features – Phase I*, Report No. 0-6946-1, Texas A&M Transportation Institute, College Station, Texas, January 2018.

31. Williams, W.F., Sheikh, N.M., Menges, W.L., Kuhn, D.L., and Bligh, R.P., *Crash Test and Evaluation of Restrained Safety-Shape Concrete Barriers on Concrete Bridge Decks*, Report No. 9-10002-15-3, Texas A&M Transportation Institute, College Station, Texas, January 2018.

32. Rosenbaugh, S.K., Rasmussen, J.D., Dixon, J.D., Loken, A., Flores, J., and Faller, R.K., *Development and Testing of an Optimized MASH Test Level 4 Bridge Rail*, Report No. TRP-03-415-20, Midwest Roadside Safety Facility, University of Nebraska-Lincoln, Lincoln, Nebraska, April 20, 2020.

33. Pena, O., Faller, R.K., Rasmussen, J.D., Steelman, J.S., Rosenbaugh, S.K., Bielenberg, R.W., Mauricio, P., and Duren, J.T., *Development of a MASH Test Level 4 Steel, Side-Mounted, Beam-and-Post, Bridge Rail*, Transportation Research Report No. TRP-03-410-20, Midwest Roadside Safety Facility, University of Nebraska-Lincoln, July 2020.

34. Fancher, P.S., Ervin, R.D., Winkeler, C.B., and Gillespie, T.D., *A Factbook of the Mechanical Properties of the Components for Single-Unit and Articulated Heavy Trucks*, Phase I Final Report, Report No. UMTRI-86-12, Transportation Research Institute, University of Michigan, March 1986.

35. Nauman, M.S., Bligh, R.P., Menges, W.L., *Determination of Minimum Height and Lateral Design Load for MASH Test Level 4 Bridge Rails,* Report No. FHWA/TX-12/9-1002-5, Texas Transportation Institute, College Station, Texas, 2011.

36. Rosenbaugh, S.K., Rasmussen, J.D., and Faller, R.K., *Development and Testing of a Test Level 4 Concrete Bridge Rail and Deck Overhang*, Midwest Roadside Safety Facility, University of Nebraska-Lincoln, Lincoln, Nebraska, August 1, 2019.

37. Rosenbaugh, S.K., Rasmussen, J.D., Dixon, J., Loken, A., Flores, J., and Faller, R.K., *Development and Testing of an Optimized MASH Test Level 4 Bridge Rail*, Report No. TRP-03-415-20, Midwest Roadside Safety Facility, University of Nebraska-Lincoln, Lincoln Nebraska, April 20, 2020.

38. Wight, J.K., and MacGregor, J.G., *Reinforced Concrete Mechanics and Design*, Sixth Edition, Pearson Education, Upper Saddle River, New Jersey, 2012.

39. Hopkins, D.J., *The Fire Performance of Engineered Timber Products and Systems*, Dissertation, Loughborough University, June 2011.

40. *ASTM Standard A307-21 Standard Specification for Carbon Steel Bolts, Studs, and Threaded Rod 60000 PSI Tensile Strength*, Revised 2021, ASTM International, West Conshohocken, Pennsylvania. DOI: https://doi.org/10.1520/A0307-21.

41. Breyer, D.E., Fridley, K.J., Cobeen, K.E., and Pollock, D.G., *Design of Wood Structures – ASD/LRFD*, Sixth Edition, McGraw-Hill, New York, New York, 2007.

42. DeLone, J., *Development of a MASH Test Level 4 Open Concrete Bridge Rail*, Study, University of Nebraska – Lincoln, July 2020.

43. *Steel Construction Manual,* American Institute of Steel Construction (AISC), Fifteenth Edition, First Printing, 2017.

5 APPENDICES

Appendix A. Previous BARRIER VII Vehicle and Bridge Railing Models

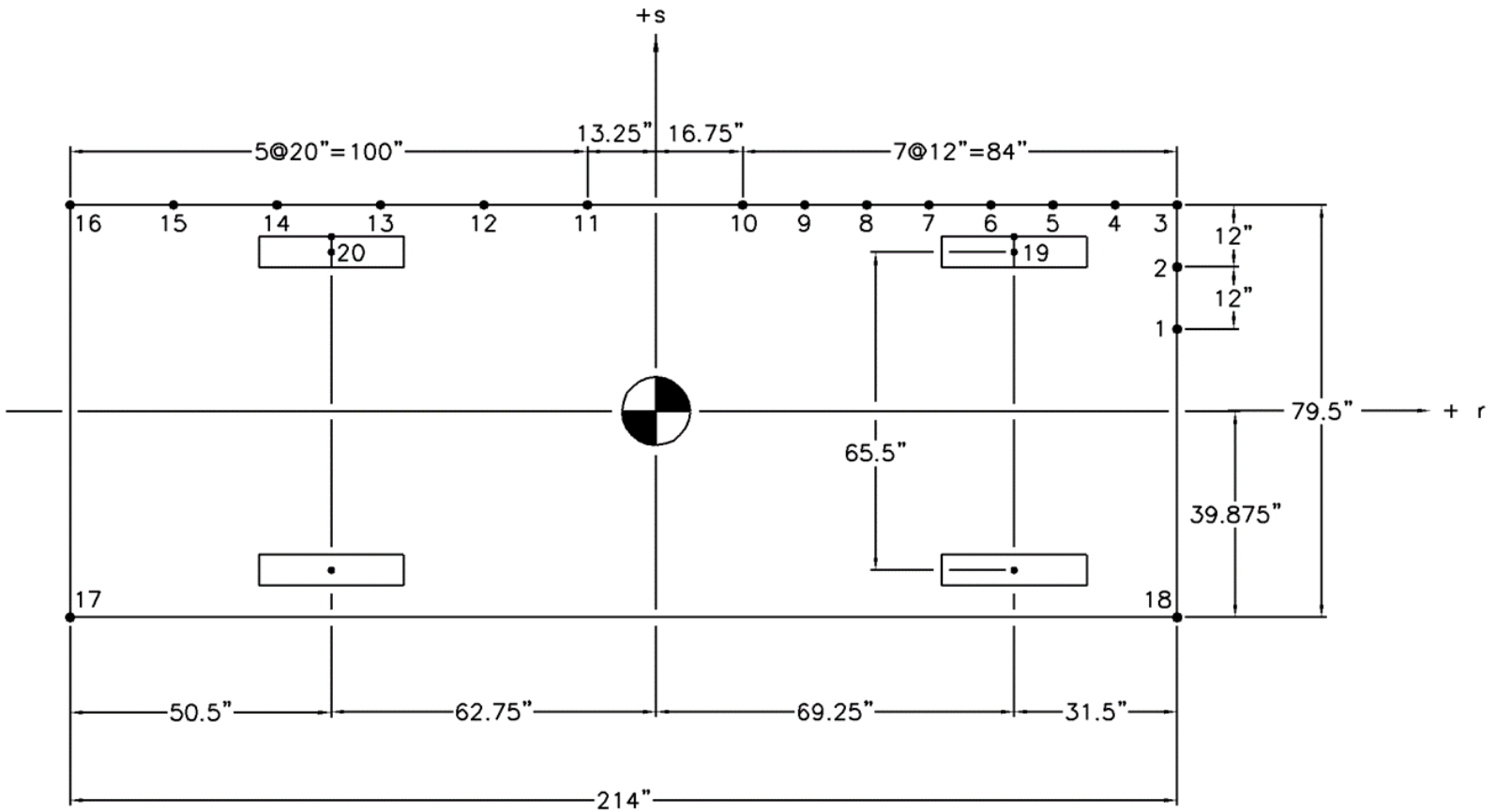

Figure A-1. BARRIER VII 2000P Pickup Truck Model

BARRIER VII 2000P Vehicle Input File

```
NCHRP 350 2000P
    4393.0   40000.0   20    6    4    0    1
    1     0.055      0.12      6.00      17.0
    2     0.057      0.15      7.00      18.0
    3     0.062      0.18     10.00      12.0
    4     0.110      0.35     12.00       6.0
    5      0.35      0.45      6.00       5.0
    6      1.45      1.50     15.00       1.0
    1    100.75    15.875    1      12.0    1    0    0    0
    2    100.75    27.875    1      12.0    1    0    0    0
    3    100.75    39.875    2      12.0    1    0    0    0
    4     88.75    39.875    2      12.0    1    0    0    0
    5     76.75    39.875    2      12.0    1    0    0    0
    6     64.75    39.875    2      12.0    1    0    0    0
    7     52.75    39.875    2      12.0    1    0    0    0
    8     40.75    39.875    2      12.0    1    0    0    0
    9     28.75    39.875    2      12.0    1    0    0    0
   10     16.75    39.875    2      12.0    1    0    0    0
   11    -13.25    39.875    3      12.0    1    0    0    0
   12    -33.25    39.875    3      12.0    1    0    0    0
   13    -53.25    39.875    3      12.0    1    0    0    0
   14    -73.25    39.875    3      12.0    1    0    0    0
   15    -93.25    39.875    3      12.0    1    0    0    0
   16   -113.25    39.875    4      12.0    1    0    0    0
   17   -113.25   -39.875    4      12.0    0    0    0    0
   18    100.75   -39.875    1      12.0    0    0    0    0
   19     69.25     37.75    5       1.0    1    0    0    0
   20    -62.75     37.75    6       1.0    1    0    0    0
    1     69.25     37.75       0.0      608.
    2     69.25    -37.75       0.0      608.
    3    -62.75     37.75       0.0      492.
    4    -62.75    -37.75       0.0      492.
    1       0.0       0.0
    3    1108.5       0.0      27.4     61.64       0.0       0.0       5.0
```

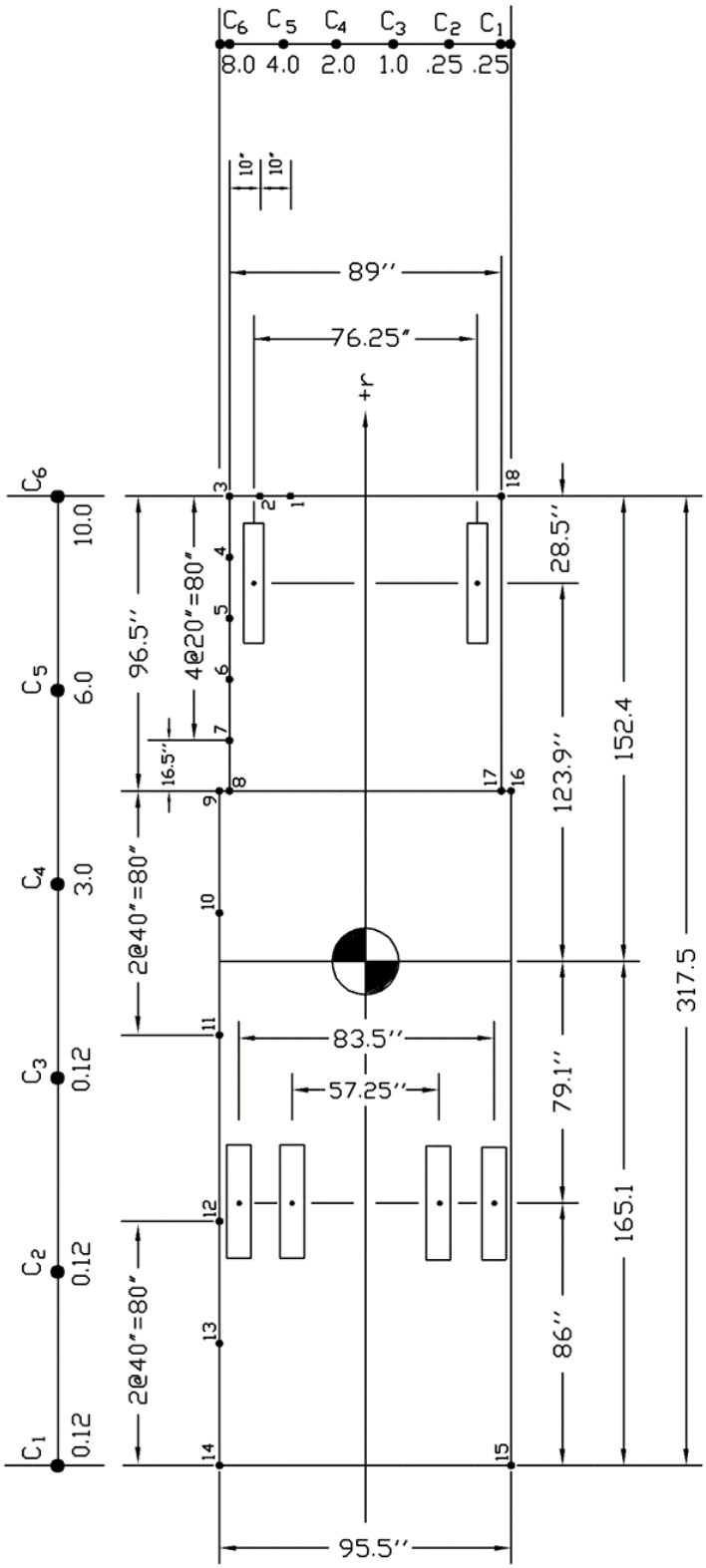

Figure A-2. BARRIER VII 8000S Single-Unit Truck Model

BARRIER VII 8000S Vehicle Input File

```
NCHRP 350 8000S
   17637.0  561483.4   20    7    6    0    1
    1     0.082      0.21       1.5      18.0
    2     0.063      0.19       2.0      12.0
    3     0.045      0.17       3.0       4.0
    4     0.800      0.95       2.5       2.5
    5     0.900      1.05       3.5       2.0
    6      0.35      0.25      10.0       3.0
    7       2.5       3.5       4.5       3.0
    1     152.4      24.5    1      10.0    1    0    0    0
    2     152.4      34.5    1      10.0    1    0    0    0
    3     152.4      44.5    1      15.0    1    0    0    0
    4     132.4      44.5    1      20.0    1    0    0    0
    5     112.4      44.5    2      20.0    1    0    0    0
    6      92.4      44.5    2      20.0    1    0    0    0
    7      72.4      44.5    2     18.25    1    0    0    0
    8      55.9      44.5    2      11.5    1    0    0    0
    9      55.9     47.75    3     23.25    0    0    0    0
   10      15.9     47.75    4      40.0    0    0    0    0
   11     -24.1     47.75    5      40.0    0    0    0    0
   12     -85.1     47.75    5      40.0    0    0    0    0
   13    -125.1     47.75    5      40.0    0    0    0    0
   14    -165.1     47.75    5      20.0    0    0    0    0
   15    -165.1    -47.75    5       1.0    0    0    0    0
   16      55.9    -47.75    3       1.0    0    0    0    0
   17      55.9     -44.5    2       1.0    0    0    0    0
   18     152.4     -44.5    1       1.0    0    0    0    0
   19     -79.1     45.75    7       1.0    1    0    0    0
   20     123.9     42.12    6       1.0    1    0    0    0
    1     123.9     38.12       0.0     2214.
    2     123.9    -38.12       0.0     2214.
    3     -79.1     41.75       0.0     2755.
    4     -79.1    -41.75       0.0     2755.
    5     -79.1     28.62       0.0     2755.
    6     -79.1    -28.62       0.0     2755.
    1       0.0       0.0
    3    1060.5       0.0      16.0     46.48       0.0       0.0      10.0
```

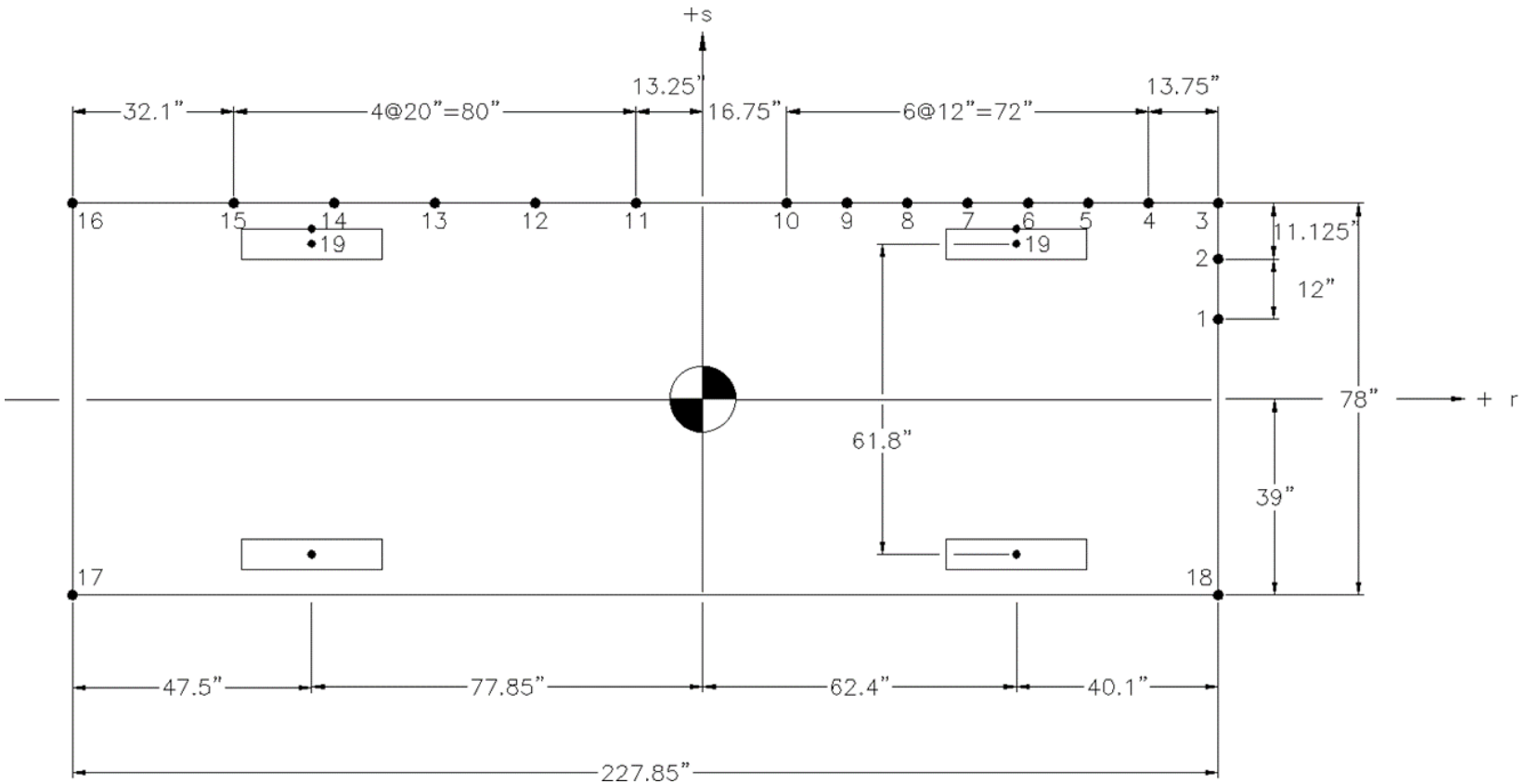

Figure A-3. BARRIER VII 2270P Pickup Truck Model

BARRIER VII 2270P Vehicle Input File

```
MASH 2270P
    5000.0   58310.0   20    6    4    0    1
    1     0.055      0.12      6.00      17.0
    2     0.057      0.15      7.00      18.0
    3     0.062      0.18     10.00      12.0
    4     0.110      0.35     12.00       6.0
    5      0.35      0.45      6.00       5.0
    6      1.45      1.50     15.00       1.0
    1    102.50    15.875    1      12.0    1    0    0    0
    2    102.50    27.875    1      12.0    1    0    0    0
    3    102.50    39.000    2      12.0    1    0    0    0
    4     88.75    39.000    2      12.0    1    0    0    0
    5     76.75    39.000    2      12.0    1    0    0    0
    6     64.75    39.000    2      12.0    1    0    0    0
    7     52.75    39.000    2      12.0    1    0    0    0
    8     40.75    39.000    2      12.0    1    0    0    0
    9     28.75    39.000    2      12.0    1    0    0    0
   10     16.75    39.000    2      12.0    1    0    0    0
   11    -13.25    39.000    3      12.0    1    0    0    0
   12    -33.25    39.000    3      12.0    1    0    0    0
   13    -53.25    39.000    3      12.0    1    0    0    0
   14    -73.25    39.000    3      12.0    1    0    0    0
   15    -93.25    39.000    3      12.0    1    0    0    0
   16   -125.35    39.000    4      12.0    1    0    0    0
   17   -125.35   -39.000    4      12.0    0    0    0    0
   18    102.50   -39.000    1      12.0    0    0    0    0
   19     62.40     33.90    5       1.0    1    0    0    0
   20    -77.85     33.90    6       1.0    1    0    0    0
    1     62.40     33.90       0.0      608.
    2     62.40    -33.90       0.0      608.
    3    -77.85     33.90       0.0      492.
    4    -77.85    -33.90       0.0      492.
    1       0.0       0.0
    3    1108.5       0.0     25.00     62.00       0.0       0.0       1.0
```

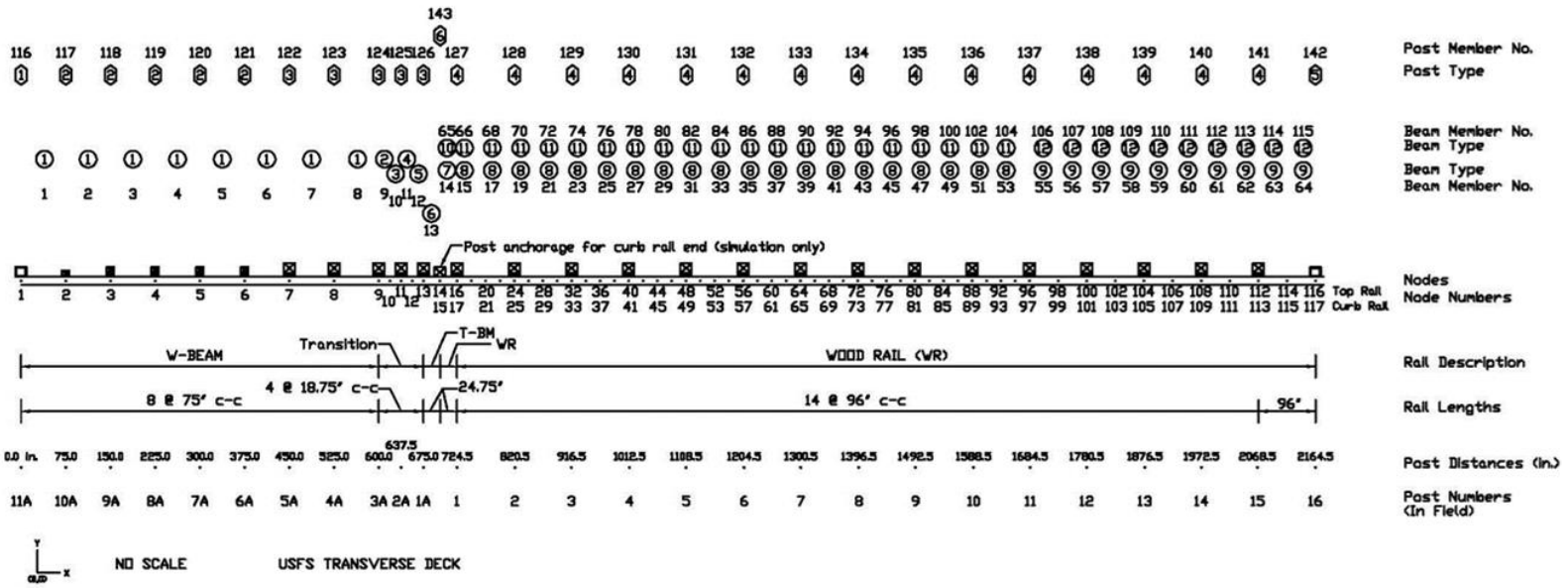

Figure A-4. Original BARRIER VII Model

Appendix B. Timber Strength Calculations

The following equations and calculations were used to determine timber strengths and were utilized in BARRIER VII models to reflect the properties of the different members used to configure the original TL-4 glulam timber rail with curb bridge railing system, as well as the properties for different component sizes in the iteration process utilized to update the system to MASH criteria. The equations as provided in AASHTO LRFD Bridge Design Specification, 9th Edition [18] and the 2018 NDS and supplements [9-17] are shown below, followed by calculations for the final rail and post members used in the bridge railing system updated to meet MASH TL-4 impact safety criteria. These members include a 10¾-in. deep by 13½-in. tall glulam beam for the upper rail, an 8¾-in. tall by 12-in. deep glulam beam for the curb rail, and an 8¾-in. wide by 10½-in. deep glulam post . It should also be noted that an additional strength modification factor, ζ, with a value of 1.33, has been added to all bending equations in order to obtain strengths more representative of a mean or 50th percentile value, as discussed in Section 2.3.2 of this study.

AASHTO LRFD Bridge Design Specification, 9th Edition [18]:

The following are the general timber strength equations from Article 8.4.4:

$$F_b = F_{b0} C_{KF} C_M (C_F \text{ or } C_v) C_{fu} C_i C_d C_\lambda \zeta \quad \text{Eq. D-1}$$

$$F_v = F_{v0} C_{KF} C_M C_i C_\lambda \quad \text{Eq. D-2}$$

$$F_t = F_{t0} C_{KF} C_M C_F C_i C_\lambda \quad \text{Eq. D-3}$$

$$F_c = F_{c0} C_{KF} C_M C_F C_i C_\lambda \quad \text{Eq. D-4}$$

$$F_{cp} = F_{cp0} C_{KF} C_M C_i C_\lambda \quad \text{Eq. D-5}$$

$$E = E_0 C_M C_i \quad \text{Eq. D-6}$$

Where: F_b = applicable adjusted bending design value (ksi)

F_v = applicable adjusted shear design value (ksi)

F_t = applicable adjusted tension design value (ksi)

F_c = applicable adjusted compression parallel to grain design value (ksi)

F_{cp} = applicable adjusted compression perpendicular to grain design value (ksi)

F_0 = reference design values F_{b0}, F_{v0}, F_{t0}, F_{c0}, or F_{cp0} specified in Article 8.4 or 2018 NDS (ksi)

E = adjusted modulus of elasticity (ksi)

E_0 = reference modulus of elasticity specified in Article 8.4.1.1.4 or 2018 NDS (ksi)

C_{KF} = format conversion factor specified in Article 8.4.4.2

C_M = wet service factor specified in Article 8.4.4.3

C_F = size factor for visually-graded dimension lumber and sawn timbers specified in Article 8.4.4.4

C_V = volume factor for structural glued-laminated timber specified in Article 8.4.4.5

C_{fu} = flat-use factor specified in Article 8.4.4.6

C_i = incising factor specified in Article 8.4.4.7

C_d = deck factor specified in Article 8.4.4.8

C_λ = time effect factor specified in Article 8.4.4.9

Moment capacity, from Article 8.6:

$$M_r = \varphi M_n = \varphi F_b S C_L \quad \text{Eq. D-7}$$

Where: M_r = factored moment resistance (k-in.)

M_n = nominal moment resistance (k-in.)

φ = resistance factor

F_b = adjusted design value in flexure (ksi)

S = section modulus (in.^{3})

C_L = beam stability factor, which should not be applied simultaneously with the Volume Factor, C_V, and calculated as follows:

$$C_L = \frac{1+A}{1.9} - \sqrt{\frac{(1+A)^2}{3.61} - \frac{A}{0.95}} \quad \text{Eq. D-8}$$

$$A = \frac{F_{be}}{F_b} \quad \text{Eq. D-9}$$

$$F_{be} = \frac{K_{be}E}{{R_b}^2} \quad \text{Eq. D-10}$$

$$R_b = \sqrt{\frac{L_e d}{b^2}} \leq 50 \quad \text{Eq. D-11}$$

$$L_e \quad \rightarrow if\ \frac{L_u}{d} < 7, then\ L_e = 2.06L_u \quad \text{Eq. D-12}$$

$$\rightarrow if\ 7 \leq \frac{L_u}{d} \leq 14.3, then\ L_e = 1.63L_u + 3d \quad \text{Eq. D-13}$$

$$\rightarrow if\ \frac{L_u}{d} > 14.3, then\ L_e = 1.84L_u \quad \text{Eq. D-14}$$

Where: A = parameter for beam stability

K_{be} = 1.10 for glulam

E = adjusted modulus of elasticity (ksi)

L_e = effective unbraced length (in.)

d = net depth of section (in.)

b = net width (height) of section (in.)

L_u = distance between points of lateral and rotational support (in.)

Shear capacity, from Article 8.7:

$$V_r = \varphi V_n = \varphi \frac{F_v b d}{1.5}$$ Eq. D-15

Where: V_r = factored shear resistance (k)

V_n = nominal shear resistance (k)

φ = resistance factor

F_v = adjusted design value in shear (ksi)

b = width of section (in.)

d = depth of section (in.)

Compression parallel to grain capacity, from Article 8.8.2:

$$P_r = \varphi P_n = \varphi F_c A_g C_p$$ Eq. D-16

Where: P_r = factored compression resistance (k)

P_n = nominal compression resistance (k)

φ = resistance factor

F_c = adjusted design value in compression parallel to grain (ksi)

A_g = gross cross-sectional area (in.^{2})

C_p = column stability factor, calculated as follows:

$$C_p = \frac{1+B}{2c} - \sqrt{\left(\frac{1+B}{2c}\right)^2 - \frac{B}{c}} \leq 1.00$$ Eq. D-17

$$B = \frac{F_{ce}}{F_c} \leq 1.00$$ Eq. D-18

$$F_{ce} = \frac{K_{cE} E d^2}{{L_e}^2}$$ Eq. D-19

Where: B = parameter for column stability

c = 0.9 for glulam

F_{ce} = Euler buckling stress

K_{cE} = Euler buckling coefficient, 0.76 for glulam

E = adjusted modulus of elasticity (ksi)

L_e = effective length (in.)

Compression perpendicular to grain capacity, from Article 8.8.3:

$$P_r = \varphi P_n = \varphi F_{cp} A_b C_b \quad \text{Eq. D-20}$$

Where: P_r = factored compression resistance (k)

P_n = nominal compression resistance (k)

φ = resistance factor

F_c = adjusted design value in compression perpendicular to grain (ksi)

A_b = bearing area (in.^{2})

C_b = bearing adjustment factor, see Table C-1

Table B-1. AASHTO LRFD Bearing Adjustment Factors

Length of Bearing Measured along the Grain (in.)							
C_b	0.5	1.0	1.5	2.0	3.0	4.0	≥6.0
	1.75	1.38	1.25	1.19	1.13	1.10	1.00

Tensile capacity, from Article 8.9:

$$P_r = \varphi P_n = \varphi F_t A_n \quad \text{Eq. D-21}$$

Where: P_r = factored tension resistance (k)

P_n = nominal tension resistance (k)

φ = resistance factor

F_t = adjusted design value in tension (ksi)

A_n = net cross-sectional area (in.^{2})

2018 NDS and 2018 Manual for Engineered Wood Construction [17]:

The following are the general timber strength equations from Article 5.3 of 2018 NDS:

$$F_b' = F_b C_M C_t C_L C_V C_{fu} C_c C_I K_F \varphi \lambda \zeta \quad \text{Eq. D-22}$$

$$F_v' = F_v C_M C_t C_{vr} K_F \varphi \lambda \quad \text{Eq. D-23}$$

$$F_t' = F_t C_M C_t K_F \varphi \lambda \quad \text{Eq. D-24}$$

$$F_c' = F_c C_M C_t C_P K_F \varphi \lambda \quad \text{Eq. D-25}$$

$$F_{c\perp}' = F_{c\perp} C_M C_t C_b K_F \varphi \quad \text{Eq. D-26}$$

$$E' = E C_M C_t \quad \text{Eq. D-27}$$

$$E_{min}' = E_{min} C_M C_t K_F \varphi \quad \text{Eq. D-28}$$

Where: F_b' = applicable adjusted bending design value (ksi)

F_v' = applicable adjusted shear design value (ksi)

F_t' = applicable adjusted tension design value (ksi)

F_c' = applicable adjusted compression parallel to grain design value (ksi)

$F_{c\perp}$' = applicable adjusted compression perpendicular to grain design value (ksi)

F = reference design values F_b, F_v, F_t, F_c, or $F_{c\perp}$ specified in Tables 5A through 5D of 2018 NDS (ksi)

E' = adjusted modulus of elasticity (ksi)

E = reference modulus of elasticity specified Tables 5A through 5D of 2018 NDS (ksi)

E_{min}' = adjusted minimum modulus of elasticity (ksi)

E_{min} = reference minimum modulus of elasticity specified Tables 5A through 5D of 2018 NDS (ksi)

C_M = wet service factor specified in Tables 5A through 5D

C_t = temperature factor specified in Article 2.3.3

C_L = beam stability factor specified in Article 3.3.3, not to be applied simultaneously with the volume factor, C_V, so use the lesser

C_V = volume factor specified in Article 5.3.6

C_{fu} = flat-use factor specified in Tables 5A through 5D or Article 5.3.7

C_c = curvature factor specified in Article 5.3.8

C_I = stress interaction factor specified in Article 5.3.9

C_{vr} = shear reduction factor specified in Article 5.3.10

C_P = column stability factor specified in Article 3.7

C_b = bearing area factor specified in Article 3.10.4

K_F = format conversion factor specified in Table 5.3.1

φ = resistance factor specified in Table 5.3.1

λ = time effect factor specified in Appendix N.3.3

Moment capacity, from Article M3.3 of 2018 Manual for Engineered Wood Construction:

$$M' = F_b'S \qquad \text{Eq. D-29}$$

Where: M' = adjusted moment capacity (k-in.)

F_b' = adjusted design value in flexure (ksi)

S = section modulus (in.^{3})

Shear capacity, from Article M3.4 of 2018 Manual for Engineered Wood Construction:

$$V' = \frac{2F_v'A}{3} \qquad \text{Eq. D-30}$$

Where: V' = adjusted shear resistance (k)

F_v' = adjusted design value in shear (ksi)

A = cross-section area (in.^{2})

Compression parallel to grain capacity, from Article M3.6 of 2018 Manual for Engineered Wood Construction:

$$P' = F_c'A \qquad \text{Eq. D-31}$$

Where: P' = adjusted compression resistance (k)

F_c' = adjusted design value in compression parallel to grain (ksi)

A = cross-sectional area (in.^{2})

Compression perpendicular to grain capacity, from Article 3.10 of 2018 NDS:

$$P' = F_{c\perp}' A_b$$ Eq. D-32

Where: P' = adjusted compression resistance (k)

$F_{c\perp}'$ = adjusted design value in compression perpendicular to grain (ksi)

A_b = bearing area (in.^{2})

Tensile capacity, from Article 8.9 of 2018 NDS:

$$P' = F_t' A_n$$ Eq. D-33

Where: P' = adjusted tension resistance (k)

F_t' = adjusted design value in tension (ksi)

A_n = net cross-sectional area (in.^{2})

Strength and Capacity Calculations for Upper Rail:

General Rail Details:

Depth = 10 ¾ in.

Height = 13 ½ in.

Length = 8 ft (distance from post to post, considered unbraced length)

Glulam Combination: Comb. 2 – DF

$F_{b0} = F_b = 1{,}800$ psi

$F_{v0} = F_v = 230$ psi

$F_{t0} = F_t = 1{,}250$ psi

$F_{c0} = F_c = 1{,}950$ psi

$F_{cp0} = F_{c\perp} = 560$ psi

$E_0 = E = 1{,}600{,}000$ psi

$E_{min} = 850{,}000$ psi

AASHTO LRFD Factors:

C_{KF}, Format Conversion Factor:

Code: Utilize 2.50/φ for all strength states other than compression perpendicular to the grain, in which 2.10/φ should be used.

Values Utilized:

For F_b, F_v, F_t, and F_c: $C_{KF} = 2.50$

For F_{cp}: $C_{KF} = 2.10$

Reasoning: According to Article 8.5.3, the resistance factor, φ, should be taken as 1.00 for extreme event limit states, and under Article 3.4.1, the Extreme Event II limit state includes collision by vehicles.

C_M, Wet Service Factor:

Code: Utilize 1.00 for glulam timber with an in-service moisture content of 16% or less, otherwise refer to Table 8.4.4.3-2.

Values Utilized:

For F_b, F_v, F_t, F_c, F_{cp}, and E: $C_M = 1.00$

Reasoning: Based on the contents of Chapter 13 in the Wood Handbook, specifically Table 13-1, which includes data for average moisture contents of wood in outdoor conditions for many cities across the U.S., and Table 13-2, which is recommended moisture contents for wood products at time of installation, it was found that typical conditions would not cause members of the bridge railing system to have a moisture content above 16% [43]. The research team recognized that some places across the U.S. have average moisture contents above 16% for some portion of the year, but when looking at the entire U.S., the number of locations are relatively few and the conditions only persist for one to two months of the year, other than in Alaska. For this reason, it was deemed appropriate and justified to use 1.00 for the wet service factors and not further decrease strength by using the lower factors.

C_F, Size Factor:

Code: Does not apply to glulam.

C_V, Volume Factor:

Code: For glulam with loads applied perpendicular to the wide face of the laminations and the depth, width, or length of the member exceeds 12.0 in., 5.125 in., or 21.0 ft, respectively, the following equation shall be used to determine the value of C_V:

$$C_V = \left[\left(\frac{12.0}{d}\right)\left(\frac{5.125}{b}\right)\left(\frac{21.0}{L}\right)\right]^a \leq 1.00$$

Where: d = depth of member (in.)

b = width of the component, height for this member (in.)

L = length of the component (ft)

a = 0.05 for SYP or 0.10 for all other species.

Value Utilized:

For F_b: Not Applicable

Reasoning: This factor is not applicable to this rail due to loads being applied parallel to the wide face of laminations.

C_{fu}, Flat-Use Factor:

Code: For glulam with loads applied parallel to the wide face of the laminations, refer to Table 8.4.4.6-2.

Value Utilized:

For F_b: $C_{fu} = 1.01$

Reasoning: From Table 8.4.4.6-2, for a member with the dimension parallel to the wide faces of the laminations being 10 ¾ in., C_{fu} should be taken as 1.01.

C_i, Incising Factor:

Code: For incised members, refer to Table 8.4.4.7-1.

Values Utilized:

For F_b, F_v, F_t, F_c, F_{cp}, and E: Not Applicable

Reasoning: The member was determined to not be incised.

C_d, Deck Factor:

Code: Only applies to certain types of decking. Does not apply to beams.

C_λ, Time Effect Factor:

Code: Based on the appropriate strength limit state, refer to Table 8.4.4.9-1.

Values Utilized:

For F_b, F_v, F_t, F_c, and F_{cp}: $C_\lambda = 1.00$

Reasoning: Table 8.4.4.9-1 does not include information for Extreme Event II, but based on Strength II, III, and Extreme Event I using a value of 1.00 for the time effect factor, 1.00 was utilized for this situation as well.

AASHTO LRFD Calculations

$$F_b = F_{b0}C_{KF}C_M(C_F \text{ or } C_v)C_{fu}C_iC_dC_\lambda\zeta = (1{,}800\ psi)(2.50)(1.00)(1.01)(1.00)(1.33) = 6{,}044.85\ psi$$

$$F_v = F_{v0}C_{KF}C_MC_iC_\lambda = (230\ psi)(2.50)(1.00)(1.00) = 575.00\ psi$$

$$F_t = F_{t0}C_{KF}C_MC_FC_iC_\lambda = (1{,}250\ psi)(2.50)(1.00)(1.00) = 3{,}125.00\ psi$$

$$F_c = F_{c0}C_{KF}C_MC_FC_iC_\lambda = (1{,}950\ psi)(2.50)(1.00)(1.00) = 4{,}875.00\ psi$$

$$F_{cp} = F_{cp0}C_{KF}C_MC_iC_\lambda = (560\ psi)(2.10)(1.00)(1.00) = 1{,}176.00\ psi$$

$$E = E_0C_MC_i = (1{,}600{,}000\ psi)(1.00)(1.00) = 1{,}600{,}000\ psi$$

Moment capacity:

$$M_r = \varphi M_n = \varphi F_b S C_L = (1.00)(6{,}044.85\ psi)(260.02\ in.^3)(0.998) = 1{,}568.64\ k-in.$$

$$S = \frac{1}{6}bd^2 = \left(\frac{1}{6}\right)(13.5\ in.)(10.75\ in.)^2 = 260.02\ in.^3$$

$$C_L = \frac{1+A}{1.9} - \sqrt{\frac{(1+A)^2}{3.61} - \frac{A}{0.95}} = \frac{1+26.15}{1.9} - \sqrt{\frac{(1+26.15)^2}{3.61} - \frac{26.15}{0.95}} = 0.998$$

$$L_e \rightarrow 7 \leq \left(\frac{L_u}{d} = \frac{(96\ in.)}{10.75\ in.} = 8.93\right) \leq 14.3, thus\ L_e = 1.63L_u + 3d$$
$$= 1.63(96\ in.) + 3(10.75\ in.) = 188.73\ in.$$

$$R_b = \left(\sqrt{\frac{L_e d}{b^2}} \leq 50\right) = \left(\sqrt{\frac{(188.73\ in.)(10.75\ in.)}{(13.5)^2}} \leq 50\right) = (3.34 \leq 50)$$

$$F_{be} = \frac{K_{be}E}{{R_b}^2} = \frac{(1.10)(1{,}600{,}000\ psi)}{(3.34)^2} = 158{,}099.61\ psi$$

$$A = \frac{F_{be}}{F_b} = \frac{158{,}099.61\ psi}{6{,}044.85\ psi} = 26.15$$

Shear Capacity:

$$V_r = \varphi V_n = \varphi \frac{F_v bd}{1.5} = (1.00)\frac{(575.00\ psi)(13.5\ in.)(10.75\ in.)}{1.5} = 55.63\ k$$

Compression parallel to grain capacity:

$$P_r = \varphi P_n = \varphi F_c A_g C_p = (1.00)(4{,}875.00\ psi)(13.5\ in. * 10.75\ in.)(0.76) = 537.51\ k$$

$$C_p = \left(\frac{1+B}{2c} - \sqrt{\left(\frac{1+B}{2c}\right)^2 - \frac{B}{c}} \leq 1.00\right) = \left(\frac{1+1.0}{2(0.9)} - \sqrt{\left(\frac{1+1.0}{2(0.9)}\right)^2 - \frac{1.0}{0.9}} \leq 1.00\right)$$
$$= (0.76 \leq 1.00)$$

$$F_{ce} = \frac{K_{cE}Ed^2}{{L_e}^2} = \frac{(0.76)(1{,}600{,}000\ psi)(10.75\ in.)^2}{(96\ in.)^2} = 15{,}247.83\ psi$$

$$B = \left(\frac{F_{ce}}{F_c} \leq 1.00\right) = \left(\frac{15{,}247.83\ psi}{4{,}875.00\ psi} \leq 1.00\right) = 1.00$$

Compression perpendicular to grain capacity:

$$P_r = \varphi P_n = \varphi F_{cp} A_b C_b = (1.00)(1{,}176\ psi)(8.75\ in. * 10.5\ in.)(1.00) = 108.05\ k$$

Area of bearing assumed to be the portion of the rail that is in contact with the front face of the post, an area that is 8.75-in. wide and 10.5-in. tall. This bearing length utilizes a bearing factor of 1.00.

Tensile capacity:

$$P_r = \varphi P_n = \varphi F_t A_n = (1.00)(3{,}125.00\ psi)(10.75\ in.* 13.5\ in. - 2 * 10.75\ in.* 1\ in.)$$
$$= 386.33\ k$$

This calculation assumed a cross-section containing two horizontal bolt holes that are each 1 in. in diameter, as could be the case at a post location.

2018 NDS Factors

C_M, Wet Service Factor:

Code: Utilize 1.00 for glulam timber with an in-service moisture content of 16% or less, otherwise refer to Table 5B.

Values Utilized:

For F_b', F_v', F_t', F_c', $F_{c\perp}$', and E': C_M = 1.00

Reasoning: Based on the contents of Chapter 13 in the Wood Handbook, specifically Table 13-1, which includes data for average moisture contents of wood in outdoor conditions for many cities across the U.S., and Table 13-2, which is recommended moisture contents for wood products at time of installation, it was found that typical conditions would not cause members of the bridge railing system to have a moisture content above 16% [43]. The research team recognizes that some places do have average moisture contents above 16% for some portion of the year, but when looking at the entire U.S., the number of locations are relatively few and the conditions only persist for one to two months of the year, other than in Alaska. For this reason, we decided that it was justified to use 1.00 for the wet service factors and not decrease strength by using the lower factors.

C_t, Temperature Factor:

Code: Refer to Table 2.3.3, which states a value of 1.00 is to be used when sustained temperatures are consistently less than 100˚F.

Values Utilized:

For F_b', F_v', F_t', F_c', $F_{c\perp}$', and E': C_t = 1.00

Reasoning: Typical temperatures in most of the U.S. would be expected to be less than 100˚F during majority of the year.

C_L, Beam Stability Factor:

Code: Refer to Article 3.3.3, where when the depth of a bending member does not exceed its breadth, C_L = 1.00.

Value Utilized:

For F_b': C_L = 1.00

Reasoning: The depth of the member is 10 ¾ in. and the breadth is 13 ½ in., therefore it satisfies the criteria in Article 3.3.3, as written above.

C_V, Volume Factor:

Code: For glulam with loads applied perpendicular to the wide face of the laminations and the depth, width, or length of the member exceeds 12.0 in., 5.125 in., or 21.0 ft, respectively, the following equation shall be used to determine the value of C_V:

$$C_V = \left(\frac{21.0}{L}\right)^{1/x} \left(\frac{12.0}{d}\right)^{1/x} \left(\frac{5.125}{b}\right)^{1/x} \leq 1.00$$

Where: L = length of the component (ft)

d = depth of member (in.)

b = width of the component, height for this member (in.)

x = 20 for SYP or 10 for all other species.

Value Utilized:

For F_b': Not Applicable

Reasoning: This factor is not applicable to this rail due to loads being applied parallel to the wide face of laminations.

C_{fu}, Flat-Use Factor:

Code: For glulam with loads applied parallel to the wide face of the laminations, refer to Table 5B.

Value Utilized:

For F_b': C_{fu} = 1.01

Reasoning: From Table 5B, for a member with the dimension parallel to the wide faces of the laminations being 10 ¾ in., C_{fu} should be taken as 1.01.

C_c, Curvature Factor:

Code: For curved members, refer to Article 5.3.8.

Value Utilized:

For F_b': Not Applicable

Reasoning: The member does not have any curvature.

C_I, Stress Interaction Factor:

Code: For tapered members, refer to Article 5.3.9.

Value Utilized:

For F_b': Not Applicable

Reasoning: The member is not tapered.

C_{vr}, Shear Reduction Factor:

Code: For members subjected to impact loading, use a factor of 0.72.

Value Utilized:

For F_v': $C_{vr} = 0.72$

Reasoning: The member is to be subjected to impact loading.

C_P, Column Stability Factor:

Code: For members loaded in axial compression, C_P shall be determined as follows:

$$C_p = \left(\frac{1 + (F_{cE}/F_c^*)}{2c} - \sqrt{\left(\frac{1 + (F_{cE}/F_c^*)}{2c} \right)^2 - \frac{(F_{cE}/F_c^*)}{c}} \leq 1.00 \right)$$

$$= \left(\frac{1 + 2.49}{2(0.9)} - \sqrt{\left(\frac{1 + 2.49}{2(0.9)} \right)^2 - \frac{2.49}{0.9}} \leq 1.00 \right) = (0.94 \leq 1.00)$$

$$E'_{min} = E_{min} C_M C_t K_F \varphi = (850{,}000\ psi)(1.00)(1.00)(1.76)(0.85)$$
$$= 1{,}271{,}600.00\ psi$$

$$F_{cE} = \frac{0.822 E_{min}{}'}{(l_e/d)^2} = \frac{(0.822)(1{,}271{,}600\ psi)}{(96\ in./10.75\ in.)^2} = 13{,}106.80\ psi$$

$$F_c^* = F_c C_M C_t K_F \varphi \lambda = (1{,}950\ psi)(1.00)(1.00)(2.40)(0.90)(1.25)$$
$$= 5{,}265.00\ psi$$

$$c = 0.9\ for\ structural\ glulam.$$

Value Utilized:

For F_c': C_p = 0.94

Reasoning: Following the calculations above, the value of the column stability factor was determined to be 0.94 for this scenario.

C_b, Bearing Area Factor:

Code: Refer to Table C-2, or Table 3.10.4 in 2018 NDS.

Table B-2. 2018 NDS Bearing Adjustment Factors

Length of Bearing Measured along the Grain (in.)							
C_b	0.5	1.0	1.5	2.0	3.0	4.0	≥6.0
	1.75	1.38	1.25	1.19	1.13	1.10	1.00

Value Utilized:

For $F_{c\perp}$': C_b = 1.00

Reasoning: The bearing length from the upper rail being in contact with the post would be 8 ¾ in., equal to the width of the posts. This length corresponds to a bearing area factor of 1.00.

K_F, Format Conversion Factor:

Code: Refer to the values in Table 5.3.1.

Values Utilized:

For F_b': K_F = 2.54

For F_v': K_F = 2.88

For F_t': K_F = 2.70

For F_c': K_F = 2.40

For $F_{c\perp}$': K_F = 1.67

For E_{min}': K_F = 1.76

Reasoning: The values taken for the format conversion were taken directly from Table 5.3.1.

φ, Resistance Factor:

Code: Refer to the values in Table 5.3.1.

Values Utilized:

For F_b': φ = 0.85

For F_v': φ = 0.75

For F_t': φ = 0.80

For F_c': φ = 0.90

For $F_{c\perp}$': φ = 0.90

For E_{min}': φ = 0.85

Reasoning: The values taken for the format conversion were taken directly from Table 5.3.1.

λ, Time Effect Factor:

Code: Based on the appropriate load combination, refer to Appendix N.3.3 and Table N3.

Values Utilized:

For F_b', F_v', F_t', and F_c': λ = 1.25

Reasoning: Table N3 states that a factor of 1.25 should be used when live loading is from impact, as is the case for this beam.

2018 NDS Calculations

$$F_b' = F_b C_M C_t C_L C_V C_{fu} C_c C_I K_F \varphi \lambda \zeta$$
$$= (1{,}800\ psi)(1.00)(1.00)(1.00)(1.01)(2.54)(0.85)(1.25)(1.33)$$
$$= 6{,}525.42\ psi$$

$$F_v' = F_v C_M C_t C_{vr} K_F \varphi \lambda = (230\ psi)(1.00)(1.00)(0.72)(2.88)(0.75)(1.25) = 447.12\ psi$$

$F_t' = F_t C_M C_t K_F \varphi\lambda = (1{,}250\ psi)(1.00)(1.00)(2.70)(0.80)(1.25) = 3{,}375.00\ psi$

$F_c' = F_c C_M C_t C_P K_F \varphi\lambda = (1{,}950\ psi)(1.00)(1.00)(0.94)(2.40)(0.90)(1.25) = 4{,}962.61\ psi$

$F_{c\perp}' = F_{c\perp} C_M C_t C_b K_F \varphi = (560\ psi)(1.00)(1.00)(1.00)(1.67)(0.90) = 841.68\ psi$

$E' = E C_M C_t = (1{,}600{,}000\ psi)(1.00)(1.00) = 1{,}600{,}000\ psi$

$E_{min}{}' = E_{min} C_M C_t K_F \varphi = (850{,}000\ psi)(1.00)(1.00)(1.76)(0.85) = 1{,}271{,}600.00\ psi$

Moment capacity:

$M' = F_b' S = (6{,}525.42\ psi)(260.02\ in^3) = 1{,}696.71\ k - in.$

$S = \frac{1}{6} b d^2 = \left(\frac{1}{6}\right)(13.5\ in.)(10.75\ in.)^2 = 260.02\ in.^3$

Shear capacity:

$V' = \frac{2F_v{}' A}{3} = \frac{2(447.12\ psi)(10.75\ in. * 13.5 in.)}{3} = 43.26\ k$

Compression parallel to grain capacity:

$P' = F_c' A = (4{,}962.61\ psi)(10.75\ in. * 13.5\ in.) = 720.20\ k$

Compression perpendicular to grain capacity:

$P' = F_{c\perp}' A_b = (841.68\ psi)(8.75\ in. * 10.5\ in.) = 77.33\ k$

The area of bearing is calculated as the portion of the rail that is in contact with the front face of the post, an area that is 8.75-in. wide and 10.5-in. tall.

Tensile capacity:

$P' = F_t' A_n = (3{,}375.00\ psi)(10.75\ in. * 13.5\ in. - 2 * 10.75\ in. * 1\ in.) = 417.23\ k$

This calculation assumed a cross-section containing two horizontal bolt holes that are each 1 in. in diameter, as could be the case at a post location.

Upper Rail Summary

Table B-3. Upper Rail Strength and Capacity Summary

Strength/Capacity	AASHTO LRFD	2018 NDS
Bending Strength (psi)	6,044.85	6,525.42
Shear Strength (psi)	575.00	447.12
Tension Strength (psi)	3,125.00	3,375.00
Comp. Par. Strength (psi)	4,875.00	4,962.61
Comp. Perp. Strength (psi)	1,176.00	841.68
Moment Capacity (k-in.)	1,568.64	1,696.71
Shear Capacity (k)	55.63	43.26
Comp. Par. Capacity (k)	537.51	720.20
Comp. Perp. Capacity (k)	108.05	77.33
Tensile Capacity (k)	386.33	471.23

Strength and Capacity Calculations for Curb Rail:

General Rail Details:

Depth = 12 in.

Height = 8 ¾ in.

Length = 8 ft (distance from post to post, considered unbraced length)

Glulam Combination: Comb. 1 – DF

$F_{b0} = F_b = 1{,}250$ psi

$F_{v0} = F_v = 265$ psi

$F_{t0} = F_t = 950$ psi

$F_{c0} = F_c = 1{,}550$ psi

$F_{cp0} = F_{c\perp} = 560$ psi

$E_0 = E = 1{,}500{,}000$ psi

$E_{min} = 790{,}000$ psi

AASHTO LRFD Factors:

C_{KF}, Format Conversion Factor:

Values Utilized:

For F_b, F_v, F_t, and F_c: $C_{KF} = 2.50$

For F_{cp}: $C_{KF} = 2.10$

Reasoning: Refer to Factors for Upper Rail.

C_M, Wet Service Factor:

Values Utilized:

For F_b, F_v, F_t, F_c, F_{cp}, and E: $C_M = 1.00$

Reasoning: Refer to Factors for Upper Rail.

C_F, Size Factor:

Code: Does not apply to glulam.

C_V, Volume Factor:

Code: For glulam with loads applied perpendicular to the wide face of the laminations and the depth, width, or length of the member exceeds 12.0 in., 5.125 in., or 21.0 ft, respectively, the following equation shall be used to determine the value of C_V:

$$C_V = \left(\left[\left(\frac{12.0}{d}\right)\left(\frac{5.125}{b}\right)\left(\frac{21.0}{L}\right)\right]^a \leq 1.00\right) = \left(\left[\left(\frac{12.0}{12}\right)\left(\frac{5.125}{8.75}\right)\left(\frac{21.0}{8}\right)\right]^{0.10} \leq 1.00\right) = 1.00$$

Where: d = depth of member (in.)

b = width of the component, height for this member (in.)

L = length of the component (ft)

a = 0.05 for SYP or 0.10 for all other species.

Value Utilized:

For F_b: $C_V = 1.00$

Reasoning: Following the calculations above, the value of the volume factor was determined to be 1.00 for this scenario.

C_{fu}, Flat-Use Factor:

Value Utilized:

For F_b: Not Applicable

Reasoning: This member is not loaded parallel to the wide faces of the laminations.

C_i, Incising Factor:

Values Utilized:

For F_b, F_v, F_t, F_c, F_{cp}, and E: Not Applicable

Reasoning: The member was determined to not be incised.

C_d, Deck Factor:

Code: Only applies to certain types of decking. Does not apply to beams.

C_λ, Time Effect Factor:

Values Utilized:

For F_b, F_v, F_t, F_c, and F_{cp}: $C_\lambda = 1.00$

Reasoning: Refer to Factors for Upper Rail.

AASHTO LRFD Calculations

$$F_b = F_{b0}C_{KF}C_M(C_F \text{ or } C_v)C_{fu}C_iC_dC_\lambda\zeta = (1{,}250\ psi)(2.50)(1.00)(1.00)(1.00)(1.33) = 4{,}156.25\ psi$$

$$F_v = F_{v0}C_{KF}C_MC_iC_\lambda = (265\ psi)(2.50)(1.00)(1.00) = 662.50\ psi$$

$$F_t = F_{t0}C_{KF}C_MC_FC_iC_\lambda = (950\ psi)(2.50)(1.00)(1.00) = 2{,}375.00\ psi$$

$$F_c = F_{c0}C_{KF}C_MC_FC_iC_\lambda = (1{,}550\ psi)(2.50)(1.00)(1.00) = 3{,}875.00\ psi$$

$$F_{cp} = F_{cp0}C_{KF}C_MC_iC_\lambda = (560\ psi)(2.10)(1.00)(1.00) = 1{,}176.00\ psi$$

$$E = E_0C_MC_i = (1{,}500{,}000\ psi)(1.00)(1.00) = 1{,}500{,}000\ psi$$

Moment capacity:

$$M_r = \varphi M_n = \varphi F_bSC_L = (1.00)(4{,}156.25\ psi)(210.00\ in.^3)(0.996) = 869.25\ k-in.$$

$$S = \frac{1}{6}bd^2 = \left(\frac{1}{6}\right)(8.75\ in.)(12\ in.)^2 = 210.00\ in.^3$$

$$C_L = \frac{1+A}{1.9} - \sqrt{\frac{(1+A)^2}{3.61} - \frac{A}{0.95}} = \frac{1+13.16}{1.9} - \sqrt{\frac{(1+13.16)^2}{3.61} - \frac{13.16}{0.95}} = 0.996$$

$$L_e \rightarrow 7 \leq \left(\frac{L_u}{d} = \frac{(96\ in.)}{12\ in.} = 8.00\right) \leq 14.3, thus\ L_e = 1.63L_u + 3d = 1.63(96\ in.) + 3(12\ in.) = 192.48\ in.$$

$$R_b = \left(\sqrt{\frac{L_ed}{b^2}} \leq 50\right) = \left(\sqrt{\frac{(192.48\ in.)(12\ in.)}{(8.75)^2}} \leq 50\right) = (5.49 \leq 50)$$

$$F_{be} = \frac{K_{be}E}{{R_b}^2} = \frac{(1.10)(1{,}500{,}000\ psi)}{(5.49)^2} = 54{,}693.18\ psi$$

$$A = \frac{F_{be}}{F_b} = \frac{54{,}693.18\ psi}{4{,}156.25\ psi} = 13.16$$

Shear capacity:

$$V_r = \varphi V_n = \varphi \frac{F_v b d}{1.5} = (1.00)\frac{(662.50\ psi)(8.75\ in.)(12\ in.)}{1.5} = 46.38\ k$$

Compression parallel to grain capacity:

$$P_r = \varphi P_n = \varphi F_c A_g C_p = (1.00)(3{,}875.00\ psi)(8.75\ in.* 12\ in.)(0.76) = 309.12\ k$$

$$C_p = \left(\frac{1+B}{2c} - \sqrt{\left(\frac{1+B}{2c}\right)^2 - \frac{B}{c}} \le 1.00\right)$$

$$= \left(\frac{1+1.00}{2(0.9)} - \sqrt{\left(\frac{1+1.00}{2(0.9)}\right)^2 - \frac{1.00}{0.9}} \le 1.00\right) = (0.76 \le 1.00)$$

$$F_{ce} = \frac{K_{cE} E d^2}{{L_e}^2} = \frac{(0.76)(1{,}500{,}000\ psi)(12\ in.)^2}{(96\ in.)^2} = 17{,}812.50\ psi$$

$$B = \left(\frac{F_{ce}}{F_c} \le 1.00\right) = \left(\frac{17{,}812.50\ psi}{3{,}875.00\ psi} \le 1.00\right) = 1.00$$

Compression perpendicular to grain capacity:

$$P_r = \varphi P_n = \varphi F_{cp} A_b C_b = (1.00)(1{,}176\ psi)(8.75\ in.* 8.75\ in.)(1.00) = 90.04\ k$$

Area of bearing assumed to be the portion of the rail that is in contact with the front face of the post, an area that is 8.75-in. wide and 8.75-in. tall. This bearing length utilizes a bearing factor of 1.00.

Tensile capacity:

$$P_r = \varphi P_n = \varphi F_t A_n = (1.00)(3{,}125.00\ psi)(12\ in.* 8.75\ in. - 2 * 12\ in.* 1\ in.) = 192.38\ k$$

This calculation assumed a cross-section containing two horizontal bolt holes that are each 1 in. in diameter, as could be the case at a post location.

2018 NDS Factors

C_M, Wet Service Factor:

Values Utilized:

For F_b', F_v', F_t', F_c', $F_{c\perp}$', and E': $C_M = 1.00$

Reasoning: Refer to Factors for Upper Rail.

C_t, Temperature Factor:

Values Utilized:

For F_b', F_v', F_t', F_c', $F_{c\perp}$', and E': $C_t = 1.00$

Reasoning: Refer to Factors for Upper Rail.

C_L, Beam Stability Factor:

Code: Refer to Article 3.3.3 for scenarios when the depth of a bending member exceeds its breadth, C_L should be calculated based on the following:

$$C_L = \left(\frac{1 + (F_{bE}/F_b{}^*)}{1.9} - \sqrt{\left(\frac{1 + (F_{bE}/F_b{}^*)}{1.9} \right)^2 - \frac{(F_{bE}/F_b{}^*)}{0.95}} \leq 1.00 \right)$$

$$= \left(\frac{1 + (13.94)}{1.9} - \sqrt{\left(\frac{1 + (13.94)}{1.9} \right)^2 - \frac{(13.94)}{0.95}} \leq 1.00 \right)$$

$$= (0.996 \leq 1.00)$$

$$L_e \quad \rightarrow if\ \frac{L_u}{d} < 7, then\ L_e = 2.06L_u$$

$$\rightarrow if\ 7 \leq \frac{L_u}{d} \leq 14.3, then\ L_e = 1.63L_u + 3d$$

$$\rightarrow if\ \frac{L_u}{d} > 14.3, then\ L_e = 1.84L_u$$

$$\frac{L_u}{d} = \frac{96\ in.}{12\ in.} = 8 \rightarrow L_e = 1.63(96\ in.) + 3(12\ in.) = 192.48\ in.$$

$$R_b = \left(\sqrt{\frac{L_e d}{b^2}} \leq 50 \right) = \left(\sqrt{\frac{(192.48\ in.)(12\ in.)}{(8.75)^2}} \leq 50 \right) = (5.49 \leq 50)$$

$$E'_{min} = E_{min} C_M C_t K_F \varphi = (790{,}000\ psi)(1.00)(1.00)(1.76)(0.85)$$
$$= 1{,}181{,}840.00\ psi$$

$$F_{bE} = \frac{1.20{E_{min}}'}{{R_b}^2} = \frac{(1.20)(1{,}181{,}840\ psi)}{(5.49)^2} = 47{,}009.88\ psi$$

$$\begin{aligned} F_b^* &= F_b C_M C_t C_V C_{fu} C_c C_I K_F \varphi \lambda \\ &= (1{,}250\ psi)(1.00)(1.00)(1.00)(2.54)(0.85)(1.25) \\ &= 3{,}373.44\ psi \end{aligned}$$

Value Utilized:

For F_b': C_L = 0.996

Reasoning: Following the calculations above, the value of the beam stability factor was determined to be 0.996 for this scenario.

C_V, Volume Factor:

Code: For glulam with loads applied perpendicular to the wide face of the laminations and the depth, width, or length of the member exceeds 12.0 in., 5.125 in., or 21.0 ft, respectively, the following equation shall be used to determine the value of C_V:

$$\begin{aligned} C_V &= \left(\left(\frac{21.0}{L}\right)^{1/x}\left(\frac{12.0}{d}\right)^{1/x}\left(\frac{5.125}{b}\right)^{1/x} \leq 1.00\right) \\ &= \left(\left(\frac{21.0}{8}\right)^{1/10}\left(\frac{12.0}{12}\right)^{1/10}\left(\frac{5.125}{8.75}\right)^{1/10} \leq 1.00\right) = 1.00 \end{aligned}$$

Where: L = length of the component (ft)

d = depth of member (in.)

b = width of the component, height for this member (in.)

x = 20 for SYP or 10 for all other species.

Value Utilized:

For F_b': C_V = 1.00

Reasoning: Following the calculations above, the value of the volume factor was determined to be 1.00 for this scenario.

C_{fu}, Flat-Use Factor:

Value Utilized:

For F_b': Not Applicable

Reasoning: This member is not loaded parallel to the wide faces of the laminations.

C_c, Curvature Factor:

Value Utilized:

For F_b': Not Applicable

Reasoning: The member does not have any curvature.

C_I, Stress Interaction Factor:

Value Utilized:

For F_b': Not Applicable

Reasoning: The member is not tapered.

C_{vr}, Shear Reduction Factor:

Value Utilized:

For F_v': $C_{vr} = 0.72$

Reasoning: The member is to be subjected to impact loading.

C_P, Column Stability Factor:

Code: For members loaded in axial compression, C_P shall be determined as follows:

$$C_p = \left(\frac{1 + (F_{cE}/F_c^*)}{2c} - \sqrt{\left(\frac{1 + (F_{cE}/F_c^*)}{2c} \right)^2 - \frac{(F_{cE}/F_c^*)}{c}} \leq 1.00 \right)$$

$$= \left(\frac{1 + 3.63}{2(0.9)} - \sqrt{\left(\frac{1 + 3.63}{2(0.9)} \right)^2 - \frac{3.63}{0.9}} \leq 1.00 \right) = (0.97 \leq 1.00)$$

$$E'_{min} = E_{min} C_M C_t K_F \varphi = (790{,}000\ psi)(1.00)(1.00)(1.76)(0.85)$$
$$= 1{,}181{,}840.00\ psi$$

$$F_{cE} = \frac{0.822 E_{min}{}'}{(l_e/d)^2} = \frac{(0.822)(1{,}181{,}840\ psi)}{(96\ in./12\ in.)^2} = 15{,}179.26\ psi$$

$$F_c^* = F_c C_M C_t K_F \varphi \lambda = (1{,}550\ psi)(1.00)(1.00)(2.40)(0.90)(1.25)$$
$$= 4{,}185.00\ psi$$

$c = 0.9\ for\ structural\ glulam.$

Value Utilized:

For F_c': C_p = 0.97

Reasoning: Following the calculations above, the value of the column stability factor was determined to be 0.97 for this scenario.

C_b, Bearing Area Factor:

Value Utilized:

For $F_{c\perp}$': C_b = 1.00

Reasoning: Refer to Factors for Upper Rail.

K_F, Format Conversion Factor:

Values Utilized:

For F_b': K_F = 2.54

For F_v': K_F = 2.88

For F_t': K_F = 2.70

For F_c': K_F = 2.40

For $F_{c\perp}$': K_F = 1.67

For E_{min}': K_F = 1.76

Reasoning: Refer to Factors for Upper Rail.

φ, Resistance Factor:

Values Utilized:

For F_b': φ = 0.85

For F_v': φ = 0.75

For F_t': φ = 0.80

For F_c': φ = 0.90

For $F_{c\perp}$': φ = 0.90

For E_{min}': φ = 0.85

Reasoning: Refer to Factors for Upper Rail.

λ, Time Effect Factor:

Values Utilized:

For F_b', F_v', F_t', and F_c': λ= 1.25

Reasoning: Refer to Factors for Upper Rail.

2018 NDS Calculations

$$F_b' = F_b C_M C_t C_L C_V C_{fu} C_c C_I K_F \varphi \lambda \zeta$$
$$= (1{,}250\ psi)(1.00)(1.00)(0.996)(1.00)(2.54)(0.85)(1.25)(1.33)$$
$$= 4{,}469.47\ psi$$

$$F_v' = F_v C_M C_t C_{vr} K_F \varphi \lambda = (265\ psi)(1.00)(1.00)(0.72)(2.88)(0.75)(1.25) = 515.16\ psi$$

$$F_t' = F_t C_M C_t K_F \varphi \lambda = (950\ psi)(1.00)(1.00)(2.70)(0.80)(1.25) = 2{,}565.00\ psi$$

$$F_c' = F_c C_M C_t C_P K_F \varphi \lambda = (1{,}550\ psi)(1.00)(1.00)(0.97)(2.40)(0.90)(1.25) = 4{,}038.60\ psi$$

$$F_{c\perp}' = F_{c\perp} C_M C_t C_b K_F \varphi = (560\ psi)(1.00)(1.00)(1.00)(1.67)(0.90) = 841.68\ psi$$

$$E' = E C_M C_t = (1{,}500{,}000\ psi)(1.00)(1.00) = 1{,}500{,}000\ psi$$

$$E_{min}{}' = E_{min} C_M C_t K_F \varphi = (790{,}000\ psi)(1.00)(1.00)(1.76)(0.85) = 1{,}181{,}840.00\ psi$$

Moment capacity:

$$M' = F_b' S = (4{,}469.47\ psi)(210.00\ in^3) = 938.59\ k - in.$$

$$S = \frac{1}{6} b d^2 = \left(\frac{1}{6}\right)(8.75\ in.)(12\ in.)^2 = 210.00\ in.^3$$

Shear capacity:

$$V' = \frac{2 F_v' A}{3} = \frac{2(515.16\ psi)(12\ in. * 8.75 in.)}{3} = 36.06\ k$$

Compression parallel to grain capacity:

$$P' = F_c' A = (4{,}038.60\ psi)(12\ in. * 8.75\ in.) = 424.05\ k$$

Compression perpendicular to grain capacity:

$$P' = F_{c\perp}' A_b = (841.68\ psi)(8.75\ in. * 8.75\ in.) = 64.44\ k$$

The area of bearing is calculated as the portion of the rail that is in contact with the front face of the post, an area that is 8.75-in. wide and 8.75-in. tall.

Tensile capacity:

$$P' = F_t' A_n = (2{,}565.00\ psi)(12\ in.* 8.75\ in. - 2 * 12in.* 1\ in.) = 207.77\ k$$

This calculation assumed a cross-section containing two horizontal bolt holes that are each 1 in. in diameter, as could be the case at a post location.

Curb Rail Summary

Table B-4. Curb Rail Strength and Capacity Summary

Strength/Capacity	AASHTO LRFD	2018 NDS
Bending Strength (psi)	4,156.25	4,469.47
Shear Strength (psi)	662.50	515.16
Tension Strength (psi)	2,375.00	2,565.00
Comp. Par. Strength (psi)	3,875.00	4,038.60
Comp. Perp. Strength (psi)	1,176.00	841.68
Moment Capacity (k-in.)	869.25	938.59
Shear Capacity (k)	46.38	36.06
Comp. Par. Capacity (k)	309.12	424.05
Comp. Perp. Capacity (k)	90.04	64.44
Tensile Capacity (k)	192.38	207.77

Strength and Capacity Calculations for Posts:

General Rail Details:

For Loading Perpendicular to the Wide Face of Laminations, or Along the B-axis

Depth = 10½ in.

Width = 8¾ in.

Length = 3 ft – 1⅛ in.

Glulam Combination: Comb. 2 – DF

$F_{b0} = F_b = 1700$ psi

$F_{v0} = F_v = 265$ psi

$F_{t0} = F_t = 1{,}250$ psi

$F_{c0} = F_c = 1{,}950$ psi

$F_{cp0} = F_{c\perp} = 560$ psi

$E_0 = E = 1{,}600{,}000$ psi

$E_{min} = 850{,}000$ psi

AASHTO LRFD Factors:

C_{KF}, Format Conversion Factor:

Values Utilized:

For F_b, F_v, F_t, and F_c: $C_{KF} = 2.50$

For F_{cp}: $C_{KF} = 2.10$

Reasoning: Refer to Factors for Upper Rail.

C_M, Wet Service Factor:

Values Utilized:

For F_b, F_v, F_t, F_c, F_{cp}, and E: $C_M = 1.00$

Reasoning: Refer to Factors for Upper Rail.

C_F, Size Factor:

Code: Does not apply to glulam.

C_V, Volume Factor:

Code: For glulam with loads applied perpendicular to the wide face of the laminations and the depth, width, or length of the member exceeds 12.0 in., 5.125 in., or 21.0 ft, respectively, the following equation shall be used to determine the value of C_V:

$$C_V = \left(\left[\left(\frac{12.0}{d}\right)\left(\frac{5.125}{b}\right)\left(\frac{21.0}{L}\right)\right]^a \leq 1.00\right)$$

$$= \left(\left[\left(\frac{12.0}{10.5}\right)\left(\frac{5.125}{8.75}\right)\left(\frac{21.0}{3.09375}\right)\right]^{0.10} \leq 1.00\right) = 1.00$$

Where: d = depth of member (in.)

b = width of the component, height for this member (in.)

L = length of the component (ft)

a = 0.05 for SYP or 0.10 for all other species.

Value Utilized:

For F_b: $C_V = 1.00$

Reasoning: Following the calculations above, the value of the volume factor was determined to be 1.00 for this scenario.

C_{fu}, Flat-Use Factor:

Value Utilized:

For F_b: Not Applicable

Reasoning: This member is not loaded parallel to the wide faces of the laminations.

C_i, Incising Factor:

Values Utilized:

For F_b, F_v, F_t, F_c, F_{cp}, and E: Not Applicable

Reasoning: The member was determined to not be incised.

C_d, Deck Factor:

Code: Only applies to certain types of decking. Does not apply to beams.

C_λ, Time Effect Factor:

Values Utilized:

For F_b, F_v, F_t, F_c, and F_{cp}: $C_\lambda = 1.00$

Reasoning: Refer to Factors for Upper Rail.

AASHTO LRFD Calculations

$$F_b = F_{b0}C_{KF}C_M(C_F \text{ or } C_v)C_{fu}C_iC_dC_\lambda\zeta = (1{,}700\ psi)(2.50)(1.00)(1.00)(1.00)(1.33) = 5{,}652.50\ psi$$

$$F_v = F_{v0}C_{KF}C_MC_iC_\lambda = (265\ psi)(2.50)(1.00)(1.00) = 662.50\ psi$$

$$F_t = F_{t0}C_{KF}C_MC_FC_iC_\lambda = (1{,}250\ psi)(2.50)(1.00)(1.00) = 3{,}125.00\ psi$$

$$F_c = F_{c0}C_{KF}C_MC_FC_iC_\lambda = (1{,}950\ psi)(2.50)(1.00)(1.00) = 4{,}875.00\ psi$$

$F_{cp} = F_{cp0}C_{KF}C_M C_i C_\lambda = (560\ psi)(2.10)(1.00)(1.00) = 1{,}176.00\ psi$

$E = E_0 C_M C_i = (1{,}600{,}000\ psi)(1.00)(1.00) = 1{,}600{,}000\ psi$

Moment capacity:

$M_r = \varphi M_n = \varphi F_b S C_L = (1.00)(5{,}652.50\ psi)(160.78\ in.^3)(0.998) = 907.24\ k-in.$

$$S = \frac{1}{6}bd^2 = \left(\frac{1}{6}\right)(8.75\ in.)(10.5\ in.)^2 = 160.78\ in.^3$$

$$C_L = \frac{1+A}{1.9} - \sqrt{\frac{(1+A)^2}{3.61} - \frac{A}{0.95}} = \frac{1+29.69}{1.9} - \sqrt{\frac{(1+29.69)^2}{3.61} - \frac{29.69}{0.95}} = 0.998$$

$$L_e \rightarrow \left(\frac{L_u}{d} = \frac{(37.125\ in.)}{12\ in.} = 8.00\right) < 7, thus\ L_e = 2.06L_u = 2.06(37.125\ in.) = 76.48\ in.$$

$$R_b = \left(\sqrt{\frac{L_e d}{b^2}} \le 50\right) = \left(\sqrt{\frac{(76.48\ in.)(10.5\ in.)}{(8.75)^2}} \le 50\right) = (3.24 \le 50)$$

$$F_{be} = \frac{K_{be}E}{{R_b}^2} = \frac{(1.10)(1{,}600{,}000\ psi)}{(3.24)^2} = 167{,}805.35\ psi$$

$$A = \frac{F_{be}}{F_b} = \frac{167{,}805.35\ psi}{5{,}652.5 psi} = 29.69$$

Shear capacity:

$$V_r = \varphi V_n = \varphi\frac{F_v bd}{1.5} = (1.00)\frac{(662.50\ psi)(8.75\ in.)(10.5\ in.)}{1.5} = 40.58\ k$$

Compression parallel to grain capacity:

$P_r = \varphi P_n = \varphi F_c A_g C_p = (1.00)(4{,}875.00\ psi)(8.75\ in. * 10.5\ in.)(0.76) = 340.28\ k$

$$C_p = \left(\frac{1+B}{2c} - \sqrt{\left(\frac{1+B}{2c}\right)^2 - \frac{B}{c}} \le 1.00\right) = \left(\frac{1+1.00}{2(0.9)} - \sqrt{\left(\frac{1+1.00}{2(0.9)}\right)^2 - \frac{1.00}{0.9}} \le 1.00\right) = (0.76 \le 1.00)$$

$$F_{ce} = \frac{K_{cE} E d^2}{{L_e}^2} = \frac{(0.76)(1{,}600{,}000\ psi)(10.5\ in.)^2}{(37.125\ in.)^2} = 97{,}270.07\ psi$$

$$B = \left(\frac{F_{ce}}{F_c} \leq 1.00\right) = \left(\frac{97{,}270.07\ psi}{4{,}875.00\ psi} \leq 1.00\right) = 1.00$$

Compression perpendicular to grain capacity:

$$P_r = \varphi P_n = \varphi F_{cp} A_b C_b = (1.00)(1{,}176\ psi)(8.75\ in. * 10.5\ in.)(1.00) = 108.05\ k$$

Area of bearing assumed to be the portion of the post that is in contact with the back face of the rail, an area that is 8.75-in. wide and 10.5-in. tall. This bearing length utilizes a bearing factor of 1.00.

Tensile capacity:

$$P_r = \varphi P_n = \varphi F_t A_n = (1.00)(3{,}125.00\ psi)(10.5\ in. * 8.75\ in. - 2 * 10.5\ in. * 1\ in.) = 221.48\ k$$

This calculation assumed a cross-section containing two horizontal bolt holes that are each 1 in. in diameter.

2018 NDS Factors

C_M, Wet Service Factor:

Values Utilized:

For F_b', F_v', F_t', F_c', $F_{c\perp}$', and E': C_M = 1.00

Reasoning: Refer to Factors for Upper Rail.

C_t, Temperature Factor:

Values Utilized:

For F_b', F_v', F_t', F_c', $F_{c\perp}$', and E': C_t = 1.00

Reasoning: Refer to Factors for Upper Rail.

C_L, Beam Stability Factor:

Code: Refer to Article 3.3.3 for scenarios when the depth of a bending member exceeds its breadth, C_L should be calculated based on the following:

$$C_L = \left(\frac{1 + (F_{bE}/F_b{}^*)}{1.9} - \sqrt{\left(\frac{1 + (F_{bE}/F_b{}^*)}{1.9} \right)^2 - \frac{(F_{bE}/F_b{}^*)}{0.95}} \leq 1.00 \right)$$

$$= \left(\frac{1 + (31.71)}{1.9} - \sqrt{\left(\frac{1 + (31.71)}{1.9} \right)^2 - \frac{(31.71)}{0.95}} \leq 1.00 \right)$$

$$= (0.998 \leq 1.00)$$

$$L_e \quad \rightarrow if\ \frac{L_u}{d} < 7, then\ L_e = 2.06L_u$$

$$\rightarrow if\ 7 \leq \frac{L_u}{d} \leq 14.3, then\ L_e = 1.63L_u + 3d$$

$$\rightarrow if\ \frac{L_u}{d} > 14.3, then\ L_e = 1.84L_u$$

$$\frac{L_u}{d} = \frac{37.125\ in.}{10.5\ in.} = 3.54 \rightarrow L_e = 2.06(37.125\ in.) = 76.48\ in.$$

$$R_b = \left(\sqrt{\frac{L_e d}{b^2}} \leq 50 \right) = \left(\sqrt{\frac{(76.48\ in.)(10.5\ in.)}{(8.75)^2}} \leq 50 \right) = (3.24 \leq 50)$$

$$E'_{min} = E_{min} C_M C_t K_F \varphi = (850{,}000\ psi)(1.00)(1.00)(1.76)(0.85)$$
$$= 1{,}271{,}600.00\ psi$$

$$F_{bE} = \frac{1.20 {E_{min}}'}{{R_b}^2} = \frac{(1.20)(1{,}271{,}600\ psi)}{(3.24)^2} = 145{,}487.23\ psi$$

$$F_b^* = F_b C_M C_t C_V C_{fu} C_c C_I K_F \varphi \lambda$$
$$= (1{,}700\ psi)(1.00)(1.00)(1.00)(2.54)(0.85)(1.25)$$
$$= 4{,}587.88\ psi$$

Value Utilized:

For F_b': C_L = 0.998

Reasoning: Following the calculations above, the value of the beam stability factor was determined to be 0.998 for this scenario.

C_V, Volume Factor:

Code: For glulam with loads applied perpendicular to the wide face of the laminations and the depth, width, or length of the member exceeds 12.0 in., 5.125 in., or 21.0 ft, respectively, the following equation shall be used to determine the value of C_V:

$$C_V = \left(\left(\frac{21.0}{L}\right)^{1/x}\left(\frac{12.0}{d}\right)^{1/x}\left(\frac{5.125}{b}\right)^{1/x} \leq 1.00\right)$$

$$= \left(\left(\frac{21.0}{3.09375}\right)^{1/10}\left(\frac{12.0}{10.5}\right)^{1/10}\left(\frac{5.125}{8.75}\right)^{1/10} \leq 1.00\right) = 1.00$$

Where: L = length of the component (ft)

d = depth of member (in.)

b = width of the component, height for this member (in.)

x = 20 for SYP or 10 for all other species.

Value Utilized:

For F_b': C_V = 1.00

Reasoning: Following the calculations above, the value of the volume factor was determined to be 1.00 for this scenario.

C_{fu}, Flat-Use Factor:

Value Utilized:

For F_b': Not Applicable

Reasoning: This member is not loaded parallel to the wide faces of the laminations.

C_c, Curvature Factor:

Value Utilized:

For F_b': Not Applicable

Reasoning: The member does not have any curvature.

C_I, Stress Interaction Factor:

Value Utilized:

For F_b': Not Applicable

Reasoning: The member is not tapered.

C_{vr}, Shear Reduction Factor:

Value Utilized:

For F_v': $C_{vr} = 0.72$

Reasoning: The member is to be subjected to impact loading.

C_P, Column Stability Factor:

Code: For members loaded in axial compression, C_P shall be determined as follows:

$$C_p = \left(\frac{1 + (F_{cE}/F_c^*)}{2c} - \sqrt{\left(\frac{1 + (F_{cE}/F_c^*)}{2c} \right)^2 - \frac{(F_{cE}/F_c^*)}{c}} \leq 1.00 \right)$$

$$= \left(\frac{1 + 15.88}{2(0.9)} - \sqrt{\left(\frac{1 + 15.88}{2(0.9)} \right)^2 - \frac{15.88}{0.9}} \leq 1.00 \right) = (0.99 \leq 1.00)$$

$$E'_{min} = E_{min} C_M C_t K_F \varphi = (850{,}000\ psi)(1.00)(1.00)(1.76)(0.85)$$
$$= 1{,}271{,}600.00\ psi$$

$$F_{cE} = \frac{0.822 E_{min}{}'}{(l_e/d)^2} = \frac{(0.822)(1{,}271{,}600\ psi)}{(37.125\ in./10.5\ in.)^2} = 83{,}611.88\ psi$$

$$F_c^* = F_c C_M C_t K_F \varphi \lambda = (1{,}950\ psi)(1.00)(1.00)(2.40)(0.90)(1.25)$$
$$= 5{,}625.00\ psi$$

$$c = 0.9\ for\ structural\ glulam.$$

Value Utilized:

For F_c': $C_p = 0.99$

Reasoning: Following the calculations above, the value of the column stability factor was determined to be 0.99 for this scenario.

C_b, Bearing Area Factor:

Value Utilized:

For $F_{c\perp}$': $C_b = 1.00$

Reasoning: Refer to Factors for Upper Rail.

K_F, Format Conversion Factor:

Values Utilized:

For F_b': K_F = 2.54

For F_v': K_F = 2.88

For F_t': K_F = 2.70

For F_c': K_F = 2.40

For $F_{c\perp}$': K_F = 1.67

For E_{min}': K_F = 1.76

Reasoning: Refer to Factors for Upper Rail.

φ, Resistance Factor:

Values Utilized:

For F_b': φ = 0.85

For F_v': φ = 0.75

For F_t': φ = 0.80

For F_c': φ = 0.90

For $F_{c\perp}$': φ = 0.90

For E_{min}': φ = 0.85

Reasoning: Refer to Factors for Upper Rail.

λ, Time Effect Factor:

Values Utilized:

For F_b', F_v', F_t', and F_c': λ= 1.25

Reasoning: Refer to Factors for Upper Rail.

2018 NDS Calculations

$$F_b' = F_b C_M C_t C_L C_V C_{fu} C_c C_I K_F \varphi \lambda \zeta$$
$$= (1{,}750\ psi)(1.00)(1.00)(0.998)(1.00)(2.54)(0.85)(1.25)(1.33)$$
$$= 6{,}091.97\ psi$$

$F_v' = F_v C_M C_t C_{vr} K_F \varphi\lambda = (265\ psi)(1.00)(1.00)(0.72)(2.88)(0.75)(1.25) = 515.16\ psi$

$F_t' = F_t C_M C_t K_F \varphi\lambda = (1{,}250\ psi)(1.00)(1.00)(2.70)(0.80)(1.25) = 3{,}375.00\ psi$

$F_c' = F_c C_M C_t C_P K_F \varphi\lambda = (1{,}950\ psi)(1.00)(1.00)(0.99)(2.40)(0.90)(1.25) = 5{,}230.10\ psi$

$F_{c\perp}' = F_{c\perp} C_M C_t C_b K_F \varphi = (560\ psi)(1.00)(1.00)(1.00)(1.67)(0.90) = 841.68\ psi$

$E' = E C_M C_t = (1{,}600{,}000\ psi)(1.00)(1.00) = 1{,}600{,}000\ psi$

$E_{min}{}' = E_{min} C_M C_t K_F \varphi = (850{,}000\ psi)(1.00)(1.00)(1.76)(0.85) = 1{,}271{,}600.00\ psi$

Moment capacity:

$M' = F_b' S = (6{,}091.97\ psi)(160.78\ in^3) = 979.47\ k - in.$

$S = \frac{1}{6} b d^2 = \left(\frac{1}{6}\right)(8.75\ in.)(10.5\ in.)^2 = 160.78\ in.^3$

Shear capacity:

$V' = \frac{2F_v{}' A}{3} = \frac{2(515.16\ psi)(10.5\ in. * 8.75 in.)}{3} = 31.55\ k$

Compression parallel to grain capacity:

$P' = F_c' A = (5{,}230.10\ psi)(10.5\ in. * 8.75\ in.) = 480.52\ k$

Compression perpendicular to grain capacity:

$P' = F_{c\perp}' A_b = (841.68\ psi)(8.75\ in. * 10.5\ in.) = 77.33\ k$

The area of bearing is calculated as the portion of the post that is in contact with the back face of the upper rail, an area that is 8.75-in. wide and 10.5-in. tall.

Tensile capacity:

$P' = F_t' A_n = (3{,}375.00\ psi)(10.5\ in. * 8.75\ in. - 2 * 10.5 in. * 1\ in.) = 239.20\ k$

This calculation assumed a cross-section containing two horizontal bolt holes that are each 1 in. in diameter.

Post Summary

Table B-5. Post Strength and Capacity Summary

Strength/Capacity	AASHTO LRFD	2018 NDS
Bending Strength (psi)	5,652.50	6,091.97
Shear Strength (psi)	662.50	515.16
Tension Strength (psi)	3,125.00	3,375.00
Comp. Par. Strength (psi)	4,875.00	5,230.10
Comp. Perp. Strength (psi)	1,176.00	841.68
Moment Capacity (k-in.)	907.24	979.47
Shear Capacity (k)	40.58	31.55
Comp. Par. Capacity (k)	340.28	480.52
Comp. Perp. Capacity (k)	108.05	77.33
Tensile Capacity (k)	221.48	239.20

Appendix C. BARRIER VII 10000S Vehicle Model

BARRIER VII 10000S Vehicle Input File

```
MASH 10000S
   22046.0  702000.0   20    7    6    0    1
    1     0.082      0.21       1.5      18.0
    2     0.063      0.19       2.0      12.0
    3     0.045      0.17       3.0       4.0
    4     0.800      0.95       2.5       2.5
    5     0.900      1.05       3.5       2.0
    6      0.35      0.25      10.0       3.0
    7       2.5       3.5       4.5       3.0
    1     166.0      17.0    1      15.0    1    0    0    0
    2     166.0      32.0    1      15.0    1    0    0    0
    3     166.0      47.0    1      17.5    1    0    0    0
    4     146.0      47.0    1      20.0    1    0    0    0
    5     126.0      47.0    2      20.0    1    0    0    0
    6     106.0      47.0    2      20.0    1    0    0    0
    7      86.0      47.0    2      25.0    1    0    0    0
    8      56.0      47.0    2    15.375    1    0    0    0
    9      56.0     47.75    3    22.875    0    0    0    0
   10      11.0     47.75    4      45.0    0    0    0    0
   11     -34.0     47.75    5      42.5    0    0    0    0
   12     -74.0     47.75    5      42.5    0    0    0    0
   13    -119.0     47.75    5      45.0    0    0    0    0
   14    -164.0     47.75    5      22.5    0    0    0    0
   15    -164.0    -47.75    5       1.0    0    0    0    0
   16      56.0    -47.75    3       1.0    0    0    0    0
   17      56.0     -47.0    2       1.0    0    0    0    0
   18     166.0     -47.0    1       1.0    0    0    0    0
   19     -76.0    42.625    7       1.0    1    0    0    0
   20     130.0      40.0    6       1.0    1    0    0    0
    1     130.0      40.0       0.0     3572.
    2     130.0     -40.0       0.0     3572.
    3     -76.0    42.625       0.0     3041.
    4     -76.0   -42.625       0.0     3041.
    5     -76.0    31.375       0.0     3041.
    6     -76.0   -31.375       0.0     3041.
    1       0.0       0.0
    3    1060.5       0.0      15.0     56.00       0.0       0.0      10.0
```

Appendix D. Calibrated NCHRP Report No. 350 BARRIER VII Model

BARRIER VII Input File

```
NCHRP 350 2000P Impact – Calibrated 350 Bridge Railing System
  369   13    8    2  396   25    2    0
    0.0010    0.0010      0.80  200    0       1.0    1
    1    5    1    5    5    5    1
    1       0.0       0.0
    9     600.0       0.0
   13     675.0       0.0
   14    699.75       0.0
   15    699.75       0.0
   16     724.5       0.0
   17     724.5       0.0
   48     916.5       0.0
   49     916.5       0.0
  240    1492.5       0.0
  241    1492.5       0.0
  368    2260.5       0.0
  369    2260.5       0.0
    1    9    7    1       0.0
    9   13    3    1       0.0
   16   48   15    2       0.0
   17   49   15    2       0.0
   48  240   95    2       0.0
   49  241   95    2       0.0
  240  368   63    2       0.0
  241  369   63    2       0.0
    1  191      0.48
  368  366  364  362  360  358  356  354  352  350
  348  346  344  342  340  338  336  334  332  330
  328  326  324  322  320  318  316  314  312  310
  308  306  304  302  300  298  296  294  292  290
  288  286  284  282  280  278  276  274  272  270
  268  266  264  262  260  258  256  254  252  250
  248  246  244  242  240  238  236  234  232  230
  228  226  224  222  220  218  216  214  212  210
  208  206  204  202  200  198  196  194  192  190
  188  186  184  182  180  178  176  174  172  170
  168  166  164  162  160  158  156  154  152  150
  148  146  144  142  140  138  136  134  132  130
  128  126  124  122  120  118  116  114  112  110
  108  106  104  102  100   98   96   94   92   90
   88   86   84   82   80   78   76   74   72   70
   68   66   64   62   60   58   56   54   52   50
   48   46   44   42   40   38   36   34   32   30
   28   26   24   22   20   18   16   14   13   12
   11   10    9    8    7    6    5    4    3    2
    1
    2  178      0.48
  369  367  365  363  361  359  357  355  353  351
  349  347  345  343  341  339  337  335  333  331
  329  327  325  323  321  319  317  315  313  311
  309  307  305  303  301  299  297  295  293  291
  289  287  285  283  281  279  277  275  273  271
  269  267  265  263  261  259  257  255  253  251
  249  247  245  243  241  239  237  235  233  231
  229  227  225  223  221  219  217  215  213  211
  209  207  205  203  201  199  197  195  193  191
```

```
189  187  185  183  181  179  177  175  173  171
169  167  165  163  161  159  157  155  153  151
149  147  145  143  141  139  137  135  133  131
129  127  125  123  121  119  117  115  113  111
109  107  105  103  101   99   97   95   93   91
 89   87   85   83   81   79   77   75   73   71
 69   67   65   63   61   59   57   55   53   51
 49   47   45   43   41   39   37   35   33   31
 29   27   25   23   21   19   17   15
100   14
  1      2.29      1.99     75.00   30000.0      6.92      99.5      68.5 0.10
  2      2.48      2.13     18.75   30000.0      7.41     106.5      73.5 0.10
  3      2.83      2.41     18.75   30000.0      8.38     120.5      83.5 0.10
  4      3.17      2.68     18.75   30000.0      9.35     134.0      93.5 0.10
  5      3.52      2.96     18.75   30000.0     10.32     148.0     103.5 0.10
  6      3.76      3.10     24.75   30000.0     10.81     155.0     109.5 0.10
  7     753.7     118.1     24.75    1600.0      28.6     314.5    1070.5 0.10
  8     753.7     118.1     12.00    1600.0      28.6     314.5    1070.5 0.10
  9     753.7     118.1      6.00    1600.0      28.6     314.5    1070.5 0.10
 10     753.7     118.1     12.00    1600.0      28.6     314.5    1070.5 0.10
 11     972.0      81.0     24.75    1500.0      19.3     135.4     668.5 0.10
 12     972.0      81.0     12.00    1500.0      19.3     135.4     668.5 0.10
 13     972.0      81.0      6.00    1500.0      19.3     135.4     668.5 0.10
 14     972.0      81.0     12.00    1500.0      19.3     135.4     668.5 0.10
300    6
  1      21.0       0.0    5000.0   15000.0     100.0    7500.0    1500.0 0.10
   300.0     100.0       1.0       1.0
  2      21.0       0.0      15.0      11.0      50.0     315.0     231.0 0.10
    18.8      13.8      20.0      20.0
  3      21.0       0.0      15.0      15.0      77.0     315.0     315.0 0.10
    18.8      18.8      20.0      20.0
  4     28.25    10.125      30.6     22.44      67.6     833.1     720.0 0.10
    55.0      55.0       4.0      10.0
  5     28.25    10.125    5000.0   15000.0     100.0    7500.0    1500.0 0.10
   300.0     100.0       1.0       1.0
  6    10.125       0.0    5000.0   15000.0     100.0    7500.0    1500.0 0.10
   300.0     100.0       1.0       1.0
  1    1    2    8    1  101       0.0       0.0       0.0
  9    9   10    0    0  102       0.0       0.0       0.0
 10   10   11    0    0  103       0.0       0.0       0.0
 11   11   12    0    0  104       0.0       0.0       0.0
 12   12   13    0    0  105       0.0       0.0       0.0
 13   13   14    0    0  106       0.0       0.0       0.0
 14   14   16    0    0  107       0.0       0.0       0.0
 15   16   18   30    2  108       0.0       0.0       0.0
 31   48   50  126    2  109       0.0       0.0       0.0
127  240  242  182    2  108       0.0       0.0       0.0
183  352  354  190    2  110       0.0       0.0       0.0
191   15   17    0    0  111       0.0       0.0       0.0
192   17   19  207    2  112       0.0       0.0       0.0
208   49   51  303    2  113       0.0       0.0       0.0
304  241  243  359    2  112       0.0       0.0       0.0
360  353  355  367    2  114       0.0       0.0       0.0
368    1    0    0    0  301       0.0       0.0       0.0       0.0       0.0
369    2    0  373    1  302       0.0       0.0       0.0       0.0       0.0
374    7    0  376    1  303       0.0       0.0       0.0       0.0       0.0
377   11    0  378    2  303       0.0       0.0       0.0       0.0       0.0
379   16   17  381   16  304       0.0       0.0       0.0       0.0       0.0
```

```
382   80   81  387   32  304       0.0       0.0       0.0       0.0       0.0
388  256  257  394   16  304       0.0       0.0       0.0       0.0       0.0
395  368  369    0    0  305       0.0       0.0       0.0       0.0       0.0
396   15    0    0    0  306       0.0       0.0       0.0       0.0       0.0
  4393.0   40000.0   20    6    4    0    1
  1     0.055      0.12      6.00      17.0
  2     0.057      0.15      7.00      18.0
  3     0.062      0.18     10.00      12.0
  4     0.110      0.35     12.00       6.0
  5      0.35      0.45      6.00       5.0
  6      1.45      1.50     15.00       1.0
  1    100.75    15.875    1      12.0    1    0    0    0
  2    100.75    27.875    1      12.0    1    0    0    0
  3    100.75    39.875    2      12.0    1    0    0    0
  4     88.75    39.875    2      12.0    1    0    0    0
  5     76.75    39.875    2      12.0    1    0    0    0
  6     64.75    39.875    2      12.0    1    0    0    0
  7     52.75    39.875    2      12.0    1    0    0    0
  8     40.75    39.875    2      12.0    1    0    0    0
  9     28.75    39.875    2      12.0    1    0    0    0
 10     16.75    39.875    2      12.0    1    0    0    0
 11    -13.25    39.875    3      12.0    1    0    0    0
 12    -33.25    39.875    3      12.0    1    0    0    0
 13    -53.25    39.875    3      12.0    1    0    0    0
 14    -73.25    39.875    3      12.0    1    0    0    0
 15    -93.25    39.875    3      12.0    1    0    0    0
 16   -113.25    39.875    4      12.0    1    0    0    0
 17   -113.25   -39.875    4      12.0    0    0    0    0
 18    100.75   -39.875    1      12.0    0    0    0    0
 19     69.25     37.75    5       1.0    1    0    0    0
 20    -62.75     37.75    6       1.0    1    0    0    0
  1     69.25     37.75       0.0      608.
  2     69.25    -37.75       0.0      608.
  3    -62.75     37.75       0.0      492.
  4    -62.75    -37.75       0.0      492.
  1       0.0       0.0
  3    1108.5       0.0      27.4     61.64       0.0       0.0       5.0
```

Appendix E. Final MASH TL-4 BARRIER VII Model

BARRIER VII Input File

```
MASH 2270P Impact – Final MASH TL-4 Bridge Railing System
  369   13    8    2  412   28    2    0
    0.0010    0.0010      0.80  200    0       1.0    1
    1    5    1    5    5    5    1
    1       0.0       0.0
    9     600.0       0.0
   13     675.0       0.0
   14    699.75       0.0
   15    699.75       0.0
   16     724.5       0.0
   17     724.5       0.0
   48     916.5       0.0
   49     916.5       0.0
  240    1492.5       0.0
  241    1492.5       0.0
  368    2260.5       0.0
  369    2260.5       0.0
    1    9    7    1       0.0
    9   13    3    1       0.0
   16   48   15    2       0.0
   17   49   15    2       0.0
   48  240   95    2       0.0
   49  241   95    2       0.0
  240  368   63    2       0.0
  241  369   63    2       0.0
    1  191      0.48
  368  366  364  362  360  358  356  354  352  350
  348  346  344  342  340  338  336  334  332  330
  328  326  324  322  320  318  316  314  312  310
  308  306  304  302  300  298  296  294  292  290
  288  286  284  282  280  278  276  274  272  270
  268  266  264  262  260  258  256  254  252  250
  248  246  244  242  240  238  236  234  232  230
  228  226  224  222  220  218  216  214  212  210
  208  206  204  202  200  198  196  194  192  190
  188  186  184  182  180  178  176  174  172  170
  168  166  164  162  160  158  156  154  152  150
  148  146  144  142  140  138  136  134  132  130
  128  126  124  122  120  118  116  114  112  110
  108  106  104  102  100   98   96   94   92   90
   88   86   84   82   80   78   76   74   72   70
   68   66   64   62   60   58   56   54   52   50
   48   46   44   42   40   38   36   34   32   30
   28   26   24   22   20   18   16   14   13   12
   11   10    9    8    7    6    5    4    3    2
    1
    2  178      0.48
  369  367  365  363  361  359  357  355  353  351
  349  347  345  343  341  339  337  335  333  331
  329  327  325  323  321  319  317  315  313  311
  309  307  305  303  301  299  297  295  293  291
  289  287  285  283  281  279  277  275  273  271
  269  267  265  263  261  259  257  255  253  251
  249  247  245  243  241  239  237  235  233  231
  229  227  225  223  221  219  217  215  213  211
  209  207  205  203  201  199  197  195  193  191
```

```
189  187  185  183  181  179  177  175  173  171
169  167  165  163  161  159  157  155  153  151
149  147  145  143  141  139  137  135  133  131
129  127  125  123  121  119  117  115  113  111
109  107  105  103  101   99   97   95   93   91
 89   87   85   83   81   79   77   75   73   71
 69   67   65   63   61   59   57   55   53   51
 49   47   45   43   41   39   37   35   33   31
 29   27   25   23   21   19   17   15
100   14
  1      2.29      1.99     75.00   30000.0      6.92      99.5      68.5 0.10
  2      2.48      2.13     18.75   30000.0      7.41     106.5      73.5 0.10
  3      2.83      2.41     18.75   30000.0      8.38     120.5      83.5 0.10
  4      3.17      2.68     18.75   30000.0      9.35     134.0      93.5 0.10
  5      3.52      2.96     18.75   30000.0     10.32     148.0     103.5 0.10
  6      3.76      3.10     24.75   30000.0     10.81     155.0     109.5 0.10
  7    1397.6     145.1     24.75    1600.0      34.5     386.3    1568.6 0.10
  8    1397.6     145.1     12.00    1600.0      34.5     386.3    1568.6 0.10
  9    1397.6     145.1      6.00    1600.0      34.5     386.3    1568.6 0.10
 10    1397.6     145.1     12.00    1600.0      34.5     386.3    1568.6 0.10
 11    1260.0     105.0     24.75    1500.0      25.0     192.4     869.3 0.10
 12    1260.0     105.0     12.00    1500.0      25.0     192.4     869.3 0.10
 13    1260.0     105.0      6.00    1500.0      25.0     192.4     869.3 0.10
 14    1260.0     105.0     12.00    1500.0      25.0     192.4     869.3 0.10
300    7
  1      21.0       0.0    5000.0   15000.0     100.0    7500.0    1500.0 0.10
   300.0     100.0       1.0       1.0
  2      21.0       0.0      15.0      11.0      50.0     315.0     231.0 0.10
    18.8      13.8      20.0      20.0
  3      21.0       0.0      15.0      15.0      77.0     315.0     315.0 0.10
    18.8      18.8      20.0      20.0
  4     33.25    14.625      9.38      8.75      39.3     416.5    605.15 0.10
    30.0      30.0       4.0      10.0
  5     33.25    14.625      9.38      3.26      39.3     416.5    676.38 0.10
    30.0      30.0       4.0      10.0
  6     33.25    14.625    5000.0   15000.0     100.0    7500.0    1500.0 0.10
   300.0     100.0       1.0       1.0
  7    14.625       0.0       1.0       1.0       1.0       1.0       1.0 0.10
     1.0       1.0       1.0       1.0
  1    1    2    8    1  101       0.0       0.0       0.0
  9    9   10    0    0  102       0.0       0.0       0.0
 10   10   11    0    0  103       0.0       0.0       0.0
 11   11   12    0    0  104       0.0       0.0       0.0
 12   12   13    0    0  105       0.0       0.0       0.0
 13   13   14    0    0  106       0.0       0.0       0.0
 14   14   16    0    0  107       0.0       0.0       0.0
 15   16   18   30    2  108       0.0       0.0       0.0
 31   48   50  126    2  109       0.0       0.0       0.0
127  240  242  182    2  108       0.0       0.0       0.0
183  352  354  190    2  110       0.0       0.0       0.0
191   15   17    0    0  111       0.0       0.0       0.0
192   17   19  207    2  112       0.0       0.0       0.0
208   49   51  303    2  113       0.0       0.0       0.0
304  241  243  359    2  112       0.0       0.0       0.0
360  353  355  367    2  114       0.0       0.0       0.0
368    1    0    0    0  301       0.0       0.0       0.0       0.0       0.0
369    2    0  373    1  302       0.0       0.0       0.0       0.0       0.0
374    7    0  376    1  303       0.0       0.0       0.0       0.0       0.0
```

```
377   11    0  378    2  303       0.0       0.0       0.0       0.0       0.0
379   16   17  381   16  304       0.0       0.0       0.0       0.0       0.0
382   80   81  387   32  304       0.0       0.0       0.0       0.0       0.0
388  256  257  394   16  304       0.0       0.0       0.0       0.0       0.0
395   16   17  397   16  305       0.0       0.0       0.0       0.0       0.0
398   80   81  403   32  305       0.0       0.0       0.0       0.0       0.0
404  256  257  410   16  305       0.0       0.0       0.0       0.0       0.0
411  368  369    0    0  306       0.0       0.0       0.0       0.0       0.0
412   15    0    0    0  307       0.0       0.0       0.0       0.0       0.0
  5000.0   58310.0   20    6    4    0    1
  1     0.055      0.12      6.00      17.0
  2     0.057      0.15      7.00      18.0
  3     0.062      0.18     10.00      12.0
  4     0.110      0.35     12.00       6.0
  5      0.35      0.45      6.00       5.0
  6      1.45      1.50     15.00       1.0
  1    102.50    15.875    1      12.0    1    0    0    0
  2    102.50    27.875    1      12.0    1    0    0    0
  3    102.50    39.000    2      12.0    1    0    0    0
  4     88.75    39.000    2      12.0    1    0    0    0
  5     76.75    39.000    2      12.0    1    0    0    0
  6     64.75    39.000    2      12.0    1    0    0    0
  7     52.75    39.000    2      12.0    1    0    0    0
  8     40.75    39.000    2      12.0    1    0    0    0
  9     28.75    39.000    2      12.0    1    0    0    0
 10     16.75    39.000    2      12.0    1    0    0    0
 11    -13.25    39.000    3      12.0    1    0    0    0
 12    -33.25    39.000    3      12.0    1    0    0    0
 13    -53.25    39.000    3      12.0    1    0    0    0
 14    -73.25    39.000    3      12.0    1    0    0    0
 15    -93.25    39.000    3      12.0    1    0    0    0
 16   -125.35    39.000    4      12.0    1    0    0    0
 17   -125.35   -39.000    4      12.0    0    0    0    0
 18    102.50   -39.000    1      12.0    0    0    0    0
 19     62.40     33.90    5       1.0    1    0    0    0
 20    -77.85     33.90    6       1.0    1    0    0    0
  1     62.40     33.90       0.0      608.
  2     62.40    -33.90       0.0      608.
  3    -77.85     33.90       0.0      492.
  4    -77.85    -33.90       0.0      492.
  1       0.0       0.0
  3    1252.5       0.0     25.00     62.00       0.0       0.0       1.0
```

END OF DOCUMENT